



1 **FLUXNET-CH4: A global, multi-ecosystem dataset and analysis** 2 **of methane seasonality from freshwater wetlands**

3

4 Kyle B. Delwiche¹, Sara Helen Knox², Avni Malhotra¹, Etienne Fluet-Chouinard¹, Gavin
5 McNicol¹, Sarah Feron^{1,3}, Zutao Ouyang¹, Dario Papale^{4,5}, Carlo Trotta⁵, Eleonora Canfora⁵,
6 You-Wei Cheah⁶, Danielle Christianson⁶, M. Carmelita R. Alberto⁷, Pavel Alekseychik⁸, Mika
7 Aurela⁹, Dennis Baldocchi¹⁰, Sheel Bansal¹¹, David P. Billesbach¹², Gil Bohrer¹³
8 Rosvel Bracho¹⁴, Nina Buchmann¹⁵, David I. Campbell¹⁶, Gerardo Celis¹⁷, Jiquan Chen¹⁸,
9 Weinan Chen¹⁹, Housen Chu²⁰, Higo J. Dalmagro²¹, Sigrid Dengel⁶, Ankur R. Desai²², Matteo
10 Detto²³, Han Dolman²⁴, Elke Eichelmann²⁵, Eugenie Euskirchen²⁶, Daniela Famulari²⁷, Thomas
11 Friborg²⁸, Kathrin Fuchs²⁹, Mathias Goeckede³⁰, Sébastien Gogo³¹, Mangaliso J. Gondwe³²,
12 Jordan P. Goodrich¹⁶, Pia Gottschalk³³, Scott L. Graham³⁴, Martin Heimann³⁰, Manuel
13 Helbig^{35,36}, Carole Helfter³⁷, Kyle S. Hemes^{10,38}, Takashi Hirano³⁹, David Hollinger⁴⁰, Lukas
14 Hörtnagl¹⁵, Hiroki Iwata⁴¹, Adrien Jacotot³¹, Joachim Jansen⁴², Gerald Jurasinski⁴³, Minseok
15 Kang⁴⁴, Kuno Kasak⁴⁵, John King⁴⁶, Janina Klatt⁴⁷, Franziska Koebsch⁴³, Ken W. Krauss⁴⁸,
16 Derrick Y.F. Lai⁴⁹, Ivan Mammarella⁵⁰, Giovanni Manca⁵¹, Luca Beelli Marchesini⁵², Jaclyn
17 Hatala Matthes⁵³, Trofim Maximon⁵⁴, Lutz Merbold⁵⁵, Bhaskar Mitra⁵⁶, Timothy H. Morin⁵⁷,
18 Eiko Nemitz³⁷, Mats B. Nilsson⁵⁸, Shuli Niu¹⁹, Walter C. Oechel⁵⁹, Patricia Y. Oikawa⁶⁰,
19 Keisuke Ono⁶¹, Matthias Peichl⁵⁸, Olli Peltola⁹, Michele L. Reba⁶², Andrew D. Richardson^{63,64},
20 William Riley⁶, Benjamin R. K. Runkle⁶⁵, Youngryel Ryu⁶⁶, Torsten Sachs³³, Ayaka Sakabe⁶⁷,
21 Camilo Rey Sanchez¹⁰, Edward A. Schuur⁶⁸, Karina V.R. Schäfer⁶⁹, Oliver Sonntag⁷⁰, Jed P.
22 Sparks⁷¹, Ellen Stuart-Haëntjens⁷², Cove Sturtevant⁷³, Ryan C. Sullivan⁷⁴, Daphne J. Szutu¹⁰,
23 Jonathan E. Thom⁷⁵, Margaret S. Torn⁶, Eeva-Stiina Tuittila⁷⁶, Jessica Turner⁷⁷, Masahito
24 Ueyama⁷⁸, Alex C. Valach¹⁰, Rodrigo Vargas⁷⁹, Andrej Varlagin⁸⁰, Alma Vazquez-Lule⁷⁹,
25 Joseph G. Verfaillie¹⁰, Timo Vesala⁵⁰, George L. Vourlitis⁸¹, Eric J. Ward⁴⁸, Christian Wille³³,
26 Georg Wohlfahrt⁸², Guan Xhuan Wong⁸³, Zhen Zhang⁸⁴, Donatella Zona^{59,85}, Lisamarie
27 Windham-Myers⁸⁶, Benjamin Poulter⁸⁷, Robert B. Jackson^{1,38,88}

28

29

30

¹ Department of Earth System Science, Stanford University, Stanford, California

31

² Department of Geography, The University of British Columbia, Vancouver, British Columbia, Canada

32

³ Department of Physics, University of Santiago de Chile, Santiago, Chile

33

⁴ Dipartimento per la Innovazione nei Sistemi Biologici, Agroalimentari e Forestali, Università degli Studi della

34

Tuscia, Largo dell'Università, Viterbo, Italy e Forestali, Università

35

⁵ euroMediterranean Center on Climate Change CMCC, Lecce, Italy

36

⁶ Earth and Environmental Sciences Area, Lawrence Berkeley National Lab, Berkeley, California

37

⁷ International Rice Research Institute

38

⁸ Natural Resources Institute Finland (LUKE), Helsinki, Finland

39

⁹ Finnish Meteorological Institute, PO Box 501, 00101 Helsinki, Finland

40

¹⁰ Department of Environmental Science, Policy and Management, University of California, Berkeley, CA, USA

41

¹¹ U.S. Geological Survey, Northern Prairie Wildlife Research Center, 8711 37th St Southeast, Jamestown, ND

42

58401 USA

43

¹² University of Nebraska-Lincoln, Department of Biological Systems Engineering, Lincoln, NE 68583, USA

44

¹³ Department of Civil, Environmental & Geodetic Engineering, Ohio State University

45

¹⁴ School of Forest Resources and Conservation, University of Florida, Gainesville FL, 32611

46

¹⁵ Department of Environmental Systems Science, Institute of Agricultural Sciences, ETH Zurich, 8092 Zurich,

47

Switzerland

48

¹⁶ School of Science, University of Waikato, Hamilton, New Zealand



- 49 ¹⁷ Agronomy Department, University of Florida, Gainesville FL, 32601
50 ¹⁸ Department of Geography, Michigan State University
51 ¹⁹ Institute of Geographic Sciences and Natural Resources Research, Chinese Academy of Sciences, Beijing 100101,
52 PR China.
53 ²⁰ Climate and Ecosystem Sciences Division, Lawrence Berkeley National Lab, Berkeley, CA 94702, USA
54 ²¹ Universidade de Cuiaba, Cuiaba, Mato Grosso, Brazil
55 ²² Dept of Atmospheric and Oceanic Sciences, University of Wisconsin-Madison, Madison, WI 53706 USA
56 ²³ Department of Ecology and Evolutionary Biology, Princeton University, Princeton NJ, USA
57 ²⁴ Department of Earth Sciences, Vrije Universiteit, Amsterdam, Netherlands
58 ²⁵ School of Biology and Environmental Science, University College Dublin, Ireland
59 ²⁶ University of Alaska Fairbanks, Institute of Arctic Biology, Fairbanks, AK, USA
60 ²⁷ C NR - institute for Mediterranean Agricultural and Forest Systems, Piazzale Enrico Fermi, 1 Portici (Napoli)
61 Italy
62 ²⁸ University of Copenhagen, Department of Geosciences and Natural Resource Management
63 ²⁹ Institute of Meteorology and Climate Research - Atmos. Environ. al Research, Karlsruhe Institute of Technology
64 (KIT Campus Alpin), 82467 Garmisch-Partenkirchen, Germany
65 ³⁰ Max Planck Institute for Biogeochemistry, Jena, Germany
66 ³¹ ISTO, Université d'Orléans, CNRS, BRGM, UMR 7327, 45071, Orléans, France
67 ³² Okavango Research Institute, University of Botswana, Maun, Botswana.
68 ³³ GFZ German Research Centre for Geosciences, Telegrafenberg, 14473 Potsdam, Germany
69 ³⁴ Manaaki Whenua - Landcare Research, Lincoln, NZ
70 ³⁵ Université de Montréal, Département de géographie, Université de Montréal, Montréal, QC H2V 0B3,
71 Canada & Dalhousie University, Department of Physics and Atmospheric Science, Halifax, NS B2Y 1P3, Canada
72 ³⁷ UK Centre for Ecology and Hydrology, Edinburgh, UK
73 ³⁸ Woods Institute for the Environment, Stanford University, Stanford, California
74 ³⁹ Research Faculty of Agriculture, Hokkaido University, Sapporo, Japan
75 ⁴⁰ Northern Research Station, USDA Forest Service, Durham, NH 03824, USA
76 ⁴¹ Department of Environmental Science, Faculty of Science, Shinshu University
77 ⁴² Stockholm University, Department of Geological Sciences
78 ⁴³ University of Rostock, Rostock, Germany
79 ⁴⁴ National Center for Agro Meteorology, Seoul, South Korea
80 ⁴⁵ Department of Geography, University of Tartu, Vanemuise st 46, Tartu, 51410, Estonia
81 ⁴⁶ Department of Forestry and Environmental Resources, North Carolina State University, Raleigh, NC, USA
82 ⁴⁷ Vegetation Ecology, Institute of Ecology and Landscape, Department Landscape Architecture, Weihestephan-
83 Triesdorf University of Applied Sciences, Am Hofgarten 1, 85354 Freising, Germany
84 ⁴⁸ USGS Wetland and Aquatic Research Center, Lafayette LA
85 ⁴⁹ Department of Geography and Resource Management, The Chinese University of Hong Kong, Shatin, New
86 Territories, Hong Kong SAR, China
87 ⁵⁰ Institute for Atmospheric and Earth System Research/Physics, Faculty of Science, University of Helsinki,
88 Helsinki, Finland
89 ⁵¹ European Commission, Joint Research Centre (JRC), Ispra, Italy.
90 ⁵² Dept. of Sustainable Agro-Ecosystems and Bioresources, Research and Innovation Centre, Fondazione Edmund
91 Mach, San Michele all'Adige, Italy
92 ⁵³ Department of Biological Sciences, Wellesley College, Wellesley, MA 02481, USA
93 ⁵⁴ Institute for Biological Problems of the Cryolithozone, RAS, Yakutsk, REP. Yakutia.
94 ⁵⁵ Mazingira Centre, International Livestock Research Institute (ILRI), Old Naivasha Road, PO Box 30709, 00100
95 Nairobi, Kenya
96 ⁵⁶ Northern Arizona University, School of Informatics, Computing and Cyber Systems
97 ⁵⁷ Environmental Resources Engineering, SUNY College of Environmental Science and Forestry
98 ⁵⁸ Dept. of Forest Ecology and Management, Swedish University of Agricultural Sciences, 901 83 Umeå, Sweden
99 ⁵⁹ Dept. Biology, San Diego State University, San Diego, CA 92182, USA
100 ⁶⁰ Department of Earth and Environmental Sciences, Cal State East Bay, Hayward CA 94542 USA
101 ⁶¹ National Agriculture and Food Research Organization, Tsukuba, Japan
102 ⁶² USDA-ARS Delta Water Management Research Unit, Jonesboro, Arkansas 72401, United States
103 ⁶³ School of Informatics, Computing & Cyber Systems, Northern Arizona University, Flagstaff, AZ 86011, USA
104 ⁶⁴ Center for Ecosystem Science and Society, Northern Arizona University, Flagstaff, AZ 86011, USA



- 105 ⁶⁵ Department of Biological & Agricultural Engineering, University of Arkansas, Fayetteville, Arkansas 72701,
106 United States
107 ⁶⁶ Department of Landscape Architecture and Rural Systems Engineering, Seoul National University, South Korea
108 ⁶⁷ Hakubi center, Kyoto University, Kyoto, Japan
109 ⁶⁸ Department of Biological Sciences, Northern Arizona University, Flagstaff, AZ, USA
110 ⁶⁹ Dept of Earth and Environmental Science, Rutgers University Newark, NJ
111 ⁷⁰ Université de Montréal, Département de géographie, Université de Montréal, Montréal, QC H2V 0B3, Canada
112 ⁷¹ Department of Ecology and Evolution, Cornell
113 ⁷² USGS California Water Science Center, 6000 J Street, Placer Hall, Sacramento, CA, 95819
114 ⁷³ National Ecological Observatory Network, Battelle, 1685 38th St Ste 100, Boulder, Colorado, 80301, USA
115 ⁷⁴ Environmental Science Division, Argonne National Laboratory, Lemont, IL, USA
116 ⁷⁵ Space Sciences and Engineering Center, University of Wisconsin-Madison, Madison, WI 53706 USA
117 ⁷⁶ School of Forest Sciences, University of Eastern Finland, Joesnuu, Finland
118 ⁷⁷ Freshwater and Marine Science, University of Wisconsin-Madison
119 ⁷⁸ Graduate School of Life and Environmental Sciences, Osaka Prefecture University
120 ⁷⁹ Department of Plant and Soil Sciences, University of Delaware, Newark, DE, USA
121 ⁸⁰ A.N. Severtsov Institute of Ecology and Evolution, Russian Academy of Sciences
122 ⁸¹ California State University San Marcos, San Marcos, CA, USA
123 ⁸² University of Innsbruck, Department of Ecology, Sternwartestr. 15, 6020 Innsbruck, AUSTRIA
124 ⁸³ Sarawak Tropical Peat Research Institute, Sarawak, Malaysia
125 ⁸⁴ Department of Geographical Sciences, University of Maryland, College Park, MD 20740, USA
126 ⁸⁵ Department of Animal and Plant Sciences, University of Sheffield, Western Bank, Sheffield, S10 2TN, United
127 Kingdom
128 ⁸⁶ USGS Water Mission Area, 345 Middlefield Road, Menlo Park, CA, 94025
129 ⁸⁷ Biospheric Sciences Laboratory, NASA Goddard Space Flight Center, Greenbelt, Maryland
130 ⁸⁸ Precourt Institute for Energy, Stanford University, Stanford, California

131
132
133 *Correspondence to:* Kyle B. Delwiche (delwiche@stanford.edu)

134
135 **Abstract.** Methane (CH₄) emissions from natural landscapes constitute roughly half of global CH₄ contributions to
136 the atmosphere, yet large uncertainties remain in the absolute magnitude and the seasonality of emission quantities
137 and drivers. Eddy covariance (EC) measurements of CH₄ flux are ideal for constraining ecosystem-scale CH₄
138 emissions, including their seasonality, due to quasi-continuous and high temporal resolution of flux measurements,
139 coincident measurements of carbon, water, and energy fluxes, lack of ecosystem disturbance, and increased
140 availability of datasets over the last decade. Here, we 1) describe the newly published dataset, FLUXNET-CH₄
141 Version 1.0, the first global dataset of CH₄ EC measurements (available at [https://fluxnet.org/data/fluxnet-ch4-](https://fluxnet.org/data/fluxnet-ch4-community-product/)
142 [community-product/](https://fluxnet.org/data/fluxnet-ch4-community-product/)). FLUXNET-CH₄ includes half-hourly and daily gap-filled and non gap-filled aggregated CH₄
143 fluxes and meteorological data from 79 sites globally: 42 freshwater wetlands, 6 brackish and saline wetlands, 7
144 formerly drained ecosystems, 7 rice paddy sites, 2 lakes, and 15 uplands. Then, we 2) evaluate FLUXNET-CH₄
145 representativeness for freshwater wetland coverage globally, because the majority of sites in FLUXNET-CH₄ Version
146 1.0 are freshwater wetlands and because freshwater wetlands are a substantial source of total atmospheric CH₄
147 emissions; and 3) provide the first global estimates of the seasonal variability and seasonality predictors of freshwater
148 wetland CH₄ fluxes. Our representativeness analysis suggests that the freshwater wetland sites in the dataset cover
149 global wetland bioclimatic attributes (encompassing energy, moisture, and vegetation-related parameters) in arctic,
150 boreal, and temperate regions, but only sparsely cover humid tropical regions. Seasonality metrics of wetland CH₄
151 emissions vary considerably across latitudinal bands. In freshwater wetlands (except those between 20° S to 20° N)
152 the spring onset of elevated CH₄ emissions starts three days earlier, and the CH₄ emission season lasts 4 days longer,
153 for each degree C increase in mean annual air temperature. On average, the onset of increasing CH₄ emissions lags
154 soil warming by one month, with very few sites experiencing increased CH₄ emissions prior to the onset of soil



155 warming. In contrast, roughly half of these sites experience the spring onset of rising CH₄ emissions prior to the spring
156 increase in gross primary productivity (GPP). The timing of peak summer CH₄ emissions does not correlate with the
157 timing for either peak summer temperature or peak GPP. Our results provide seasonality parameters for CH₄
158 modeling, and highlight seasonality metrics that cannot be predicted by temperature or GPP (i.e., seasonality of CH₄
159 peak). The FLUXNET-CH₄ dataset provides an open-access resource for CH₄ flux synthesis, has a range of
160 applications, and is unique in that it includes coupled measurements of important CH₄ drivers such as GPP and
161 temperature. Although FLUXNET-CH₄ could certainly be improved by adding more sites in tropical ecosystems and
162 by increasing the number of site-years at existing sites, it is a powerful new resource for diagnosing and understanding
163 the role of terrestrial ecosystems and climate drivers in the global CH₄ cycle. All seasonality parameters are available
164 at <https://doi.org/10.5281/zenodo.4408468>. Additionally, raw FLUXNET-CH₄ data used to extract seasonality
165 parameters can be downloaded from <https://fluxnet.org/data/fluxnet-ch4-community-product/>, and a complete list of
166 the 79 individual site data DOIs is provided in Table 2 in the Data Availability section of this document.

167
168
169
170
171

172 1 Introduction

173 Methane (CH₄) has a global warming potential that is 28 times larger than carbon dioxide (CO₂) on a 100-
174 year time scale (Myhre et al., 2013), and its atmospheric concentration has increased by >1000 ppb since 1800
175 (Etheridge et al., 1998). While atmospheric CH₄ concentrations are substantially lower than those of CO₂, CH₄'s
176 higher effectiveness at absorbing longwave radiation means that CH₄ has contributed 20-25% as much radiative
177 forcing as CO₂ since 1750 (Etminan et al., 2016). Despite its importance to global climate change, natural CH₄ sources
178 and sinks remain poorly constrained, and with uncertain attribution to the various biogenic and anthropogenic sources
179 (Saunio et al., 2016, 2020). Bottom-up and top-down estimates differ by 154 TG/yr (745 vs 591 TG/yr, respectively),
180 with much of this difference arising from natural sources (Saunio et al., 2020). Vegetated wetlands and inland water
181 bodies account for most natural CH₄ emissions, as well as the majority of uncertainty in bottom-up emissions estimates
182 (Saunio et al., 2016). Better diagnosis and prediction of terrestrial CH₄ sources to the atmosphere requires high
183 frequency and continuous measurements of CH₄ exchanges across a continuum of ecological time (hours to years)
184 and space (meters to kilometers) scales.

185 Tower-based eddy covariance (EC) measurements provide ecosystem-scale CH₄ fluxes at high temporal
186 resolution across years, are coupled with measurements of key CH₄ drivers such as temperature, water and recent
187 substrate input (inferred from CO₂ flux), and thus help constrain bottom-up CH₄ budgets and improve CH₄ predictions.
188 Although EC towers began measuring CO₂ fluxes in the late 1970s (Desjardins 1974; Anderson et al., 1984), and
189 some towers began measuring CH₄ in the 1990s (Verma et al., 1992), most CH₄ flux EC measurements began within
190 the last decade. Given that many EC CH₄ sites are relatively new, the flux community has only recently compiled
191 them for global synthesis efforts (e.g., Chang et al., in review) and is still working to standardize CH₄ flux
192 measurements and establish gap-filling protocols (Nemitz et al., 2018; Knox et al., 2019). Furthermore, the growth of
193 EC networks for CH₄ fluxes has sometimes taken place in a relatively *ad hoc* fashion, often at sites that were already
194 measuring CO₂ fluxes or where higher CH₄ fluxes were expected, potentially introducing bias. The representativeness
195 and spatial distribution of CO₂ flux tower networks has been assessed to evaluate its ability to upscale fluxes regionally
196 (Hargrove et al., 2003; Hoffman et al., 2013; Papale et al., 2015; Villarreal et al., 2018, 2019) and globally (Jung et
197 al., 2009; 2020; Kumar et al., 2016). However, a relatively sparse coverage of CH₄ flux towers prompts the question
198 of how well the current observation network provides a sufficient sampling of global or ecosystem-specific bioclimatic
199 conditions.



200 Broad-scale wetland CH₄ seasonality estimates, such as when fluxes increase, peak, and decrease and the
201 predictors of seasonality, remain relatively unconstrained across wetlands globally. These key seasonality metrics
202 vary considerably across high-emitting systems such as wetlands and other aquatic systems (Desjardins, 1974; Dise,
203 1992; Melloh and Crill 1996; Wik et al., 2013; Zona et al., 2016; Treat et al., 2018). Few continuous CH₄ flux datasets
204 across representative site-years make it difficult to establish trends in seasonal dynamics, though monthly or annually
205 aggregated estimates of CH₄ fluxes from different seasons do exist for high latitudes (Zona et al., 2016; Treat et al.,
206 2018). Seasonal variability in wetland CH₄ fluxes is expected to be driven by changes in air and soil temperature, soil
207 moisture (including water table dynamics), and recent carbon substrate availability, which influence the rates of CH₄
208 production and consumption (Lai, 2009; Bridgman et al., 2013; Dean et al., 2018). Temperature has widely been found
209 to strongly affect CH₄ flux (Chu et al., 2014; Yvon-Durocher et al., 2014; Sturtevant et al., 2016), but the relationship
210 is complex (Chang et al., 2020) and varies seasonally (Koebsch et al., 2015; Helbig et al., 2017). Methane flux is also
211 driven by inundation depth since anoxic conditions are typically necessary for methanogenesis (Lai, 2009; Bridgman
212 et al., 2013), though CH₄ production under bulk-oxic conditions has been observed (Angle et al., 2017). Substrate
213 availability influences CH₄ production potential and is linked with gross primary productivity (GPP) because recent
214 photosynthate fuels methanogenesis though this relationship can vary by ecosystem type, plant functional type and
215 biome (Meronigal et al., 1999; Chanton et al., 2008; Hatala et al., 2012; Lai et al., 2014; Malhotra and Roulet, 2015;
216 Sturtevant et al., 2016). In process models, the seasonality of CH₄ emissions from wetlands globally is primarily
217 constrained by inundation (Poulter et al., 2017), with secondary within-wetland influences from temperature and
218 availability of carbon (C) substrates (Melton et al., 2013; Castro-Morales et al., 2018). Bottom-up and top-down global
219 CH₄ estimates continue to disagree on total CH₄ flux magnitudes and seasonality, including the timing of annual peak
220 emissions (Spahni et al., 2011; Saunio et al., 2020). Thus, the variability and predictors of wetland CH₄ seasonality
221 globally remain a knowledge gap that high-frequency and long-term EC data can help fill.

222 Here, we 1) describe Version 1.0 of the FLUXNET-CH₄ dataset (available at <https://fluxnet.org/data/fluxnet->
223 [ch4-community-product/](https://fluxnet.org/data/fluxnet-ch4-community-product/)). Version 1.0 of the dataset expands and formalizes the publication of data scattered among
224 regional flux networks as described previously in Knox et al., 2019. FLUXNET-CH₄ includes half-hourly and daily
225 gap-filled and non gap-filled aggregated CH₄ fluxes and meteorological data from 79 sites globally: 42 freshwater
226 wetlands, 6 brackish and saline wetlands, 7 formerly drained ecosystems, 7 rice paddy sites, 2 lakes, and 15 upland
227 ecosystems. Since the majority of sites in FLUXNET-CH₄ Version 1.0 are freshwater wetlands, and freshwater
228 wetlands are a substantial source of total atmospheric CH₄ emissions, we use the subset of data from freshwater
229 wetlands to then; 2) evaluate the representativeness of freshwater wetland coverage in the dataset relative to wetlands
230 globally; and 3) provide the first assessment of global variability and predictors of freshwater wetland CH₄ flux
231 seasonality. We quantify a suite of CH₄ seasonality metrics and evaluate temperature and GPP (a proxy for recent
232 substrate input) as predictors of seasonality across four latitudinal bands (northern, temperate, subtropical, and
233 tropical). Due to a lack of high-temporal resolution water table data at all sites, our analyses are unable to evaluate the
234 critical role of water table on CH₄ seasonality. Here we provide parameters for better understanding and modeling
235 seasonal variability in freshwater wetland CH₄ fluxes and generate new hypotheses and data resources for future
236 syntheses.

237 2. Methods

238 2.1 FLUXNET-CH₄ dataset

239 2.1.1 History and data description

240 The FLUXNET-CH₄ dataset was initiated by the Global Carbon Project (GCP) in 2017 to better constrain
241 the global CH₄ budget (<https://www.globalcarbonproject.org/methanebudget/index.htm>). Beginning with a kick off
242 meeting in May 2018 in Washington DC, hosted by Stanford University, we coordinated with the AmeriFlux
243 Management Project, the European Ecosystem Fluxes Database, and the ICOS Ecosystem Thematic Centre (ICOS-



244 ETC) in order to avoid duplication of efforts, as most sites are part of different regional networks (albeit with different
245 data products). We have collected and standardized data for FLUXNET-CH₄ with assistance from the regional flux
246 networks, AmeriFlux's "Year of Methane", FLUXNET, the EU's Readiness of ICOS for Necessities of Integrated
247 Global Observations (RINGO) project, and a USGS Powell Center working group. FLUXNET-CH₄ is a community-
248 led project, so while we developed it with assistance from FLUXNET, we do not necessarily use standard FLUXNET
249 data variables, formats, or methods.

250 FLUXNET-CH₄ includes gap-filled half-hourly CH₄ fluxes and meteorological variables. Gaps in
251 meteorological variables (TA - air temperature, SW_IN - incoming shortwave radiation, LW_IN - incoming longwave
252 radiation, VPD - vapor pressure deficient, PA - pressure, P - precipitation, WS - wind speed) were filled with the
253 ERA-Interim (ERA-I) reanalysis product (Vuichard and Papale, 2015). We used the REddyProc package (Wutzler
254 et al., 2018) to filter flux values with low friction velocity (u_*), based on relating nighttime u_* , to fill gaps in CO₂, latent
255 heat, and sensible heat fluxes, and to partition net CO₂ fluxes into gross primary production (GPP) and ecosystem
256 respiration (RECO) using both the daytime (Lasslop et al., 2010) and nighttime (Reichstein et al., 2005) approaches
257 in REddyProc. CH₄ flux data gaps were filled using artificial neural network (ANN) methods first described in Knox
258 et al. (2015) and in Knox et al. (2019), and summarized here in Sect. 2.1.2. Gap-filled data for gaps exceeding two
259 months are provided and flagged for quality. Please see Table B1 for variable description and units, as well as quality
260 flag information. For the seasonality analysis in this paper we excluded data from gaps exceeding two months, and
261 we encourage future users of FLUXNET-CH₄ to critically evaluate gap-filled values from long data gaps before
262 including them in analyses (Dengel et al., 2013; Kim et al., 2020).

263 In addition to half-hourly data, the FLUXNET-CH₄ Version 1.0 release also contains a full set of daily mean
264 values for all parameters except wind direction and precipitation. Daily precipitation is included as the daily sum of
265 the half-hourly data, and daily average wind direction is not included.

266 2.1.2 Gap-filling methods and uncertainty estimates

267 As described in Knox et al. (2015) and in Knox et al. (2019), the ANN routine used to gap-fill the CH₄ data
268 was optimized for generalizability and representativeness. To avoid biasing the ANN toward environmental conditions
269 with typically better data coverage (e.g., summer-time and daytime measurements), the explanatory data were divided
270 into a maximum of 15 clusters using a k-means clustering algorithm. Data used to train, test, and validate the ANN
271 were proportionally sampled from these clusters. For generalizability, the simplest ANN architecture with good
272 performance (<5% gain in model accuracy for additional increases in architecture complexity) was selected for 20
273 extractions of the training, test, and validation data. Within each extraction, each tested ANN architecture was
274 reinitialized 10 times, and the initialization with the lowest root-mean-square-error was selected to avoid local minima.
275 The median of the 20 predictions was used to fill each gap. A standard set of variables available across all sites were
276 used to gap-fill CH₄ fluxes (Dengel et al., 2013), which included the previously mentioned meteorological variables
277 TA, SW_IN, WS, PA, and sine and cosine functions to represent seasonality. These meteorological variables were
278 selected since they are relevant to CH₄ exchange and were gap-filled using the ERA-I reanalysis data. Other variables
279 related to CH₄ flux (e.g., water table depth and soil temperature) were not included as explanatory variables as they
280 were not available across all sites or had large gaps that could not be filled using the ERA-I reanalysis data (Knox et
281 al., 2019). The ANN gap-filling was performed using MATLAB (MathWorks 2018, version 9.4.0).

282 While the median of the 20 predictions was used to fill each gap, the spread of the predictions was used to
283 provide a measure of uncertainty resulting from the ANN gap-filling procedure. Specifically, for gap-filled values,
284 the combined annual gap-filling and random uncertainty was calculated from the variance of the cumulative sums of
285 the 20 ANN predictions (Knox et al., 2015; Anderson et al., 2016; Oikawa et al., 2017). The (non-cumulative) variance
286 of the 20 ANN predictions was also used to provide gap-filling uncertainty for each half-hourly gap-filled value
287 included in the dataset. While this is useful for data-model comparisons, it cannot be used to estimate cumulative



288 annual gap-filling error because gap-filling error is not random, which is why the cumulative sums of the 20 ANN
289 predictions are used to estimate annual gap-filling error.

290 Random errors in EC fluxes follow a double exponential (Laplace) distribution with the standard deviation
291 varying with flux magnitude (Richardson et al., 2006; Richardson et al., 2012). For half-hourly CH₄ flux
292 measurements, random error was estimated using the residuals of the median ANN predictions, providing a
293 conservative “upper limit” estimate of the random flux uncertainty (Moffat et al., 2007; Richardson et al., 2008). The
294 annual cumulative uncertainty at 95% confidence was estimated by adding the cumulative gap-filling and random
295 measurement uncertainties in quadrature (Richardson and Hollinger, 2007; Anderson et al., 2016). Annual
296 uncertainties for individual site-years are provided in Table B7. Throughout this paper, we include uncertainties on
297 individual site years when discussing single years of data. In sites with multiple years of data, we report the standard
298 deviation of the multiple years.

299 2.1.3 Dataset structure and site metadata

300 To enable data use by the broader flux community, we have partnered with regional flux networks and
301 FLUXNET to provide standardized and gap-filled EC CH₄ data. FLUXNET-CH₄ Version 1.0 contains two comma-
302 separated data files per site at half-hourly and daily resolutions. Half-hourly and daily aggregations are available for
303 download at <https://fluxnet.org/data/fluxnet-ch4-community-product/>, along with a file containing select site
304 metadata. Each site has a unique FLUXNET-CH₄ DOI. All site data are available under CC BY 4.0
305 (<https://creativecommons.org/licenses/by/4.0/>) copyright license.

306 Metadata (Table B2) include site coordinates, ecosystem classification based on site literature,
307 presence/absence and dominance for specific vegetation types, and DOI link, as well as calculated data such as annual
308 and quarterly flux values. FLUXNET-CH₄ Version 1.0 sites were classified based on site-specific literature as fen,
309 bog, swamp, marsh, salt marsh, lake, mangrove, rice paddy/field, wet tundra, upland, or drained ecosystems that
310 previously could have been wetlands, seasonally flooded pastures, or agricultural areas. To the extent possible, we
311 followed classification systems of previous wetland CH₄ syntheses (Olefeldt et al., 2013; Turetsky et al., 2014; Treat
312 et al., 2018). Drained systems are former wetlands that have subsequently been drained but may maintain a relatively
313 shallow water table. Upland ecosystems are further divided into alpine meadows, grasslands, needleleaf forests, mixed
314 forest, crops, tundra, and urban. Freshwater wetland classifications follow hydrological definitions of bog
315 (ombrotrophic), fen (minerotrophic), wet tundra, marshes and swamps, and were designated as per primary literature
316 on the site. For all sites, vegetation was classified for presence or absence of brown mosses, *Sphagnum* mosses,
317 ericaceous shrubs, trees (of any height) and aerenchymatous species (mostly Order Poales but includes exceptions).
318 These categories closely follow Treat et al., (2018), except that aerenchymatous species had to be expanded beyond
319 Cyperaceae to incorporate wetlands globally. Presence/absence of vegetation groups was designated based on species
320 lists in primary literature from the site. Out of the vegetation groups present, the dominant (most abundant) group is
321 also reported and is based on data from a survey of lead site investigators.

322 In addition to the variable description table (Table B1) and the site metadata (Table B2), we provide several
323 more tables to complement our analysis. Table B3 includes the climatic data for the representativeness analysis.
324 Seasonality parameters for CH₄ flux, air temperature, soil temperature (for sites with multiple probes, Table B4
325 includes parameters from the probe closest to the ground surface), and GPP are provided in Table B4, with the full set
326 of soil temperature parameters from all probes in Table B5. Table B6 contains the soil temperature probe depths.
327 Table B7 contains the annual flux and uncertainty. All Appendix B tables are also available at
328 <https://doi.org/10.5281/zenodo.4408468>.

329



330 2.1.4 Annual fluxes

331 Annual fluxes were calculated from gap-filled data for site-years with data gaps shorter than two consecutive
332 months, or for sites above 20° N where >2 month data gaps occurred outside of the highest CH₄-emission months of
333 May 1 through October 31. Since we did not sum gap-filled values for >2 month gaps during the winter, annual sums
334 from these years will be an underestimate since winter fluxes can be important (Zona et al., 2016; Treat et al., 2018).
335 Several sites had less than one year of data, and we report gap-filled flux annual sums for sites with between six
336 months and one year of data (BW-Gum = 228 days, CH-Oe2 = 200 days, JP-Swl = 210 days, US-EDN = 182 days).
337 While these sums will be an underestimate of annual flux since they do not span a full year (and we therefore do not
338 use them in the seasonality analysis), their relative magnitude can still be informative. For example, site JP-SWL is a
339 lake site, and even with less than a year of data the summed flux of 66 g C m⁻² is relatively high (Taoka et al., 2020).
340 In addition to sites with short time series, the annual sum for site ID-Pag represents 365 days spanning June 2016 to
341 June 2017.

342 2.1.5 Subset analysis on freshwater wetland CH₄ flux

343 In addition to the FLUXNET-CH₄-wide description of site class distributions and annual fluxes, we also
344 include a subset analysis on freshwater wetlands, given that it is the dominant ecosystem type in our dataset and an
345 important global CH₄ source (Saunois et al., 2016). First, we analyze freshwater wetland representativeness, and
346 subsequently the seasonality of their CH₄ emissions. Freshwater wetlands included in the seasonality and
347 representativeness analysis are indicated in Table B2, column “IN_SEASONALITY_ANALYSIS”.

348

349 2.2 Wetland representativeness

350 2.2.1 Principal Component Analysis

351 To understand how the distribution of FLUXNET-CH₄ Version 1.0 sites compares with the global wetland
352 distribution, we evaluated the representativeness of the FLUXNET-CH₄ Version 1.0 wetland sites in the entire global
353 wetland cover along four bioclimatic gradients. Only freshwater wetland sites were included in this analysis, with
354 coastal sites excluded because, due to a lack of global gridded datasets, salinity could not be included as an
355 environmental variable despite being an important control on CH₄ production (Bartlett et al., 1987; Poffenbarger et
356 al., 2011). The four bioclimatic variables used were: mean annual air temperature (MAT), latent heat flux (LE),
357 enhanced vegetation index (EVI), and water index (SRWI; data sources in Table B3). EVI is a more direct
358 measurement than GPP from global gridded products and is considered a reasonable proxy for GPP (Sims et al.,
359 2006). Thus, we used EVI instead of GPP. Together, these environmental variables account for or are proxies for key
360 controls of CH₄ production, oxidation at the surface, and transport (Bridgham et al., 2013). We use a principal
361 components analysis (PCA) to visualize the site distribution across the four environmental drivers at once. For this
362 analysis, we consider the annual average bioclimatic conditions over 2003-2015. In the PCA output, we evaluate the
363 coverage of the 42 freshwater sites over 0.25° grid cells containing >5% wetland mean cover in Wetland Area and
364 Dynamics for Methane Modeling (WAD2M; Zhang et al., In Review) for the same time period.

365 2.2.2 Global Dissimilarity and Constituency Analysis

366 To further identify geographical gaps in the coverage of the FLUXNET-CH₄ Version 1.0 network, we
367 quantified the dissimilarity of global wetlands from the tower network, using a similar approach to that taken for CO₂
368 flux towers (Kumar et al., 2016; Meyer and Pebesma 2020). We calculated the 4-dimensional Euclidean distance from
369 the four bioclimatic variables between every point at the land surface to every tower location at the FLUXNET-CH₄
370 network. We then divided these distances by the average distance between towers to produce a dissimilarity index.
371 Dissimilarity scores <1 represent areas whose nearest tower is closer than the average distance among towers, while



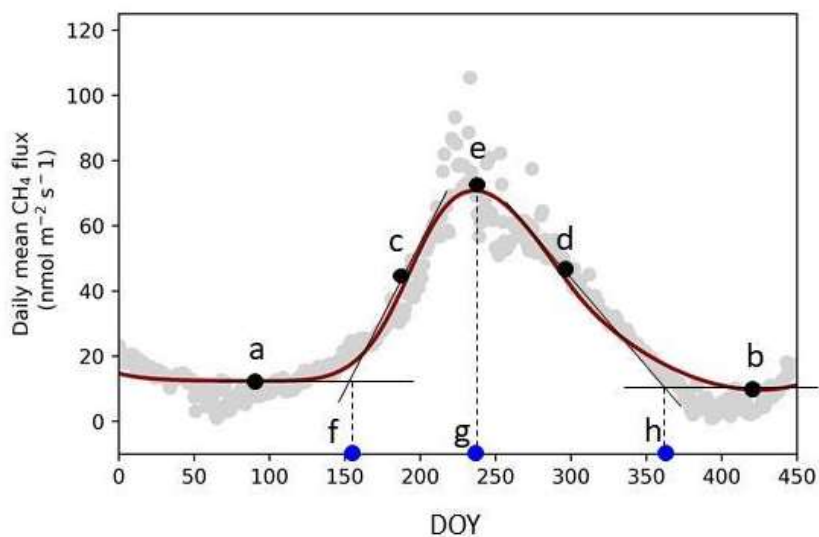
372 areas with scores >1 are more distant. Lastly, we identified the importance of an individual tower in the network by
373 estimating the geographical area to which it is most analogous in bioclimate space. We divided the world's land
374 surface according to closest towers in bioclimatic space. The area to which each tower is nearest is defined as the
375 tower's constituency.

376 2.3 Wetland CH₄ seasonality

377 To examine freshwater wetland CH₄ seasonality across the global range of sites in FLUXNET-CH4
378 Version 1.0, we extracted seasonality parameters for CH₄, temperature, and GPP using Timesat, a software package
379 designed to analyse seasonality of environmental systems (Jönsson and Eklundh, 2002; Jönsson and Eklundh, 2004;
380 Eklundh and Jönsson, 2015). Timesat calculates a range of seasonality parameters, including baseline flux, peak
381 flux, and the slope of spring flux increase and fall decrease (Fig. 1). We also calculate parameters such as amplitude
382 (“e” - baseline, which is the average of “a” and “b”, in Fig. 1), and relative peak timing ($(“g” - “f”) / (“h” - “f”)$ in
383 Fig. 1). Timesat uses a double-logistic fitting function to create a series of localized fits centered on data minima and
384 maxima. Localized fits are minimized using a merit function and the Levenberg-Marquardt method (Madsen et al.,
385 2004; Nielsen, 1999). These localized fits are then merged using a global function to create a smooth fit over the
386 full time interval. To fit CH₄ time-series in Timesat, we used gap-filled data after removing gaps exceeding two
387 months. We do not report Timesat parameters when large gaps occur during CH₄ emissions spring increase, peak, or
388 fall decrease.

389 We estimate ‘start of elevated emissions season’ when CH₄ emissions begin to increase in the spring (“f”
390 in Fig. 1), and ‘end of elevated emissions season’ when the period of elevated flux ends in the fall (“h” in Fig. 1), as
391 the intercept between the Timesat fitted baseline parameter and shoulder-season slope (similar to Gu et al., 2009).
392 To extract seasonality parameters with Timesat, sites need a sufficiently pronounced seasonality, a sufficiently long
393 time period, and minimal data gaps (we note that while Timesat is capable of fitting two peaks per year, all the
394 freshwater wetland sites have a single annual peak). We excluded site-years in restored wetlands when wetlands
395 were still under construction. We were able to fit 36 freshwater wetland sites using Timesat, with 141 site-years of
396 data, using the double-logistic fitting method which followed site data well (representative examples in Fig. 2). For
397 extratropical sites in the Southern Hemisphere, we shifted all data by 182 days so that maximum solar insolation
398 seasonality would be congruent across the globe.

399 We also used Timesat to extract seasonality metrics for GPP, partitioned using the daytime-based approach
400 (Lasslop et al., 2010) (GPP_DT), air temperature (TA), and soil temperature (TS_1, TS_2, etc). For sites where
401 winter soil temperatures fall significantly below 0 °C, Timesat fits a soil temperature “start of elevated season” date
402 to periods when the soil is still frozen. In order for Timesat to define the soil temperature seasonality within the
403 thawed season, we converted all negative soil temperatures to zero (simply removing these values results in too
404 many missing values for Timesat to fit). Many sites have more than one soil temperature probe, so we extracted
405 separate seasonality metrics from each individual probe (although we used the metrics from the shallowest
406 temperature probe in our analysis). Tables B4 contain the Timesat seasonality parameters used in the seasonality
407 analysis. We did not include water table depth in the seasonality analysis because many sites either lack water table
408 depth measurements or have sparse data.

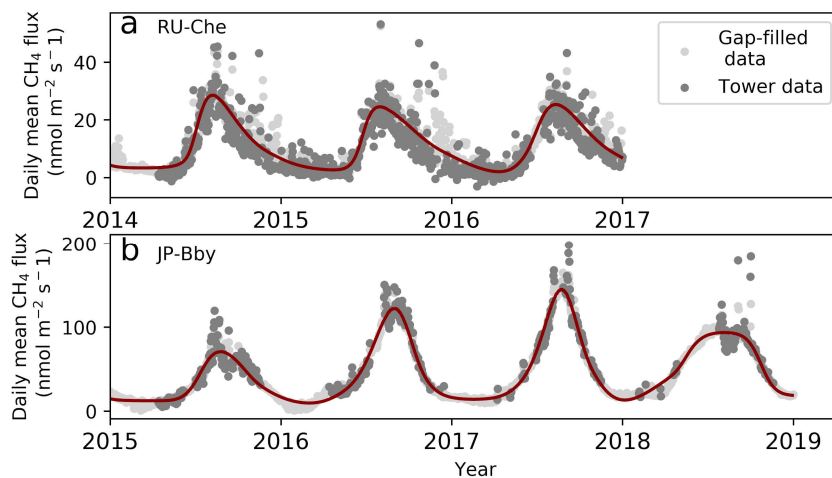


409

410 Figure 1: TIMESAT parameter description. (a) and (b) base values (Timesat reports the average of these two values), (c)
411 and (d) slopes of seasonal curves (lines drawn between 20% and 80% of the amplitude), (e) peak value, and day of year
412 (DOY) for the start (f), peak (g), and end (h) of the elevated CH₄ emissions season. Data points are the mean daily gap-
413 filled CH₄ fluxes from site JP-Bby in 2015.

414

415



416

417 Figure 2: Examples of Timesat fits for two FLUXNET-CH₄ sites, (a) RU-Che and (b) JP-BBY. Flux data showing daily
418 average flux tower data, with several high outliers excluded to improve the plot (dark gray), gap-filled values (light gray),



419 and Timesat-fitted curve (dark red line) for sites JP-BBY and RU-Che. Timesat captures peak shape as well as size (note
420 different scale on y-axes).

421

422 We regressed the CH₄ seasonality parameters from Timesat against a range of temperature, moisture, and
423 GPP (proxy for recent carbon input available as substrate) metrics using linear mixed-effect modeling with the *lmer*
424 command (with site as a random effect) from the R (R Core Team 2018, version 3.6.2) package *lmerTest*. For these
425 regressions we present the marginal R² outputs from *lmer*, which represent the variance explained only by the fixed
426 effects. Mixed-effect modeling was necessary to account for the non-independence between measurements taken at
427 the same site during different years (Zona et al., 2016; Treat et al., 2018). We also compared how seasonality
428 metrics varied across latitudinal bands by dividing sites into northern (> 60° N), temperate (between 40° N and 60°
429 N), subtropical (absolute value between 20° and 40° latitude, with site NZ-KOP being the only Southern
430 hemisphere site), and tropical (absolute value below 20°). Site-year totals for the northern, temperate, subtropical,
431 and tropical bands were $n = 57, 36, 39,$ and $9,$ respectively. We used the Kruskal-Wallis test to establish whether
432 groups (either across quarters or across latitudes) were from similar distributions, and the post hoc multiple
433 comparison “Dwass, Steel, Critchlow, and Fligner” procedure for inter-group comparisons. Kruskal-Wallis and
434 post-hoc tests were implemented in Python Version 3.7.4, using stats from *scipy* for Kruskal-Wallis and
435 *posthoc_dscf* from *scikit_posthocs*.

436 In addition to comparing CH₄ flux seasonality across latitudinal bands and to the seasonality of potential
437 drivers, we also compared quarterly flux sums by dividing data into quarterly periods: January/February/March
438 (JFM), April/May/June (AMJ), July/August/September (JAS), and October/November/December (OND). For the
439 sake of simplicity, we chose to compare quarterly periods rather than site-specific growing/non-growing season
440 periods so that all time periods would be the same length. Quarterly sums were computed from the gap-filled CH₄
441 fluxes when the longest continuous data gap within the quarter did not exceed 30 days, leading to site-year counts of
442 67, 92, 95, 72 for JFM, AMJ, JAS, and OND, respectively. We compared quarterly fluxes across latitudinal bands
443 both for the total flux, and for the quarterly percentage of the annual flux. Quarterly statistics were also conducted
444 with the Kruskal-Wallis test and the post hoc multiple comparison “Dwass, Steel, Critchlow, and Fligner” procedure
445 implemented in Python. Quarterly values are provided in Table B2, and the sum of mean quarterly flux does not
446 always equal mean annual flux because some quarters either do not have data, or have data gaps that exceed 30
447 days.

448

449 3. Results and Discussion

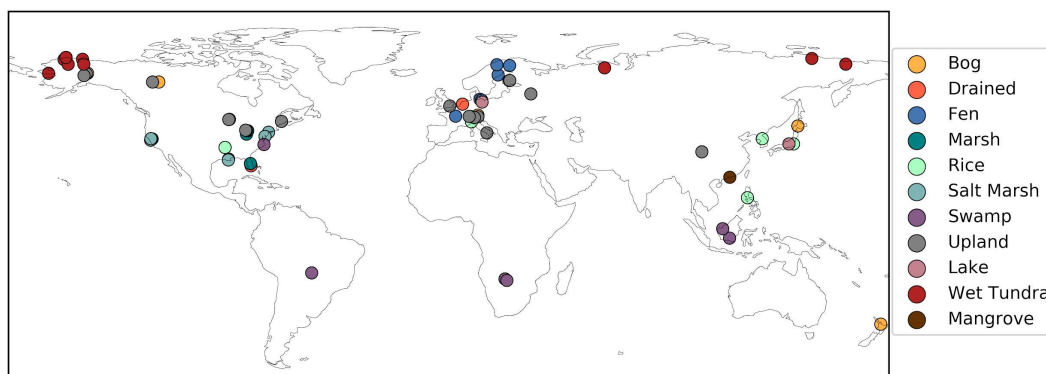
450 3.1 FLUXNET-CH₄ dataset

451 3.1.1 Dataset description

452 Version 1.0 of the FLUXNET-CH₄ dataset contains 79 unique sites, 293 total site-years of data, and 201
453 site-years with sufficient data to estimate annual CH₄ emissions. A previous synthesis paper, published prior to the
454 public data release of FLUXNET-CH₄ Version 1.0, had 60 unique sites and 139 site-years with annual CH₄ emissions
455 estimates (Knox et al., 2019). Freshwater wetlands make up the majority of sites ($n = 42$), and the dataset also includes
456 five salt marshes and one mangrove wetland. Notable additions to FLUXNET-CH₄ Version 1.0 from the previous
457 unpublished dataset used in Knox et al., (2019) include six tropical sites (between 20°S and 20°N), including one site
458 in South America, two sites in southern Africa, and three sites in Southeast Asia. The 15 upland sites include six
459 needleleaf forests, three crop sites (excluding rice), two alpine meadows, one grassland, one mixed forest, one tundra,
460 and one urban site. The drained sites represent former wetlands that have been artificially drained for use as grasslands



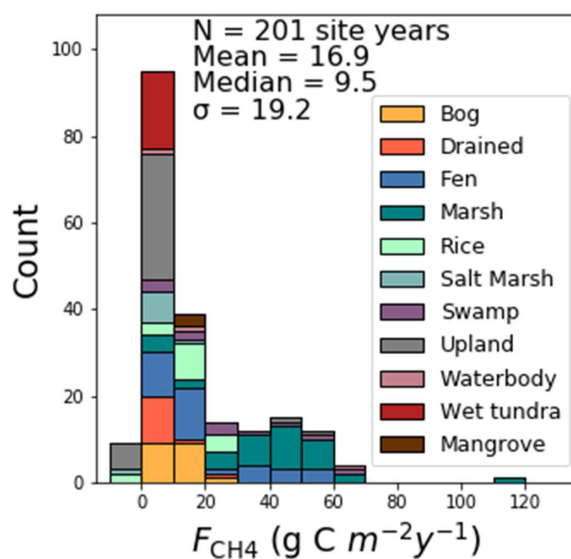
461 ($n = 3$) or croplands ($n = 3$). FLUXNET-CH₄ Version 1.0 sites span the globe, though are concentrated in North
462 America and Europe (Fig. 3). Table B2 includes characteristics of all sites in the dataset.



463

464 **Figure 3. Global map of FLUXNET-CH₄ Version 1.0 site locations colored by site type. The bog and upland site in the**
465 **Northwest Territories of Canada have been slightly offset from each other so that both are visible.**

466



467

468 **Figure 4. Histogram of annual CH₄ fluxes (g C m⁻² yr⁻¹) grouped by site type.**

469 Sites represent a range of ecosystem types, latitudes, median fluxes, and seasonality patterns (Table 1).
470 Across all FLUXNET-CH₄ Version 1.0 sites, mean average annual flux is positively skewed with a median flux of
471 9.5 g C m⁻² yr⁻¹, a mean flux of 16.9 g C m⁻² yr⁻¹, and numerous annual fluxes exceeding 60 g C m⁻² yr⁻¹. The
472 addition of 19 sites from the 60 sites aggregated in Knox et al., (2019) therefore do not significantly change the
473 distribution of annual CH₄ fluxes. Marshes and swamps have the highest median flux, and upland, salt marsh, and



474 tundra sites have the lowest (Fig. 4). Lake emissions are highly variable due to one high-flux lake site (JP-SWL).
 475 Flux data at many sites show strong seasonality in CH₄ emissions, but data coverage is also lower outside the
 476 growing season. Data coverage is lowest during the JFM quarter (on average 20% of half-hourly time periods
 477 contain flux data) reflecting the predominance of Northern hemisphere sites and the practical difficulties in
 478 maintaining EC tower sites during colder winter months (Table 1). Bogs, fens, and marshes have pronounced
 479 seasonality, with fluxes being highest in the AMJ and JAS quarters. In contrast, CH₄ fluxes from uplands, drained
 480 sites, and salt marshes are more uniform and low year-round.

481 **Table 1: Summary table of sites grouped by ecosystem class reporting annual mean flux (Ann_Flux) and standard**
 482 **deviation from inter-annual variability (Ann_Flux_SD), site-years of data, % data cover per quarter, and median (med.)**
 483 **flux across site class.**

	# of Sites	# of Site-Years	Ann_Flux g C m ⁻² year ⁻¹	Ann_Flux_SD g C m ⁻² year ⁻¹	JFM coverage (%)	AMJ coverage (%)	JAS coverage (%)	OND coverage (%)	JFM flux (med.)	AMJ flux (med.)	JAS flux (med.)	OND flux (med.)
Salt marsh	5	10	2.9	4.7	7	42	50	37	1.5	1.7	2.1	1.6
Wet tundra	11	39	3.8	1.8	8	28	40	18	0.4	2.6	8.1	3.2
Upland	15	47	4.0	10.5	23	35	39	28	1.2	0.5	1.4	0.8
Drained	7	20	6.3	7.1	22	39	39	29	4.6	3.6	5.1	3.6
Bog	7	32	10.5	6.4	8	27	37	18	7.2	11.0	24.8	9.5
Mangrove	1	3	11.1	0.5	46	28	30	41	3.2	7.2	22.5	14.1
Rice	7	20	14.4	8.8	16	37	45	27	3.2	11.9	43.1	4.2
Fen	8	40	20.5	16.0	29	43	40	30	2.8	14.2	26.0	6.4
Swamp	6	15	26.4	19.9	24	34	29	19	14.7	24.9	31.0	24.4
Lake	2	4	28.2	33.4	15	13	27	36	0.2	47.6	90.2	40.3
Marsh	10	42	40.8	20.7	22	43	53	30	13.5	55.0	85.8	36.1

484



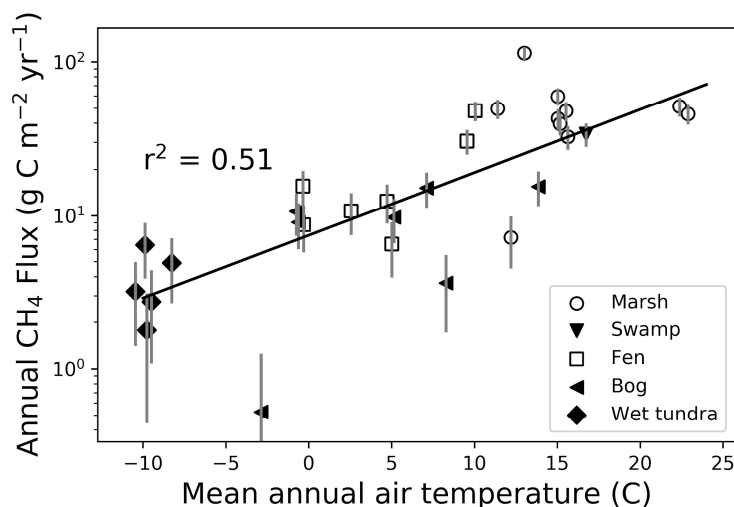
485

486 3.1.2 Freshwater wetland CH₄ characteristics

487 The FLUXNET-CH₄ Version 1.0 dataset contains 42 freshwater wetlands that span 37°S to 69°N, including
488 bogs, fens, wet tundra, marshes, and swamps, and a range of annual CH₄ emission rates (Fig. 4). The majority of
489 wetlands in our dataset emit 0-20 g C m⁻² yr⁻¹, with 10 emitting 20-60 g C m⁻² yr⁻¹, and one more than 60 g C m⁻² yr⁻¹.
490 Differences in annual flux among wetland types is partially driven by temperature (which is often linked to site type),
491 with mean annual air temperature explaining 51% of the variance between sites (Fig. 5, exponential relationship). The
492 global relationship between annual methane emissions and temperature can be described using a Q₁₀ relationship
493 where $Q_{10} = R_2/R_1^{((T_2-T_1)/10)}$, with R₂ and R₁ being the methane emission rates at temperatures T₂ and T₁, respectively
494 (temperature in degrees C). The Q₁₀ based on Fig. 5 data is 2.57. Annual CH₄ flux is not correlated with mean annual
495 water table depth in FLUXNET-CH₄ Version 1.0, unlike in Knox set al (2019; which used a subset of the FLUXNET-
496 CH₄ Version 1.0 sites) where CH₄ flux was correlated with water table depth only for sites with water table below
497 ground for 90% of measured days (r₂ = 0.31, p<0.05, n = 27 site years, Knox et al., 2019). Freshwater wetland
498 seasonality is further described in Sect. 3.3.

499

500



501

502 Figure 5: Relationship between mean annual wetland flux (g C m⁻² yr⁻¹) and mean annual air temperature (°C,
503 logarithmic scale) for each freshwater wetland site, with wetland type indicated by symbol. The difference in emissions
504 across site types is partially driven by difference in mean annual temperature. Markers represent individual site means,
505 with vertical error bars representing the standard deviation of interannual variability.

506

507

508

509 3.1.3 Non-wetland CH₄ characteristics

510 Upland agricultural sites are characterized by a lack of seasonal pattern in CH₄ emissions, relatively low flux,
511 and some negative daily flux (i.e., CH₄ uptake) averages. All of the upland non-agricultural sites in FLUXNET-CH₄



512 Version 1.0 are net (albeit weak) CH₄ sources except for the needleleaf forest site US-Ho1, which has mean annual
513 flux of -0.1 ± 0.1 g C m⁻² yr⁻¹ (see Table B2 for site acronyms and metadata). The average agricultural site emissions
514 are 1.3 ± 0.8 g C m⁻² yr⁻¹ and non-agricultural site emissions are 1.6 ± 1.2 g C m⁻² yr⁻¹ across sites.

515 Rice sites (n = 7) have average annual emissions across all sites of 16.7 ± 7.7 g C m⁻² yr⁻¹ and are
516 characterized by strong seasonal patterns, with either one or more CH₄ emission peaks per year depending on the
517 number of rice seasons and field water management. One peak is typically observed during the reproductive period
518 for the continuously flooded sites with one rice season (i.e., US-HRC, JP-MSE) (Iwata et al., 2018; Runkle et al.,
519 2019; Hwang et al., 2020). For sites with only one rice season but with single or multiple drainage and re-flooding
520 periods, a secondary peak may appear before the reproductive peak (i.e., KR-CRK, IT-Cas, and US-HRA; Mejjide et
521 al., 2011; Runkle et al., 2019; Hwang et al., 2020). Two reproductive peaks appear for sites with two rice seasons (i.e.
522 PH-RiF), and each reproductive peak may be accompanied by a secondary peak due to drainage events (Alberto et al.,
523 2015). Even sites with one, continuously flooded rice season may experience a second peak if the field is flooded
524 during the fallow season to provide habitat for migrating birds (e.g. US-Twt; Knox et al., 2016).

525 The dataset has one year of urban data from site UK-LBT in London, England. UK-LBT observes CH₄ fluxes
526 from a 190 m tall communications tower in the center of London, and had a mean annual flux of 46.5 ± 5.6 g C m⁻²
527 yr⁻¹. This flux is more than twice as high as the mean annual flux across all FLUXNET-CH₄ Version 1.0 sites, 16.9
528 g C m⁻² yr⁻¹. The London site has higher CH₄ emissions in the winter compared to summer, which is attributed to a
529 seasonal increase in natural gas usage (Helfter et al., 2016).

530 3.1.4 Non-freshwater wetland CH₄ characteristics

531 Three of the five saltwater wetlands in FLUXNET-CH₄ Version 1.0 (US-Edn, US-MRM, and US-Srr) have
532 a very low mean annual flux (see Table B7 for individual site-year flux sums and associated uncertainty) and minimal
533 seasonality. Two other FLUXNET-CH₄ Version 1.0 saltwater sites (US-La1, US-StJ) have significantly higher
534 fluxes, with annual sums of 12.6 ± 0.6 and 9.6 ± 1.0 g C m⁻² yr⁻¹ respectively, while the mangrove site HK-MPM has
535 annual mean fluxes of 11.1 ± 0.5 g C m⁻² yr⁻¹. This range of CH₄ fluxes across different saltwater ecosystems could
536 be valuable for exploring the effect of salinity and different biogeochemical pathways of CH₄ production and transport
537 of CH₄ (Bartlett et al., 1987; Poffenbarger et al., 2011). Saltwater wetlands along the coast have unique CH₄ dynamics
538 attributable to the presence of abundant electron acceptors, most importantly sulphates, which inhibit methanogenesis
539 (Pattnaik et al., 2000; Mishra et al., 2003; Weston et al., 2006), but at low concentrations can have no effect (Chambers
540 et al., 2011) or even increase methanogenesis (Weston et al., 2011). In fact, estuarine wetlands with moderate salinity
541 can still be significant sources of CH₄ (Liu et al., 2020). Even under sulfate-rich conditions, high CH₄ production can
542 be found via methylotrophic methanogenesis (Seyfferth et al., 2020) or because the processes of sulfate reduction and
543 methanogenesis are spatially separated (Koebsch et al., 2019).
544

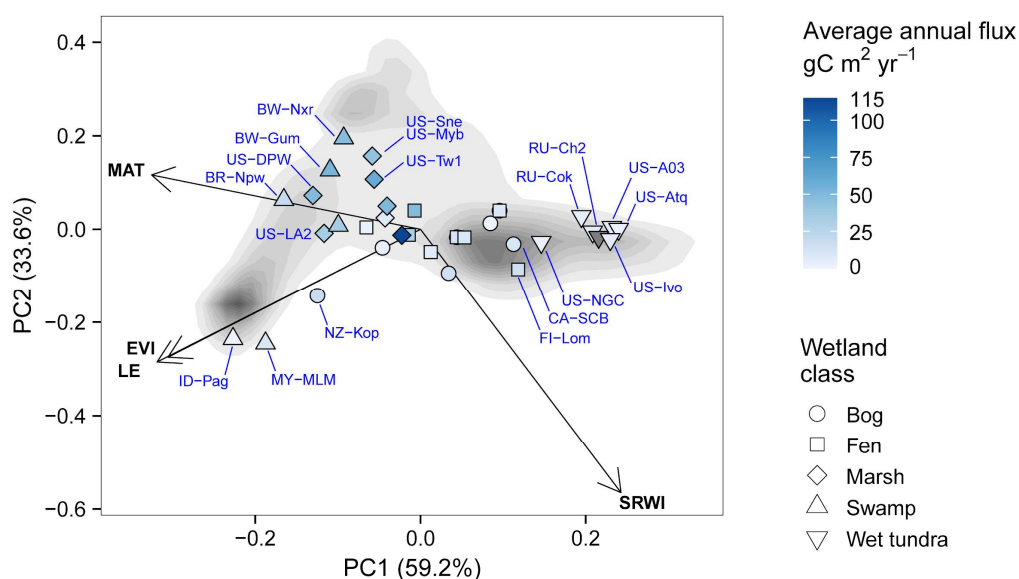
545 3.2 Wetland Representativeness

546 We evaluated the representativeness of freshwater wetland sites in the FLUXNET-CH₄ Version 1.0 dataset
547 against wetlands globally. Specifically, we asked how representative the bioclimatic conditions of our sites are,
548 relative to bioclimatic conditions in all wetlands globally. Parameters defining bioclimatic conditions are selected
549 from those known to affect CH₄ production, consumption, and transport processes (e.g., energy, moisture, substrate
550 availability, and vegetation). When evaluating bioclimatic variables individually, the distribution across the network
551 was significantly different from the global distribution ($\alpha > 0.05$; two-tailed Kolmogorov-Smirnov tests; see Table
552 B3).

553 When considering the four bioclimatic variables, MAT, LE, EVI and SRWI in a PCA, we found that our
554 tower network generally samples the bioclimatic conditions of global wetland cover, but some noticeable gaps remain



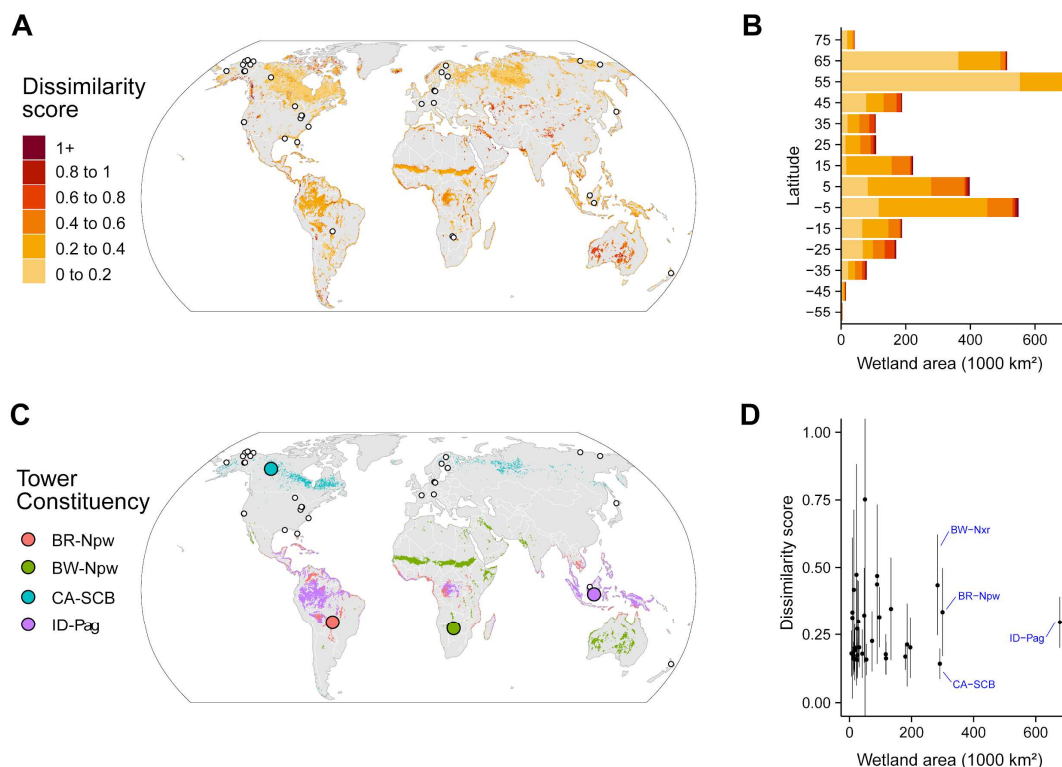
555 (Fig. 6). Three clusters of the world's wetland-dense regions are identified, but are not equally sampled by the network.
556 A cluster of low temperature wetlands is sampled by a large number of high-latitude sites. The other two wetland
557 clusters are not as well sampled: a high temperature and LE cluster is represented only by two towers (ID-Pag and
558 MY-MLM), while drier and temperate and subtropical wetlands including large swathes of the Sahel only have a site
559 in Botswana as their closest tower.
560



561
562 **Figure 6: Principal Component Analysis displaying the distribution of freshwater wetland sites (blue points) along the two**
563 **main principal components together accounting for 91.9% of variance. Tower sites are represented as the larger points of**
564 **shapes representing wetland type and color shade representing the annual CH₄ flux (greyed points represent sites for which**
565 **<6 months of flux data was available to estimate annual budget). The size of wetland points are made larger for visual**
566 **clarity and site codes are labelled in blue. The background shades of grey represent the density of land pixels (excluding**
567 **Greenland and Antarctica) that have a >5% wetland fraction according to the WAD2M map (Zhang et al., In Review).**
568 **Loading variables are represented by the arrows: mean annual temperature (MAT), simple ratio water index (SRWI),**
569 **latent heat flux (LE) and enhanced vegetation index (EVI).**

570
571 Evaluating the bioclimatic dissimilarity of global wetlands to the FLUXNET-CH₄ Version 1.0 network
572 shows the least captured regions are in the tropics and mountainous regions (Fig. 7A). Sparse coverage in the tropics
573 also means that the few existing towers occupy a critical place in the network, particularly as tropical wetlands are the
574 largest CH₄ emitters (Bloom et al., 2017; Poulter et al., 2017). Highly dissimilar wetlands are limited in extent and
575 distributed across all latitudes, but the average dissimilarity is higher in temperate and tropical latitudes (Fig. 7B). To
576 evaluate the importance of individual towers in the network, we estimated the geographical area to which it is most
577 analogous in bioclimate-space (Fig. 7C). We found that some towers have disproportionately large constituencies (i.e.,
578 wetland areas that share the same closest bioclimatic analog tower). Towers in Indonesia (ID-Pag), Brazilian Pantanal
579 (BR-Npw), and Botswana floodplains (BW-Nxr) represent the closest climate analog for much of the tropics (678,
580 300 & 284 thousand km² respectively) while CA-SCB represents a vast swath (291 thousand km²) of boreal/arctic
581 regions (Fig. 7D).

582



583

584 **Figure 7: (A) Distance in bioclimatic space between global land surface and the FLUXNET-CH₄ Version 1.0 tower network.**
 585 **The Euclidean distance was computed on the five bioclimatic variables and was then standardized by the average distance**
 586 **within-network. Most of the land surface has a dissimilarity score lower than 1, meaning these areas are closer than the**
 587 **average tower distance (lower dissimilarity score means a similar bioclimate to that represented by towers in the network).**
 588 **However, this pattern reflects more the sparsity of the tower network than a similarity of the land surface to the network.**
 589 **Areas with <5% coverage by wetlands were excluded to focus on wetland-dense regions. (B) Latitudinal distribution of**
 590 **dissimilarity score, (C) Map of the four largest tower constituencies, (D) Scatterplot of wetland area in each tower**
 591 **constituency plotted against the average dissimilarity score (point) and +/- standard deviation (error bar).**

592 Our assessment of wetland CH₄ tower coverage determines the ability of our dataset to represent global
 593 wetland distributions and highlights some clear representation gaps in the network - tropical, humid, and mountainous
 594 regions. Other geographic regions such as India, China and Australia, where towers exist but are not included in the
 595 current network should be prioritized when expanding the network, even though they are not among the most distant
 596 areas to the current network. Similar representativeness assessments have been developed for CO₂ tower networks to
 597 identify gaps and priorities for expansion (Jung et al., 2009; Kumar et al., 2016). To improve the geographic coverage
 598 of the network for representing global-scale fluxes, locations for new tower sites can be targeted to cover bio-
 599 climatically distant areas from the current network (Villarreal et al., 2019). Candidate regions for expansion that are
 600 both high CH₄ emitting and under-sampled are: African Sahel, Amazon basin, Congo basin, South-East Asia.
 601 Moreover, sites should be established in other ecosystem types, especially lakes and reservoirs (Bastviken et al., 2011;
 602 Deemer et al., 2016; Matthews et al., 2020) in most climatic zones in order to capture CH₄ fluxes from these
 603 ecosystems. Understanding the representativeness of the network is essential when inferring general patterns of flux
 604 magnitude, seasonality, and drivers from the tower data (Villarreal et al., 2018). We produced a first-order
 605 representativeness of average bioclimatic conditions, but temporal representativeness (across seasons, climate
 606 anomalies and extreme events) is particularly needed given the episodic nature of CH₄ fluxes (Chu et al., 2017;
 607 Mahecha et al., 2017; Göckede et al., 2019).



608 Assessing representation of wetland CH₄ sites is complicated by the fact that wetlands occupy only a fraction
609 of most landscapes (except wetland dense regions such as Siberian Lowlands, Hudson Bay Lowlands, Congo basin,
610 etc.) and that not all relevant factors affecting CH₄ production and consumption could be considered in our analysis.
611 For instance, our assessment of representation did not consider wetland types as such maps are limited (Gallant, 2015).
612 The attribution of representativeness is further complicated by the fact that many EC tower locations are subject to
613 small-scale variability within the field of view, or footprint, of the sensor. Consequently, the individual time steps
614 within EC flux time series may represent a mixture of different wetland types, or different fractions of wetland
615 contribution to the total flux, varying with wind direction, atmospheric stability, or season. This further complicates
616 upscaling efforts. Additionally, this representativeness analysis did not apply weights to the drivers to reflect their
617 varying influence on CH₄ flux. Such weights can be included in future versions as they are generated by a cross-
618 validated machine learning approach (Jung et al., 2020). Future efforts will include the dissimilarity index from this
619 analysis as a metric of extrapolation in a CH₄ flux upscaling effort.

620

621 3.3 Freshwater wetland flux seasonality

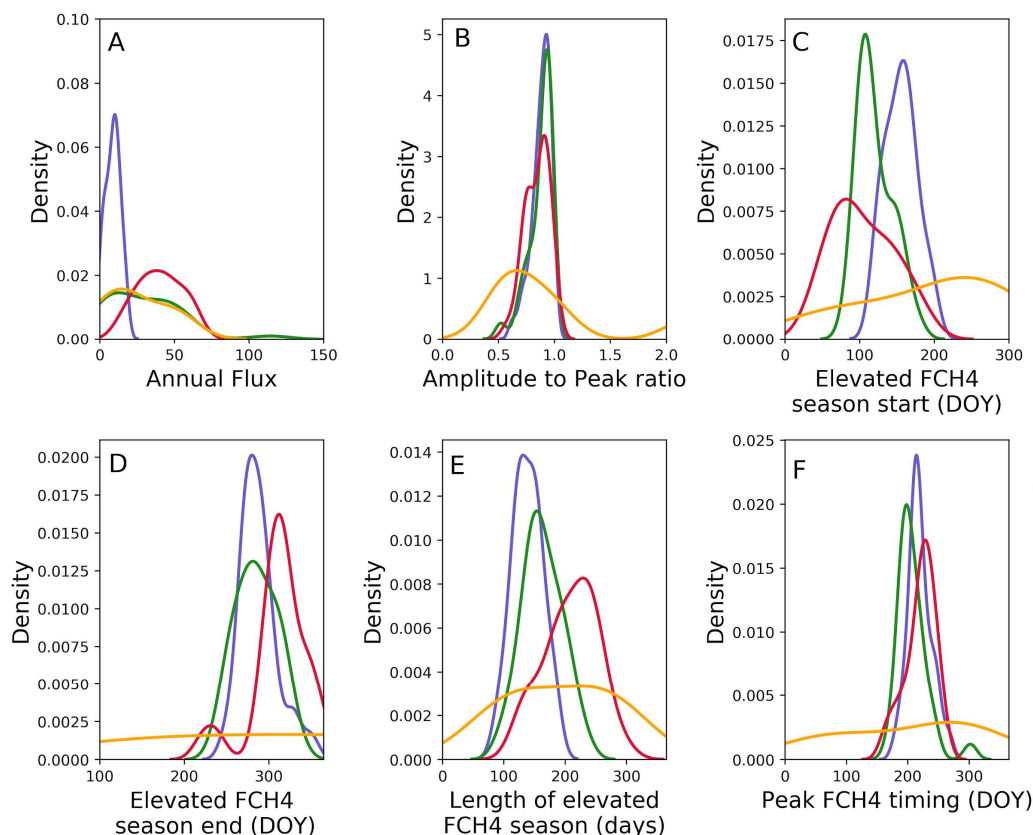
622 We used seasonality parameters extracted by Timesat to describe typical seasonal patterns in freshwater wetland
623 CH₄ fluxes, and to compare them with seasonality in soil temperature and GPP. Of the 42 freshwater wetland sites
624 in FLUXNET-CH₄ Version 1.0, 36 had sufficient data series to extract seasonality parameters.

625 3.3.1 Seasonal flux comparisons by latitudinal bands

626 CH₄ flux and seasonality varied substantially across latitudinal bands (northern, temperate, subtropical, and
627 tropical) (Fig. 8). Annual fluxes for temperate, and subtropical sites were significantly higher than for northern sites
628 (8.7 ± 5.0 , 29.7 ± 25.2 , 40.1 ± 14.6 , and 24.5 ± 20.7 g C m⁻² yr⁻¹ for northern, temperate, subtropical, and tropical
629 respectively, $p < 0.0001$ using Kruskal Wallis and post hoc comparisons; Fig. 8a), and tropical sites were similar to all
630 other latitudinal bands likely because of their small sample size. The ratio of seasonal amplitude to peak flux provides
631 a measure of the relative seasonal increase in emissions compared with baseline, where a ratio of zero indicates no
632 seasonal change in amplitude, a ratio of one indicates the off-season flux is zero, and values over one means the off-
633 season baseline CH₄ fluxes were negative (i.e., uptake). Average amplitude to peak flux ratios were similar across all
634 latitudinal bands (0.9 ± 0.1 , 0.9 ± 0.1 , 0.9 ± 0.1 , 1.0 ± 0.7 , for northern, temperate, subtropical, and tropical,
635 respectively; Fig. 8b). The spring increase in CH₄ emissions begins later in northern sites compared with temperate
636 and subtropical sites (end of May versus April, respectively, $p = 0.001$; Fig. 8c), while tropical sites vary widely in
637 elevated emission season start date. Northern sites also have shorter CH₄ flux season lengths (138 ± 24 days) compared
638 to temperate sites (162 ± 32 days), and both are shorter than subtropical sites (209 ± 43 days; $p < 0.0001$; Fig. 8d). On
639 average, CH₄ flux peaks earlier for temperate sites compared to northern ($p = 0.008$) and subtropical sites ($p = 0.02$;
640 mid to late July compared with early August; Fig. 8e), while tropical sites again vary widely. Given their unique
641 seasonality, and low number of site-years ($n = 9$), tropical systems are discussed separately in Sect. 3.3.3, and not
642 included in the comparisons in the remainder of this section. While our results on CH₄ seasonality corroborate
643 expected trends for these latitudinal bands, they provide some of the first estimates of CH₄ seasonality parameters and
644 ranges across a global distribution of sites.

645

646



647
 648
 649
 650
 651
 652
 653
 654
 655
 656
 657

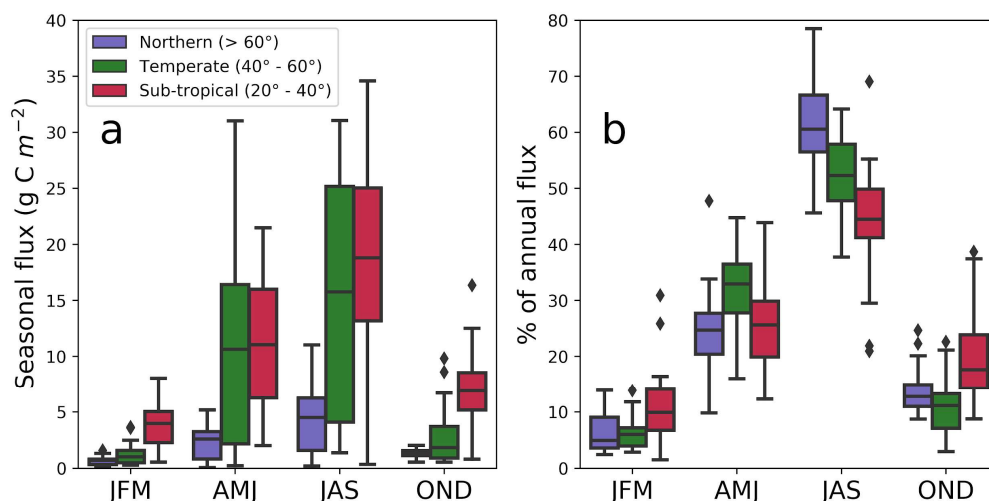
Figure 8: (a) Annual flux ($\text{g C m}^{-2} \text{yr}^{-1}$), (b) Ratio of seasonal amplitude to seasonal peak, where values of 0 indicate uniform annual flux, values of one indicate zero off-season fluxes, and values exceeding one indicate negative off-season fluxes, (c) CH_4 flux elevated emissions season start, (d) Length of CH_4 flux season, and (e) peak timing metrics for high, mid, and lower latitude wetlands (purple, green, red, respectively) plotted using the kernel density function. Latitudinal bands are as follows: northern ($> 60^\circ$), temperate (between 40° and 60°), subtropical (between 20° and 40°), and tropical ($< 20^\circ$), though the site-year totals vary between these groups ($n = 57$, $n = 36$, $n = 39$, and $n = 9$ respectively). All total flux values and elevated season start values are positive, and the apparent continuation of the data distribution into negative values is an artifact of the kernel density function. Southern Hemisphere sites below 20°S were shifted by 182 days.

658
 659
 660
 661
 662
 663
 664
 665
 666
 667
 668

We found that latitudinal groups show strong differences in absolute flux across quarters, and narrower differences in percentage of annual flux (Fig. 9a versus 9b). Thus, the AMJ quarter has a similar contribution to the annual flux across latitudes, regardless of the absolute annual flux. Methane fluxes (Fig. 9a) are highest during JAS for northern, temperate, and subtropical sites and highest in AMJ and JAS for temperate sites ($p < 0.01$). Though CH_4 fluxes in northern sites are most commonly measured during warm summer months (Sachs et al., 2010; Parmentier et al., 2011), fluxes in JFM and OND (50% of the yearly duration) on average make up $18.1 \pm 3.6\%$, $15.3 \pm 0.1\%$, and $31.2 \pm 0.1\%$ (northern, temperate, subtropical, respectively) of annual emissions. This pattern indicates that a substantial fraction of annual CH_4 fluxes occurs during cooler months. The fraction would be even higher if we added April, May, and September emissions to the northern ($> 60^\circ \text{N}$) sites, as done in (Zona et al., 2016), where $> 50\%$ of emissions were found to come from non-growing season months. The contribution of non-growing season CH_4 emissions to annual fluxes has previously been described for arctic and boreal regions (Zona et al., 2016; Treat et al.,



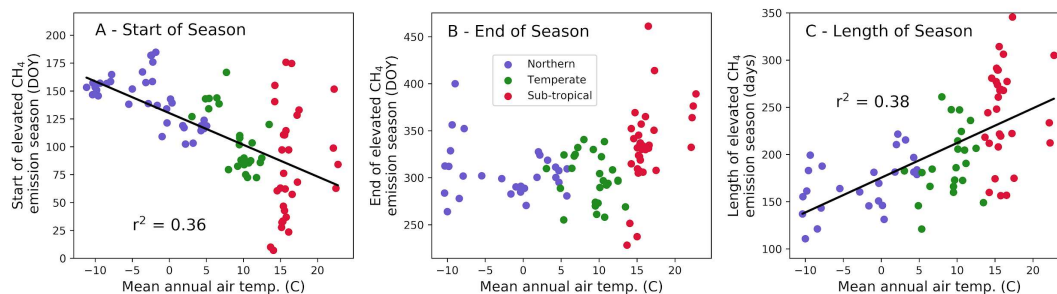
669 2018) and our analysis suggests comparable contributions in temperate and subtropical systems for the same quarterly
670 periods.
671
672
673



674
675
676 **Figure 9: (A) Quarterly contribution to total annual flux in g C m^{-2} , and (B) percentage of annual flux. Sites were divided**
677 **into northern ($> 60^\circ \text{N}$), temperate ($40^\circ \text{N} - 60^\circ \text{N}$), and subtropical ($20^\circ \text{N} - 40^\circ \text{N}$). Quarters with continuous data gaps**
678 **exceeding 30 days were excluded. We used the following quarterly periods: January/February/March (JFM),**
679 **April/May/June (AMJ), July/August/September (JAS), and October/November/December (OND). Tropical sites are**
680 **discussed separately in Sect. 3.3.3 because of their unique seasonality and low number of sites.**
681

682 3.3.2 Predictors of CH_4 flux phenology

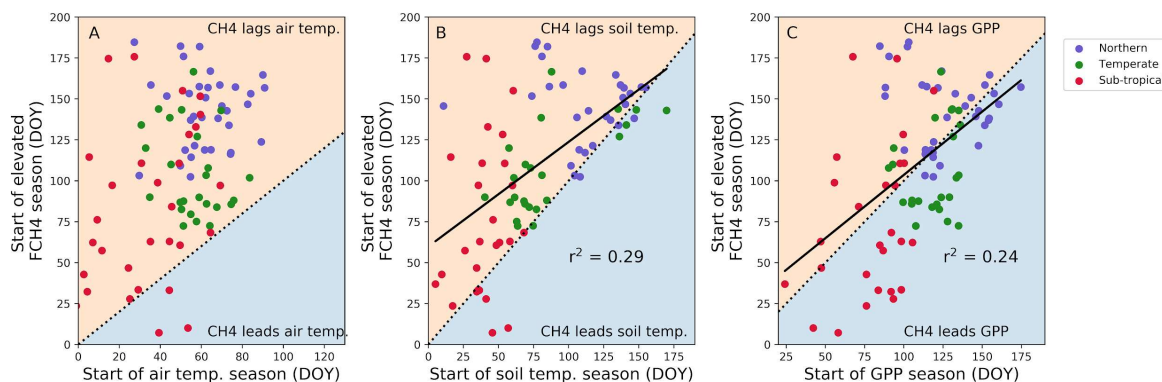
683 The start of the elevated CH_4 flux season, and how long the elevated flux season lasts, correlates strongly
684 with mean annual air temperature (Fig. 10; $p < 0.0001$ for each). Methane flux begins to increase roughly two
685 months earlier in the warmest systems (mean annual temperature $> 20^\circ \text{C}$) compared to the coldest (mean annual
686 temperature near -10°C), though several of the warmer sites have high variability. Our data suggest that the CH_4
687 season starts 2.8 ± 0.5 days earlier for every degree Celsius increase in mean annual temperature (Fig. 10a). In
688 contrast, the end of the CH_4 emission season is not correlated with mean annual temperature but a positive trend
689 exists despite high variability in warmest and coldest sites (Fig. 10b). The high variability seen in the end of CH_4
690 season at northern sites is important to note and would likely be better resolved by incorporating other seasonality or
691 phenological characteristics, such as moisture, active layer depth, and plant community composition. Plants with
692 aerenchymatous tissue, for example, influence the timing of plant-mediated CH_4 flux and are a key source of
693 uncertainty while predicting CH_4 seasonality for northern wetlands (Xu et al., 2016). Despite the relative lack of
694 trend with season end date, the season length is still positively correlated with mean annual temperature, with the
695 warmest sites having roughly three more months of seasonally elevated CH_4 emissions than the coldest sites (Fig.
696 10c). Methane season length increases 3.6 ± 0.6 days for every $^\circ \text{C}$ increase in mean annual temperature (note that
697 these relationships are correlations, and we cannot disentangle causality with this analysis). Temperature is highly
698 correlated with other parameters (i.e., radiation, days of snow cover, etc.), so CH_4 flux is also likely to correlate with
699 other environmental parameters.



700

701 **Figure 10.** The (a) start of the elevated CH₄ emission season ($y = -2.8x + 130$, with ‘x’ in °C and ‘y’ in day of year), (b) the
 702 end of the emission season, and (c) the length of the emission season with mean annual site air temperature ($y = 3.6x +$
 703 176.6 , with ‘x’ in °C and ‘y’ in days). Each point represents a site-year of data and all reported r^2 are significant to $p <$
 704 0.0001). Tropical sites are discussed separately in Sect. 3.3.3.

705 Although the spring onset of increasing CH₄ emissions correlates with mean annual air temperature, on
 706 average it lags the spring increase in the shallowest soil temperatures by 31 ± 40 days (Fig. 11), with very few
 707 instances of CH₄ emissions beginning before seasonal soil temperatures increase (and by 20 ± 50 days for the
 708 deepest temperature probes). In contrast, for roughly half of the sites, CH₄ emission increases prior to seasonal GPP
 709 (a proxy for fresh substrate availability) increases. This suggests that the initiation of increased CH₄ fluxes at the
 710 beginning of the season is not limited by availability of substrate derived from recent photosynthate, especially in
 711 cooler climates. Additionally, the onset of CH₄ fluxes tends to occur closer to the onset of soil temperature increase
 712 for cooler temperature sites (sites with later start dates tend to be cooler; Fig. 11a). This result is likely attributable to
 713 the direct influence of increased temperature on microbial processes as well as the indirect influences of snow melt,
 714 both via release of CH₄ from the snowpack as well as a higher water table leading to more CH₄ production
 715 (Hargreaves et al., 2001; Tagesson et al., 2012; Mastepanov et al., 2013; Helbig et al., 2017). These observed trends
 716 hold for the entire temperature or GPP range of freshwater wetland sites, but are not necessarily applicable within
 717 individual latitudinal bands.



718

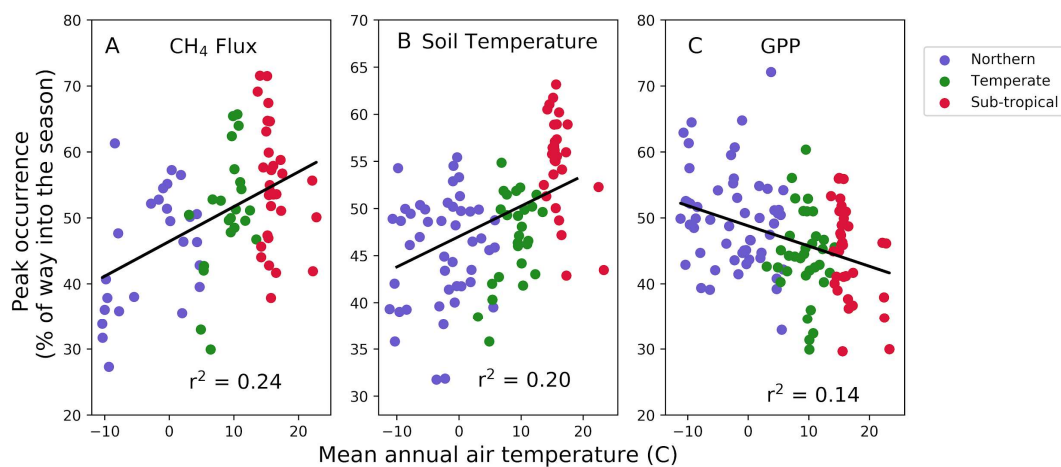
719

720 **Figure 11.** Relationship between the onset of the onset of the CH₄ emission season to (a) the beginning of the air warming,
 721 (b) soil warming at the shallowest probe depth per site, and (c) gross primary productivity (GPP) increase for the subset
 722 of sites with soil temperature data. Each point represents a site-year of data. Dashed lines represent a 1:1 relationship,



723 solid lines are regression fits. On average, the CH₄ emission season lags the soil temperature increase by 31 ± 40 days,
724 and is more synchronous with GPP.

725 In contrast with the CH₄ season-start timing, the timing of the CH₄ peak does not correlate with either the
726 timing of the soil temperature peak or the GPP peak (Fig. A1). For 63% of the sites, the average timing of peak CH₄
727 emissions lags the soil temperature peak, and at 83% of the sites average peak CH₄ lags peak GPP (Fig. A1).
728 Although there is no simple relationship between absolute CH₄ peak timing and the environmental drivers we
729 investigated, there is a correlation ($p = 0.0005$) between the relative timing of peak CH₄ compared to season onset
730 (calculated as described in Section 2.3) and mean annual air temperature (Fig. 12a). For cooler sites, the peak of
731 seasonal CH₄ emissions occurs closer to the onset of the CH₄ emission season than the end of the season, resulting in
732 an asymmetrical seasonal flux shape that is illustrated in Fig. 2a. Soil temperature also peaks earlier in the season
733 for cooler wetlands, though the relationship is not as pronounced ($p = 0.009$, Fig. 12b). In contrast, GPP peaks later
734 in the season for cooler wetlands ($p = 0.009$, Fig. 12c). Previous work on Arctic sites (sites US-Ivo, US-Beo, US-
735 Atq, US-Bes, and RU-CH2) has highlighted the asymmetrical annual CH₄ peak, with higher fall emissions being
736 attributed to the “zero curtain” period when soil below the surface remains thawed for an extended period of time
737 due to snow insulation (Zona et al., 2016; Kittler et al., 2017). Furthermore, soils can stay above the “zero curtain”
738 range for an extended time into the fall and winter (Helbig et al., 2017), which may also be caused by snow
739 insulation. The rapid onset of emissions in the spring following snowmelt could be attributed to the release of
740 accumulated CH₄ (Friborg et al., 1997), and other high latitude sites have seen similarly sharp increases in CH₄
741 emissions at snowmelt (Dise, 1992; Windsor, 1992). However, not all studies in high latitudes have observed
742 asymmetrical CH₄ emission peaks, pointing to the inherent complexity of these ecosystems (Rinne et al., 2007;
743 Tagesson et al., 2012).



744

745 Figure 12. Site-year peak CH₄ emission (a) and peak soil temperature (b) occur earlier in the season for sites with lower
746 mean annual temperatures. (c) GPP tends to peak earlier in the season for warmer sites, though the trend is weak. All r^2
747 values are significant at $p < 0.001$. Each point represents a site-year of data.

748 3.3.3 Uniqueness of tropical wetlands

749 Tropical wetlands typically do not experience the large swings in temperature and GPP that contribute to
750 CH₄ flux seasonality in temperate and northern sites. Indeed, the relatively constant high temperatures and high
751 GPP in tropical ecosystems may lead to the lower ratio between seasonal amplitude and peak CH₄ flux compared
752 with temperate and northern sites (Fig. 8b). Tropical flux sites have historically been under-studied, leading to a



753 lack of synthesized information about these ecosystems. FLUXNET-CH4 Version 1.0 has five tropical wetland sites
754 (latitude between 20° S and 20° N), and one tropical rice site, representing 13 site-years of data. The tropical sites
755 are especially insightful as they provide the first estimates of CH₄ fluxes from large seasonal floodplain systems
756 found in the tropics.

757
758 We find a broad range of annual CH₄ fluxes across tropical sites in FLUXNET-CH4 Version 1.0. Annual
759 CH₄ flux emissions from two Southeast Asian flooded peat forests were relatively low, 0.01 ± 0.1 and 9.5 ± 0.6 g C
760 m⁻² yr⁻¹ for ID-PAG and MY-MLM, respectively, which is consistent with annual CH₄ fluxes measured at another
761 peat forest in Indonesia (Deshmukh et al., 2020). In contrast, mean annual flux for a seasonally flooded swamp in
762 the Brazilian Pantanal region (BR-NPW) was over twice as high as MY-MLM, at 19.2 ± 2.5 g C m⁻² yr⁻¹. Similarly
763 high annual fluxes were observed at the two Botswana swamp sites in the Okavango Delta (51.7 ± 10.6 and $47.3 \pm$
764 3.7 g C m⁻² yr⁻¹ for BW-GUM and BW-NXR, respectively), one of which is seasonally inundated and surrounded by
765 grassland (BW-NXR) and the other is a permanently flooded lagoon covered in a floating papyrus mat (BW-GUM).
766 The relatively low fluxes found at the two Southeast Asian peat forest sites indicate that these ecosystems may be
767 smaller CH₄ sources than expected, given their location in the humid tropics. Even the higher-emitting tropical sites
768 in Brazil and Botswana are still well within the range of annual flux typical in cooler latitudes (Fig. 1).

769 In addition to having highly variable flux magnitudes, the tropical sites differ from each other in their
770 seasonality. Methane flux hits a minimum around July for two sites (BW-GUM, latitude 18.965 °S and MY-MLM,
771 latitude 1.46 °N), while CH₄ flux increases through July and the subsequent months for the other Botswana site, BW-
772 NXR (latitude 19.548 °S). Site ID-Pag (latitude 2.32 °S) has minimal seasonality, whereas the flooded forest site in
773 Brazil (BR-NPW, latitude 16.49 °S) has near-zero fluxes from approximately July to January, and consistently high
774 fluxes for the remainder of the year. The rice site PH-RiF (latitude 14.14 °N) has two annual CH₄ flux peaks, which
775 is consistent with some other rice sites and likely reflects management practices. Baseline flux values also differ, with
776 the two Botswana sites having the highest off-season fluxes (29 and 133 nmol m⁻² s⁻¹ for BW-NXR and BW-GUM,
777 respectively, estimated by Timesat), MY-MLM having an intermediate baseline flux (16 nmol m⁻² s⁻¹, estimated by
778 Timesat), and the remainder of the sites having essentially zero flux at baseline. While more tropical wetland data will
779 be needed to extract broad scale conclusions about these ecosystems, the six tropical sites in FLUXNET-CH4 provide
780 an important starting point for synthesis studies and highlight tropical wetland CH₄ variability.

781

782 4.0 Data Availability

783 Half-hourly and daily aggregations are available for download at [https://fluxnet.org/data/fluxnet-ch4-](https://fluxnet.org/data/fluxnet-ch4-community-product/)
784 [community-product/](https://fluxnet.org/data/fluxnet-ch4-community-product/), along with a table containing site metadata compiled from Table B2. Variable descriptions and
785 units are provided in Table B1, and at <https://fluxnet.org/data/fluxnet-ch4-community-product/>. Each site has a unique
786 FLUXNET-CH4 DOI as listed in Table B2. All site data are available under the CC BY 4.0
787 (<https://creativecommons.org/licenses/by/4.0/>) copyright policy. The individual site DOIs are provided below in
788 Table 2. All seasonality parameters used in these analyses are available at <https://doi.org/10.5281/zenodo.4408468>.

789

790 **Table 2: Site identification (SITE_ID), data DOI, and DOI reference for each FLUXNET-CH4 site.**

SITE ID	DOI	DOI REFERENCE
AT-Neu	10.18140/FLX/1669365	Wohlfahrt et al., 2020.
BR-Npw	10.18140/FLX/1669368	Vourlitis et al., 2020.



BW-Gum	10.18140/FLX/1669370	Helfter, 2020a.
BW-Nxr	10.18140/FLX/1669518	Helfter, 2020b.
CA-SCB	10.18140/FLX/1669613	Sonntag and Helbig, 2020a.
CA-SCC	10.18140/FLX/1669628	Sonntag and Helbig, 2020b.
CH-Cha	10.18140/FLX/1669629	Hörtnagl et al., 2020a.
CH-Dav	10.18140/FLX/1669630	Hörtnagl et al., 2020b.
CH-Oe2	10.18140/FLX/1669631	Hörtnagl, et al., 2020c.
CN-Hgu	10.18140/FLX/1669632	Niu and Chen, 2020.
DE-Dgw	10.18140/FLX/1669633	Sachs et al, 2020a.
DE-Hte	10.18140/FLX/1669634	Koebisch and Jurasinski, 2020.
DE-SfN	10.18140/FLX/1669635	Klatt et al., 2020.
DE-Zrk	10.18140/FLX/1669636	Sachs et al., 2020b.
FI-Hyy	10.18140/FLX/1669637	Mammarella et al. 2020.
FI-Lom	10.18140/FLX/1669638	Aurela et al., 2020.
FI-Si2	10.18140/FLX/1669639	Vesala et al., 2020a.
FI-Sii	10.18140/FLX/1669640	Vesala et al., 2020b
FR-LGt	10.18140/FLX/1669641	Jacotot et al., 2020.
HK-MPM	10.18140/FLX/1669642	Lai and Liu, 2020.
ID-Pag	10.18140/FLX/1669643	Sakabe et al., 2020.
IT-BCi	10.18140/FLX/1669644	Magliulo et al., 2020.
IT-Cas	10.18140/FLX/1669645	Manca and Goded, 2020.
JP-BBY	10.18140/FLX/1669646	Ueyama et al., 2020.
JP-Mse	10.18140/FLX/1669647	Iwata, 2020a.
JP-SwL	10.18140/FLX/1669648	Iwata, 2020b.
KR-CRK	10.18140/FLX/1669649	Ryu et al., 2020.
MY-MLM	10.18140/FLX/1669650	Tang et al., 2020.
NL-Hor	10.18140/FLX/1669651	Dolman et al., 2020a.
NZ-Kop	10.18140/FLX/1669652	Campbell and Goodrich, 2020.
PH-RiF	10.18140/FLX/1669653	Albert and Wassmann, 2020.
RU-Ch2	10.18140/FLX/1669654	Goekede, 2020.
RU-Che	10.18140/FLX/1669655	Merbold et al., 2020.
RU-Cok	10.18140/FLX/1669656	Dolman et al., 2020b.
RU-Fy2	10.18140/FLX/1669657	Varlagin, 2020.
SE-Deg	10.18140/FLX/1669659	Nilsson and Peichl, 2020.
UK-LBT	10.18140/FLX/1670207	Helfter, 2020c.
US-A03	10.18140/FLX/1669661	Billesbach and Sullivan, 2020a.
US-A10	10.18140/FLX/1669662	Billesbach and Sullivan, 2020b.
US-Atq	10.18140/FLX/1669663	Zona and Oechel, 2020a.
US-Beo	10.18140/FLX/1669664	Zona and Oechel, 2020b.
US-Bes	10.18140/FLX/1669665	Zona and Oechel, 2020c.
US-Bil	10.18140/FLX/1669666	Rey-Sanchez et al., 2020a.



US-Bi2	10.18140/FLX/1669667	Rey-Sanchez et al., 2020b.
US-BZB	10.18140/FLX/1669668	Euskirchen and Edgar, 2020a.
US-BZF	10.18140/FLX/1669669	Euskirchen and Edgar, 2020b.
US-BZS	10.18140/FLX/1669670	Euskirchen and Edgar, 2020c.
US-CRT	10.18140/FLX/1669671	Chen and Chu, 2020a.
US-DPW	10.18140/FLX/1669672	Hinkle and Bracho, 2020.
US-EDN	10.18140/FLX/1669673	Oikawa, 2020.
US-EML	10.18140/FLX/1669674	Schuur, 2020.
US-Ho1	10.18140/FLX/1669675	Richardson and Hollinger, 2020.
US-HRA	10.18140/FLX/1669676	Runkle et al., 2020.
US-HRC	10.18140/FLX/1669677	Reba et al., 2020.
US-ICs	10.18140/FLX/1669678	Euskirchen et al., 2020d.
US-Ivo	10.18140/FLX/1669679	Zona and Oechel, 2020d.
US-LA1	10.18140/FLX/1669680	Holm et al., 2020a.
US-LA2	10.18140/FLX/1669681	Holm et al., 2020b.
US-Los	10.18140/FLX/1669682	Desai and Thom, 2020a.
US-MAC	10.18140/FLX/1669683	Sparks, 2020.
US-MRM	10.18140/FLX/1669684	Schafer, 2020.
US-Myb	10.18140/FLX/1669685	Matthes et al., 2020.
US-NC4	10.18140/FLX/1669686	Noormets et al., 2020.
US-NGB	10.18140/FLX/1669687	Torn and Dengel, 2020a.
US-NGC	10.18140/FLX/1669688	Torn and Dengel, 2020b.
US-ORv	10.18140/FLX/1669689	Bohrer and Morin, 2020a.
US-OWC	10.18140/FLX/1669690	Bohrer et al., 2020b.
US-PFa	10.18140/FLX/1669691	Desai and Thom, 2020b.
US-Snd	10.18140/FLX/1669692	Detto et al., 2020.
US-Sne	10.18140/FLX/1669693	Short et al., 2020.
US-Srr	10.18140/FLX/1669694	Windham-Myers et al., 2020.
US-StJ	10.18140/FLX/1669695	Vazquez-Lule and Vargas, 2020.
US-Tw1	10.18140/FLX/1669696	Valach et al., 2020a.
US-Tw3	10.18140/FLX/1669697	Chamberlain et al., 2020.
US-Tw4	10.18140/FLX/1669698	Eichelmann et al., 2020.
US-Tw5	10.18140/FLX/1669699	Valach et al., 2020b.
US-Twt	10.18140/FLX/1669700	Knox et al., 2020.
US-Uaf	10.18140/FLX/1669701	Iwata et al., 2020c.
US-WPT	10.18140/FLX/1669702	Chen and Chu, 2020b.

791

792

793



794 5.0 Conclusions

795 The breadth and scope of CH₄ flux data in the FLUXNET-CH₄ Version 1.0 dataset make it possible to
796 study the global patterns of CH₄ fluxes, particularly for global freshwater wetlands which release a substantial
797 fraction of atmospheric CH₄. We provide the first global estimates of flux patterns and predictors in CH₄ seasonality
798 using freshwater wetland data. In the seasonality analysis, we find that, on average, the seasonal increase in CH₄
799 emissions begins about three months earlier and lasts about four months longer at the warmest sites compared with
800 the coolest sites. We also find that the beginning of the CH₄ emission season lags the beginning of seasonal soil
801 warming by approximately one month, with almost no instances of CH₄ increasing before temperature increases.
802 Additionally, roughly half the sites have CH₄ emissions increasing prior to GPP increase; highlighting the
803 importance of substrate vs temperature limitations on wetland CH₄ emissions. Furthermore, relative to warmer
804 climates, wetland CH₄ emissions in cooler climates increase faster in the warming season and decrease slower in the
805 cooling season. This phenomenon has previously been noted on a regional scale and we show that it persists at the
806 global scale. Constraining the seasonality of CH₄ fluxes on a global scale can help improve the accuracy of global
807 wetland models.

808 FLUXNET-CH₄ is an important new resource for the research community, but critical data gaps and
809 opportunities remain. The current FLUXNET-CH₄ Version 1.0 is biased towards sites in boreal and temperate
810 regions, which influence the relationships presented in our analyses. Tropical ecosystems are estimated to account
811 for 64% of potential natural CH₄ emissions (<30° N, Saunois et al., 2020) but only account for 13% of the
812 FLUXNET-CH₄ Version 1.0 sites in the dataset. Unsurprisingly, tropical sites in our network do not represent the
813 range of bioclimatic wetland conditions present in the tropics. Therefore, while maintaining flux towers in tropical
814 ecosystems is challenging, it is necessary to further constrain the global CH₄ cycle. Coastal wetlands are also poorly
815 represented in FLUXNET-CH₄ even though there is evidence of substantial CH₄ emissions from these ecosystems,
816 so better representation across salinity gradients is warranted. Lastly, the average time series for FLUXNET-CH₄
817 Version 1.0 is relatively short, only 3.7 site-years on average compared with 7.2 for CO₂ sites in FLUXNET
818 (Pastorello et al., 2020). Adding additional site-years of data from existing sites, as a complement to adding new
819 sites, will increase the community's ability to explain interannual variability in CH₄ emission and seasonality.
820 Nevertheless, FLUXNET-CH₄ is an important and unprecedented resource with which to diagnose and understand
821 drivers of the global CH₄ cycle.

822

823 Author contribution

824 Kyle B. Delwiche oversaw the data release, performed the seasonality analysis, gathered metadata, and
825 prepared the manuscript with contributions from all co-authors. Sara Helen Knox gathered and standardized the
826 data, and gap-filled the CH₄ flux data. Avni Malhotra prepared the manuscript and gathered metadata. Etienne
827 Fluet-Chouinard did the representativeness analysis and prepared the manuscript. Gavin McNicol gathered data and
828 prepared the manuscript. Robert B. Jackson oversaw the data collection, processing, analysis, and release. Danielle
829 Christianson and You-Wei Cheah oversaw the FLUXNET-CH₄ dataset release on fluxnet.org. Dario Papale,
830 Eleonora Canfora, and Carlo Trotta did the data collection, curation, and processing for a majority of the non-
831 American sites. Remaining co-authors contributed eddy-covariance data to FLUXNET-CH₄ Version 1.0 dataset
832 and/or participated in editing the manuscript.

833 Competing interests

834 The authors declare that they have no conflict of interest.



835

836

837 **Acknowledgements**

838 We acknowledge primary support from the Gordon and Betty Moore Foundation (Grant GBMF5439,
839 “Advancing Understanding of the Global Methane Cycle”; Stanford University) and from the John Wesley
840 Powell Center for Analysis and Synthesis of the U.S. Geological Survey (“Wetland FLUXNET Synthesis for
841 Methane” working group). Benjamin R. K. Runkle was supported by National Science Foundation Award
842 1752083. Ankur R. Desai acknowledges support of the DOE AmeriFlux Network Management Project.
843 Masahito Ueyama was supported by ArCS II (JPMXD1420318865) and JSPS KAKENHI (20K21849). Dario
844 Papale and Nina Buchmann acknowledge the support of the RINGO (GA 730944) H2020 EU project. Nina
845 Buchmann and Kathrin Fuchs acknowledge the SNF project M4P (40FA40_154245/1) and InnoFarm
846 (407340_172433). Nina Buchmann acknowledges support from the SNF for ICOS-CH Phases 1 and 2
847 (20FI21_148992, 20FI20_173691). Carlo Trotta acknowledges the support of the E-SHAPE (GA 820852)
848 H2020 EU project. William J. Riley was supported by the US Department of Energy, BER, RCGM,
849 RUBISCO project under contract no. DEAC02-05CH11231. Jessica Turner acknowledges support from NSF
850 GRFP (DGE-1747503) and NTL LTER (DEB-1440297). Minseok Kang was supported by the National
851 Research Foundation of Korea (NRF-2018 R1C1B6002917). Carole Helfter acknowledges the support of the
852 UK Natural Environment Research Council (the Global Methane Budget project, grant number
853 NE/N015746/1). Rodrigo Vargas acknowledges support from the National Science Foundation (1652594).
854 Dennis Baldocchi acknowledges the California Department of Water Resources for a funding contract from
855 the California Department of Fish and Wildlife and the United States Department of Agriculture (NIFA
856 grant #2011-67003-30371), as well as the U.S. Department of Energy’s Office of Science (AmeriFlux contract
857 #7079856) for funding the AmeriFlux core sites. US-A03 and US-A10 are operated by the Atmospheric
858 Radiation Measurement (ARM) user facility, a U.S. Department of Energy Office of Science user facility
859 managed by the Biological and Environmental Research Program (doi:10.5439/1025039,
860 doi:10.5439/1025274, doi:10.5439/1095578). Work at ANL was supported by the U.S. Department of Energy,
861 Office of Science, Office of Biological and Environmental Research, under contract DE-AC02-06CH11357.
862 Any use of trade, firm, or product names is for descriptive purposes only and does not imply endorsement by
863 the U.S. Government. The CH-Dav, DE-SfN, FI-Hyy, FI-Lom, FI-Sii, FR-LGt, IT-BCi, SE-Deg and SE-Sto
864 sites are part of the ICOS European Research Infrastructure. Oliver Sonntag acknowledges funding by
865 the Canada Research Chairs, Canada Foundation for Innovation Leaders Opportunity Fund, and Natural
866 Sciences and Engineering Research Council Discovery Grant Programs for work at CA-SCC and CA-SCB.
867 Benjamin Poulter acknowledges support from the NASA Carbon Cycle and Ecosystems Program. We thank
868 Nathaniel Goenawan for his help with the representativeness analysis.

869 **References**

- 870 Alberto, M. C. R., Wassmann, R., Gummert, M., Buresh, R. J., Quilty, J. R., Correa, T. Q., Centeno, C. A. R., &
871 Oca, G. M. Straw incorporated after mechanized harvesting of irrigated rice affects net emissions of CH₄ and
872 CO₂ based on eddy covariance measurements. *Field Crop. Res.*, 184, 162–175.
873 <https://doi.org/10.1016/j.fcr.2015.10.004>. 2015.
874 Alberto, M., & Wassmann, R. FLUXNET-CH₄ PH-RiF Philippines Rice Institute flooded. Philippines.
875 <https://doi.org/10.18140/FLX/1669653>. 2020.
876 Anderson, D. E., Verma, S. B., & Rosenberg, N. J. Eddy correlation measurements of CO₂, latent heat, and sensible
877 heat fluxes over a crop surface. *Bound. Lay. Meteorol.*, 29(3), 263–272. <https://doi.org/10.1007/bf00119792>.
878 1984.



- 879 Anderson, F. E., Bergamaschi, B., Sturtevant, C., Knox, S., Hastings, L., Windham-Myers, L., Detto, M., Hestir, E.
880 L., Drexler, J., Miller, R. L., Matthes, J. H., Verfaillie, J., Baldocchi, D., Snyder, R. L., & Fujii R. Variation of
881 energy and carbon fluxes from a restored temperate freshwater wetland and implications for carbon market
882 verification protocols. *J. of Geophys. Res. – Biogeo.*, 121(3), 777–795. <https://doi.org/10.1002/2015JG003083>.
883 2016.
- 884 Angle, J. C., Morin, T. H., Solden, L. M., Narrowe, A. B., Smith, G. J., Borton, M. A., Rey-Sanchez, C., Daly, R.
885 A., Mirfenderesgi, G., Hoyt, D. W., Riley, W. J., Miller, C. S., Bohrer, G., & Wrighton, K. C. Methanogenesis
886 in oxygenated soils is a substantial fraction of wetland methane emissions. *Nat. Comm.*, 8(1), 1567.
887 <https://doi.org/10.1038/s41467-017-01753-4>. 2017.
- 888 Aurela, M., Lohila, A., J.-P., Hatakka, J., Rainne, J., Mäkelä, T., & Lauria, T. FLUXNET-CH4 FI-Lom
889 Lompolojankka. Finland. <https://doi:10.18140/FLX/1669638>. 2020.
- 890 Bartlett, K. B., Bartlett, D. S., Harriss, R. C., & Sebacher, D. I. Methane emissions along a salt marsh salinity
891 gradient. *Biogeochemistry*, 4(3), 183–202. <https://doi.org/10.1007/bf02187365>. 1987.
- 892 Bastviken, D., Tranvik, L. J., Downing, J. A., Crill, P. M., & Enrich-Prast, A. Freshwater methane emissions offset
893 the continental carbon sink. *Science*, 331(6013), 50. <https://doi.org/10.1126/science.1196808>. 2011.
- 894 Billesbach, D., & Sullivan, R. FLUXNET-CH4 US-A03 ARM-AMF3-Oliktok. United States. <https://doi:10.18140/FLX/1669661>. 2020a.
- 895 Billesbach, D., & Sullivan, R. FLUXNET-CH4 US-A10 ARM-NSA-Barrow. United States.
896 <https://doi:10.18140/FLX/1669662>. 2020b.
- 897 Bloom, A. A., Bowman, K. W., Lee, M., Turner, A. J., Schroeder, R., Worden, J. R., Weidner, R., McDonald, K.
898 C., & Jacob, D. J. A global wetland methane emissions and uncertainty dataset for atmospheric chemical
899 transport models (WetCHARTs version 1.0). *Geosci. Model Dev.*, 10, 2141–2156.
900 <https://doi.org/10.5194/gmd-10-2141-2017>. 2017.
- 901 Bridgman, S. D., Cadillo-Quiroz, H., Keller, J. K., & Zhuang, Q. Methane emissions from wetlands:
902 biogeochemical, microbial, and modeling perspectives from local to global scales. *Glob. Change Biol.*, 19(5),
903 1325–1346. <https://doi.org/10.1111/gcb.12131>. 2013.
- 904 Bohrer, G., & Morin, T. H. FLUXNET-CH4 US-ORv Olentangy River Wetland Research Park. United States.
905 <https://doi:10.18140/FLX/1669689>. 2020a.
- 906 Bohrer, G., Kerns, J., Morin, T. H., Rey-Sanchez, A. C., Villa, J., & Ju, Y. FLUXNET-CH4 US-OWC Old Woman
907 Creek. United States. <https://doi:10.18140/FLX/1669690>. 2020b.
- 908 Campbell, D., & Goodrich, J. FLUXNET-CH4 NZ-Kop Kopuatai. New Zealand.
909 <https://doi:10.18140/FLX/1669652>. 2020.
- 910 Castro-Morales, K., Kleinen, T., Kaiser, S., Zaehle, S., Kitzler, F., Kwon, M. J., Beer, C., & Göckede, M. Year-
911 round simulated methane emissions from a permafrost ecosystem in Northeast Siberia. *Biogeosciences*, 15(9),
912 2691–2722. <https://doi.org/10.5194/bg-15-2691-2018>. 2018.
- 913 Chamberlain, S. D., Oikawa, P., Sturtevant, C., Szutu, D., Verfaillie, J., & Baldocchi, D. FLUXNET-CH4 US-Tw3
914 Twitchell Alfalfa. United States. <https://doi:10.18140/FLX/1669697>. 2020.
- 915 Chambers, L. G., Ramesh Reddy, K., & Osborne, T. Z. Short-Term Response of Carbon Cycling to Salinity Pulses
916 in a Freshwater Wetland. *Soil Sci. Soc. Am. J.*, 75(5), 2000–2007. <https://doi.org/10.2136/sssaj2011.0026>.
917 2011.
- 918 Chang, K. Y., W. J. Riley, S. H. Knox, R. B. Jackson, G. McNicol, B. Poulter, M. Aurela, D. Baldocchi, S. Bansal,
919 G. Bohrer, D. I. Campbell, A. Cescatti, H. Chu, K. B. Delwiche, A. Desai, E. Euskirchen, T. Friborg, M.
920 Goeckede, G. Holm, M. Kang, T. Keenan, K. W. Krauss, A. Lohila, I. Mammarella, A. Miyata, M. B. Nilsson,
921 A. Noormets, D. Papale, B. R. K. Runkle, Y. Ryu, T. Sachs, K. V. R. Schäfer, H. P. Schmid, N. Shurpali, O.
922 Sonntag, A. C. I. Tang, M. S. Torn, C. Trotta, M. Ueyama, R. Vargas, T. Vesala, L. Windham-Myers, Z.
923 Zhang, & D. Zona. Global wetland methane emissions have hysteretic responses to seasonal temperature. In
924 Review: Nature Communications.
- 925 Chanton, J. P., Glaser, P. H., Chasar, L. S., Burdige, D. J., Hines, M. E., Siegel, D. I., Tremblay, L. B., & Cooper,
926 W. T. Radiocarbon evidence for the importance of surface vegetation on fermentation and methanogenesis in
927 contrasting types of boreal peatlands. *Global Biogeochem. Cy.*, 22(4). <https://doi.org/10.1029/2008gb003274>.
928 2008.
- 929 Chen, J., & Chu, H. FLUXNET-CH4 US-CRT Curtice Walter-Berger cropland. United States.
930 <https://doi:10.18140/FLX/1669671>. 2020a.
- 931 Chen, J., & Chu, H. FLUXNET-CH4 US-WPT Winous Point North Marsh. United States.
932 <https://doi:10.18140/FLX/1669702>. 2020b.
- 933



- 934 Chu, H., Chen, J., Gottgens, J. F., Ouyang, Z., John, R., Czajkowski, K., & Becker, R. Net ecosystem methane and
935 carbon dioxide exchanges in a Lake Erie coastal marsh and a nearby cropland. *J. Geophys. Res.: Biogeo.*,
936 119(5), 722–740. <https://doi.org/10.1002/2013JG002520>. 2014.
- 937 Chu, H., Baldocchi, D. D., John, R., Wolf, S., & Reichstein, M. Fluxes all of the time? A primer on the temporal
938 representativeness of FLUXNET. *Journal of Geophysical Research: Biogeosciences*, 122(2), 289–307.
939 <https://doi.org/10.1002/2016JG003576>. 2017.
- 940 Dean, J. F., Middelburg, J. J., Röckmann, T., Aerts, R., Blauw, L. G., Egger, M., Jetten, M. S. M., de Jong, A. E. E.,
941 Meisel, O. H., Rasigraf, O., Slomp, C. P., in't Zandt, M. H., & Dolman, A. J. Methane Feedbacks to the Global
942 Climate System in a Warmer World. *Rev. Geophys.*, 56(1), 207–250. <https://doi.org/10.1002/2017rg000559>.
943 2018.
- 944 Deemer, B. R., Harrison, J. A., Li, S., Beaulieu, J. J., DelSontro, T., Barros, N., Bezerra-Neto, J. F., Powers, S. M.,
945 Dos Santos, M. A., & Vonk, J. A. Greenhouse Gas Emissions from Reservoir Water Surfaces: A New Global
946 Synthesis. *Bioscience*, 66(11), 949–964. <https://doi.org/10.1093/biosci/biw117>. 2016.
- 947 Dengel, S., Zona, D., Sachs, T., Aurela, M., Jammot, M., Parmentier, F.-J. W., Oechel, W., & Vesala, T. Testing the
948 applicability of neural networks as a gap-filling method using CH₄ flux data from high latitude wetlands.
949 *Biogeosciences*, 10, 8185–8200. <https://doi.org/10.5194/bg-10-8185-2013>. 2013.
- 950 Deshmukh, C. S., Julius, D., Evans, C. D., Nardi, Susanto, A. P., Page, S. E., Gauci, V., Laurén, A., Sabiham, S.,
951 Agus, F., Asyhari, A., Kurnianto, S., Suardiwerianto, Y., & Desai, A. R. Impact of forest plantation on
952 methane emissions from tropical peatland. *Glob. Change Biol.*, 26, 2477–2495.
953 <https://doi.org/10.1111/gcb.15019>. 2020.
- 954 Desai, A. R., & Thom, J. FLUXNET-CH₄ US-Los Lost Creek. United States. <https://doi:10.18140/FLX/1669682>.
955 2020a.
- 956 Desai, A. R., & Thom, J. FLUXNET-CH₄ US-PFa Park Falls/WLEF. United States.
957 <https://doi:10.18140/FLX/1669691>. 2020b.
- 958 Desjardins, R. L. A technique to measure CO₂ exchange under field conditions. *Int. J. Biometeorol.*, 18(1), 76–83.
959 <https://doi.org/10.1007/bf01450667>. 1974.
- 960 Detto, M., Sturtevant, C., Oikawa, P., Verfaillie, J., & Baldocchi, D. FLUXNET-CH₄ US-Snd Sherman Island.
961 United States. <https://doi:10.18140/FLX/1669692>. 2020.
- 962 Dise, N. Winter fluxes of methane from Minnesota peatlands. *Biogeochemistry*, 17(2).
963 <https://doi.org/10.1007/bf00002641>. 1992.
- 964 Dolman, H., Hendriks, D., Parmentier, F.-J., Marchesini, L. B., Dean, J., & van Huissteden, K. FLUXNET-CH₄
965 NL-Hor Horstermeer. Netherlands. <https://doi:10.18140/FLX/1669651>. 2020a.
- 966 Dolman, H., van der Molen, H., Parmentier, F.-J., Marchesini, L. B., Dean, J., van Huissteden, K., & Maximov, T.
967 FLUXNET-CH₄ RU-Cok Chokurdakh. Russian Federation. <https://doi:10.18140/FLX/1669656>. 2020b.
- 968 Eichelmann, E., Knox, S., Rey Sanchez, C., Valach, A., Sturtevant, C., Szutu, D., Verfaillie, J., & Baldocchi, D.
969 FLUXNET-CH₄ US-Tw4 Twitchell East End Wetland. United States. <https://doi:10.18140/FLX/1669698>.
970 2020.
- 971 Eklundh, L., & Jönsson, P. TIMESAT: A Software Package for Time-Series Processing and Assessment of
972 Vegetation Dynamics. *Remote Sensing Time Series* (pp. 141–158). [https://doi.org/10.1007/978-3-319-15967-](https://doi.org/10.1007/978-3-319-15967-6_7)
973 [6_7](https://doi.org/10.1007/978-3-319-15967-6_7). 2015.
- 974 Etheridge, D. M., Steele, L. P., Francey, R. J., & Langenfelds, R. L. Atmospheric methane between 1000 A.D. and
975 present: Evidence of anthropogenic emissions and climatic variability. *J. Geophys. Res. – Atmos.*, 103(D13),
976 15979–15993. <https://doi.org/10.1029/98jd00923>. 1998.
- 977 Etminan, M., Myhre, G., Highwood, E. J., & Shine, K. P. Radiative forcing of carbon dioxide, methane, and nitrous
978 oxide: A significant revision of the methane radiative forcing. *Geophys. Res. Lett.*, 43(24), 12,614–12,623.
979 <https://doi.org/10.1002/2016gl017930>. 2016.
- 980 Euskirchen, E., & Edgar, C. FLUXNET-CH₄ US-BZB Bonanza Creek Thermokarst Bog. United States.
981 <https://doi:10.18140/FLX/1669668>. 2020a.
- 982 Euskirchen, E., & Edgar, C. FLUXNET-CH₄ US-BZF Bonanza Creek Rich Fen. United States.
983 <https://doi:10.18140/FLX/1669669>. 2020b.
- 984 Euskirchen, E., & Edgar, C. FLUXNET-CH₄ US-BZS Bonanza Creek Black Spruce. United States.
985 <https://doi:10.18140/FLX/1669670>. 2020c.
- 986 Euskirchen, E., Bret-Harte, M., & Edgar, C. Marion Bret-Harte. FLUXNET-CH₄ US-ICs Imnavait Creek
987 Watershed Wet Sedge Tundra. United States. <https://doi:10.18140/FLX/1669678>. 2020d.
- 988 Gallant, A. The Challenges of Remote Monitoring of Wetlands. *Remote Sensing*, 7(8), 10938–10950.
989 <https://doi.org/10.3390/rs70810938>. 2015.



- 990 Göeckede, M., Kittler, F., & Schaller, C. Quantifying the impact of emission outbursts and non-stationary flow on
991 eddy covariance CH₄ flux measurements using wavelet techniques. *Biogeosciences*, 16(16), 3113–3131.
992 <https://doi.org/10.5194/bg-16-3113-2019>. 2019.
- 993 Goeckede, M. FLUXNET-CH₄ RU-Ch₂ Chersky reference. Russian Federation.
994 <https://doi.org/10.18140/FLX/1669654>. 2020.
- 995 Gu, L., Post, W. M., Baldocchi, D. D., Andrew Black, T., Suyker, A. E., Verma, S. B., Vesala, T., & Wofsy, S. C.
996 Characterizing the Seasonal Dynamics of Plant Community Photosynthesis Across a Range of Vegetation
997 Types. In: Noormets A. (eds) *Phenology of Ecosystem Processes*. Springer, New York, NY. pp. 35–58.
998 https://doi.org/10.1007/978-1-4419-0026-5_2. 2009.
- 999 Hargreaves, K. J., Fowler, D., Pitcairn, C. E. R., & Aurela, M. Annual methane emission from Finnish mires
1000 estimated from eddy covariance campaign measurements. *Theor. Appl. Climatol.*, 70, 203–213.
1001 <https://doi.org/10.1007/s007040170015>. 2001.
- 1002 Hargrove, W. W., Hoffman, F. M., & Law, B. E. New analysis reveals representativeness of the AmeriFlux
1003 network. *Eos, Transactions American Geophysical Union*, 84(48), 529.
1004 <https://doi.org/10.1029/2003EO480001>. 2003.
- 1005 Hatala, J. A., Detto, M., & Baldocchi, D. D. Gross ecosystem photosynthesis causes a diurnal pattern in methane
1006 emission from rice. *Geophys. Res. Lett.*, 39(6). <https://doi.org/10.1029/2012gl051303>. 2012.
- 1007 Helbig, M., Quinton, W. L., & Sonnentag, O. Warmer spring conditions increase annual methane emissions from a
1008 boreal peat landscape with sporadic permafrost. *Environ. Res. Lett.*, 12(11), 115009.
1009 <https://doi.org/10.1088/1748-9326/aa8c85>. 2017.
- 1010 Helfter, C., Tremper, A. H., Halios, C. H., Kotthaus, S., Bjoerkegren, A., Grimmond, C. S. B., Barlow, J. F., &
1011 Nemitz, E. Spatial and temporal variability of urban fluxes of methane, carbon monoxide and carbon dioxide
1012 above London, UK. *Atmos. Chem. Phys.* 16, 10543–10557. <https://doi.org/10.5194/acp-2016-216-ac1>. 2016.
- 1013 Helfter, C. FLUXNET-CH₄ BW-Gum Guma. Botswana. <https://doi.org/10.18140/FLX/1669370>. 2020a.
- 1014 Helfter, C. FLUXNET-CH₄ BW-Nxr Nxaraga. Botswana. <https://doi.org/10.18140/FLX/1669518>. 2020b.
- 1015 Helfter, C. FLUXNET-CH₄ UK-LBT London_BT. United Kingdom. <https://doi.org/10.18140/FLX/1670207>. 2020c.
- 1016 Hinkle, C. R., & Bracho, R. FLUXNET-CH₄ US-DPW Disney Wilderness Preserve Wetland. United States.
1017 <https://doi.org/10.18140/FLX/1669672>. 2020.
- 1018 Hoffman, F. M., Kumar, J., Mills, R. T., & Hargrove, W. W. Representativeness-based sampling network design for
1019 the State of Alaska. *Landscape Ecol.*, 28(8), 1567–1586. <https://doi.org/10.1007/s10980-013-9902-0>. 2013.
- 1020 Holm, G. O., Perez, B. C., McWhorter, D. E., Krauss, K. W., Raynie, R. C., & Killebrew, C. J. FLUXNET-CH₄
1021 US-LA1 Pointe-aux-Chenes Brackish Marsh. United States. <https://doi.org/10.18140/FLX/1669680>. 2020a.
- 1022 Holm, G. O., Perez, B. C., McWhorter, D. E., Krauss, K. W., Raynie, R. C., & Killebrew, C. J. FLUXNET-CH₄
1023 US-LA2 Salvador WMA Freshwater Marsh. United States. <https://doi.org/10.18140/FLX/1669681>. 2020b.
- 1024 Hörtnagl, L., Feigenwinter, I. Fuchs, K., Merbold, L., Buchmann, N., Eugster, W., Zeeman, M., Pluess, P., Käslin,
1025 F., Meier, P., Koller, P., & Baur, T. FLUXNET-CH₄ CH-Cha Chamau. Switzerland.
1026 <https://doi.org/10.18140/FLX/1669629>. 2020a.
- 1027 Hörtnagl, Lukas, Werner Eugster, Lutz Merbold, Nina Buchmann, Mana Gharun, Sophia Etzold, Rudolf Haesler,
1028 Matthias Haeni, Philip Meier, Florian Käslin, Thomas Baur, & Peter Pluess. FLUXNET-CH₄ CH-Dav Davos.
1029 Switzerland. <https://doi.org/10.18140/FLX/1669630>. 2020b.
- 1030 Hörtnagl, Lukas, Regine Maier, Werner Eugster, Nina Buchmann, Carmen Emmel, Patrick Koller, Thomas Baur,
1031 Peter Pluess, Florian Käslin, & Philip Meier. FLUXNET-CH₄ CH-Oe2 Oensingen crop. Switzerland.
1032 <https://doi.org/10.18140/FLX/1669631>. 2020c.
- 1033 Hwang, Y., Ryu, Y., Huang, Y., Kim, J., Iwata, H., & Kang, M. Comprehensive assessments of carbon dynamics in
1034 an intermittently-irrigated rice paddy. *Agr. Forest Met.*, 285–286, 107933.
1035 <https://doi.org/10.1016/j.agrformet.2020.107933>. 2020.
- 1036 Iwata, H., Mano, M., Ono, K., Tokida, T., Kawazoe, T., Kosugi, Y., Sakabe, A., Takahashi, K., & Miyata, A.
1037 Exploring sub-daily to seasonal variations in methane exchange in a single-crop rice paddy in central Japan.
1038 *Atmos. Environ.*, 179, 156–165. <https://doi.org/10.1016/j.atmosenv.2018.02.015>. 2018.
- 1039 Iwata, Hiroki. FLUXNET-CH₄ JP-Mse Mase rice paddy field. Japan. <https://doi.org/10.18140/FLX/1669647>. 2020a.
- 1040 Iwata, Hiroki. FLUXNET-CH₄ JP-SwL Suwa Lake. Japan. <https://doi.org/10.18140/FLX/1669648>. 2020b.
- 1041 Iwata, Hiroki, Masahito Ueyama, & Yoshinobu Harazono. FLUXNET-CH₄ US-Uaf University of Alaska,
1042 Fairbanks. United States. <https://doi.org/10.18140/FLX/1669701>. 2020c.
- 1043 Jacotot, Adrien, Sébastien Gogo, & Fatima Laggoun-Défarge. FLUXNET-CH₄ FR-LGt La Guette. France.
1044 <https://doi.org/10.18140/FLX/1669641>. 2020.



- 1045 Jung, M., Reichstein, M., & Bondeau, A. Towards global empirical upscaling of FLUXNET eddy covariance
1046 observations: validation of a model tree ensemble approach using a biosphere model. *Biogeosciences*, 6(10),
1047 2001–2013. <https://doi.org/10.5194/bg-6-2001-2009>. 2009.
- 1048 Jung, M., Schwalm, C., Migliavacca, M., Walther, S., Camps-Valls, G., Koirala, S., Anthoni, P., Besnard, S.,
1049 Bodesheim, P., Carvalhais, N., Chevallier, F., Gans, F., Goll, D. S., Haverd, V., Kohler, P., Ichii, K., Jain, A.
1050 K., Liu, J., Lombardozzi, D., Nabel, J. E. M. S., Nelson, J. A., O’Sullivan, M., Pallandt, M., Papale, D., Peters,
1051 W., Pongrats, J., Rodenbeck, C., Sitch, S., Tramontana, G., Walker, A., Weber, U., & Reichstein, M. Scaling
1052 carbon fluxes from eddy covariance sites to globe: synthesis and evaluation of the FLUXCOM approach.
1053 *Biogeosciences*, 17(5), 1343–1365. <https://doi.org/10.5194/bg-17-1343-2020>. 2020.
- 1054 Kim, Y., Johnson, M. S., Knox, S. H., Andrew Black, T., Dalmagro, H. J., Kang, M., Kim, J., & Baldocchi, D. Gap-
1055 filling approaches for eddy covariance methane fluxes: A comparison of three machine learning algorithms and
1056 a traditional method with principal component analysis. *Glob. Change Biol.*, 26(3), 1499–1518.
1057 <https://doi.org/10.1111/gcb.14845>. 2020.
- 1058 Kittler, F., Heimann, M., Kolle, O., Zimov, N., Zimov, S., & Göckede, M. Long-Term Drainage Reduces CO₂
1059 Uptake and CH₄ Emissions in a Siberian Permafrost Ecosystem: Drainage impact on Arctic carbon cycle.
1060 *Global Biogeochem. Cy.*, 31(12), 1704–1717. <https://doi.org/10.1002/2017GB005774>. 2017.
- 1061 Klatt, Janina, Hans Peter Schmid, Matthias Mauder, & Rainer Steinbrecher. FLUXNET-CH₄ DE-StfN Schechenfilz
1062 Nord. Germany. <https://doi.org/10.18140/FLX/1669635>. 2020.
- 1063 Knox, S. H., Sturtevant, C., Matthes, J. H., Koteen, L., Verfaillie, J., & Baldocchi, D. Agricultural peatland
1064 restoration: effects of land-use change on greenhouse gas (CO₂ and CH₄) fluxes in the Sacramento-San
1065 Joaquin Delta. *Glob. Change Biol.*, 21(2), 750–765. <https://doi.org/10.1111/gcb.12745>. 2015.
- 1066 Knox, S. H., Matthes, J. H., Sturtevant, C., Oikawa, P. Y., Verfaillie, J., & Baldocchi, D. Biophysical controls on
1067 interannual variability in ecosystem-scale CO₂ and CH₄ exchange in a California rice paddy. *J. Geophys. Res.-*
1068 *Biogeo.*, 121(3), 978–1001. <https://doi.org/10.1002/2015jg003247>. 2016.
- 1069 Knox, S. H., Jackson, R. B., Poulter, B., McNicol, G., Fluet-Chouinard, E., Zhang, Z., Hugelius, G., Bousquet, P.,
1070 Canadell, J. G., Saunio, M., Papale, D., Chu, H., Keenan, T. F., Baldocchi, D., Torn, M. S., Mammarella, I.,
1071 Trotta, C., Aurela, M., Bohrer, G., Campbell, D.I., Cescatti, A., Chamberlain, S., Chen, J., Chen, W., Dengel,
1072 S., Desai, A.R., Euskirchen, E., Friberg, T., Gasbarra, D., Goded, I., Goeckede, M., Heimann, M., Helbig, M.,
1073 Hirano, T., Hollinger, D.Y., Iwata, H., & Others. FLUXNET-CH₄ Synthesis Activity: Objectives,
1074 Observations, and Future Directions. *B. Am. Meteorol. Soc.*, 100(12), 2607–2632. [https://doi.org/10.1175/bams-](https://doi.org/10.1175/bams-d-18-0268.1)
1075 [d-18-0268.1](https://doi.org/10.1175/bams-d-18-0268.1). 2019.
- 1076 Knox, Sara, Jaclyn Hatala Matthes, Joseph Verfaillie, & Dennis Baldocchi. FLUXNET-CH₄ US-Twt Twitchell
1077 Island. United States. <https://doi.org/10.18140/FLX/1669700>. 2020.
- 1078 Koebisch, F., Jurasinski, G., Koch, M., Hofmann, J., & Glatzel, S. Controls for multi-scale temporal variation in
1079 ecosystem methane exchange during the growing season of a permanently inundated fen. *Agr. Forest*
1080 *Meteorol.*, 204, 94–105. <https://doi.org/10.1016/j.agrformet.2015.02.002>. 2015.
- 1081 Koebisch, F., Winkel, M., Liebner, S., Liu, B., Westphal, J., Schmiedinger, I., Spitz, A., Gehre, M., Jurasinski, G.,
1082 Köhler, S., & Others. Sulfate deprivation triggers high methane production in a disturbed and rewetted coastal
1083 peatland. *Biogeosciences*, 16, 1937–1953. <https://doi.org/10.5194/bg-16-1937-2019>. 2019.
- 1084 Koebisch, Franziska, & Gerald Jurasinski. FLUXNET-CH₄ DE-Hte Huettelmoor. Germany.
1085 <https://doi.org/10.18140/FLX/1669634>. 2020.
- 1086 Kumar, J., Hoffman, F. M., Hargrove, W. W., & Collier, N. Understanding the representativeness of FLUXNET for
1087 upscaling carbon flux from eddy covariance measurements. *Earth Syst. Sci. Data* [preprint].
1088 <https://doi.org/10.5194/essd-2016-36>. 2016.
- 1089 Lai, D. Y. F. Methane Dynamics in Northern Peatlands: A Review. *Pedosphere*, 19(4), 409–421.
1090 [https://doi.org/10.1016/s1002-0160\(09\)00003-4](https://doi.org/10.1016/s1002-0160(09)00003-4). 2009.
- 1091 Lai, D. Y. F., Roulet, N. T., & Moore, T. R. The spatial and temporal relationships between CO₂ and CH₄
1092 exchange in a temperate ombrotrophic bog. *Atmos. Environ.*, 89, 249–259.
1093 <https://doi.org/10.1016/j.atmosenv.2014.02.034>. 2014.
- 1094 Lai, Derrick Y.F., & Jiangong Liu. FLUXNET-CH₄ HK-MPM Mai Po Mangrove. Hong Kong.
1095 <https://doi.org/10.18140/FLX/1669642>. 2020.
- 1096 Lasslop, G., Reichstein, M., Papale, D., Richardson, A. D., Arneeth, A., Barr, A., Stoy, P., & Wohlfahrt, G.
1097 Separation of net ecosystem exchange into assimilation and respiration using a light response curve approach:
1098 critical issues and global evaluation. *Glob. Change Biol.*, 16(1), 187–208. [https://doi.org/10.1111/j.1365-](https://doi.org/10.1111/j.1365-2486.2009.02041.x)
1099 [2486.2009.02041.x](https://doi.org/10.1111/j.1365-2486.2009.02041.x). 2010.



- 1100 Liu, J., Zhou, Y., Valach, A., Shortt, R., Kasak, K., Rey-Sanchez, C., Hemes, K. S., Baldocchi, D., & Lai, D. Y. F.
1101 Methane emissions reduce the radiative cooling effect of a subtropical estuarine mangrove wetland by half.
1102 *Glob. Change Biol.*, 26(9), 4998–5016. <https://doi.org/10.1111/gcb.15247>. 2020.
- 1103 Madsen, K., Nielsen, H. B., & Tingleff, O. Methods for non-linear least squares problems. Informatics and
1104 Mathematical Modelling, Technical University of Denmark. 2nd Edition. 2004.
- 1105 Magliulo, Vincenzo, Paul Di Tommasi, Daniela Famulari, Daniele Gasbarra, Luca Vitale, Antonio Manco,
1106 Ferdinando di Matteo, Andrea Esposito, & Maurizio Tosca. FLUXNET-CH4 IT-BCi Borgo Cioffi. Italy.
1107 <https://doi.org/10.18140/FLX/1669644>. 2020.
- 1108 Mahecha, M. D., Gans, F., Sippel, S., Donges, J. F., Kaminski, T., Metzger, S., Migliavacca, M., Papale, D.,
1109 Rammig, A., & Zscheischler, J. Detecting impacts of extreme events with ecological in situ monitoring
1110 networks. *Biogeosciences*, 14(18), 4255–4277. <https://doi.org/10.5194/bg-14-4255-2017>. 2017.
- 1111 Malhotra, A., & Roulet, N. T. Environmental correlates of peatland carbon fluxes in a thawing landscape: do
1112 transitional thaw stages matter? *Biogeosciences*, 12(10), 3119–3130. <https://doi.org/10.5194/bg-12-3119-2015>.
1113 2015.
- 1114 Mammarella, Ivan, Timo Vesala, Petri Keronen, Pasi Kolari, Samuli Launiainen, Jukka Pumpanen, Üllar Rannik,
1115 Erkki Siivola, Janne Levula, & Toivo Pohja. FLUXNET-CH4 FI-Hyy Hyytiala. Finland.
1116 <https://doi.org/10.18140/FLX/1669637>. 2020.
- 1117 Manca, Giovanni, & Ignacio Goded. FLUXNET-CH4 IT-Cas Castellaro. Italy. <https://doi.org/10.18140/FLX/1669645>.
1118 2020.
- 1119 Mastepanov, M., Sigsgaard, C., Tagesson, T., Ström, L., Tamstorf, M. P., Lund, M., & Christensen, T. R.
1120 Revisiting factors controlling methane emissions from high-Arctic tundra. *Biogeosciences*, 10(7), 5139–5158.
1121 <https://doi.org/10.5194/bg-10-5139-2013>. 2013.
- 1122 Matthes, Jaelyn Hatala, Cove Sturtevant, Patty Oikawa, Samuel D Chamberlain, Daphne Szutu, Ariane Arias Ortiz,
1123 Joseph Verfaillie, & Dennis Baldocchi. FLUXNET-CH4 US-Myb Mayberry Wetland. United States.
1124 <https://doi.org/10.18140/FLX/1669685>. 2020.
- 1125 Matthews, E., Johnson, M. S., Genovese, V., Du, J., & Bastviken, D. Methane emission from high latitude lakes:
1126 methane-centric lake classification and satellite-driven annual cycle of emissions. *Sci. Rep.- UK*, 10(1), 12465.
1127 <https://doi.org/10.1038/s41598-020-68246-1>. 2020.
- 1128 Megonigal, J. P., Whalen, S. C., Tissue, D. T., Bovard, B. D., Allen, A. S., & Albert, D. B. A Plant-Soil-
1129 Atmosphere Microcosm for Tracing Radiocarbon from Photosynthesis through Methanogenesis. *Soil Sci. Soc.*
1130 *Am. J.* 63(3), 665–671. <https://doi.org/10.2136/sssaj1999.03615995006300030033x>. 1999.
- 1131 Mejjide, A., Manca, G., Goded, I., Magliulo, V., Di Tommasi, P., Seufert, G., & Cescatti, A. Seasonal trends and
1132 environmental controls of methane emissions in a rice paddy field in Northern Italy. *Biogeosciences*, 8(12),
1133 3809. <https://doi.org/10.5194/bg-8-3809-2011>. 2011.
- 1134 Melloh, R. A., & Crill, P. M. Winter methane dynamics in a temperate peatland. *Global Biogeochem. Cy.*, 10(2),
1135 247–254. <https://doi.org/10.1029/96gb00365>. 1996.
- 1136 Melton, J. R., Wania, R., Hodson, E. L., Poulter, B., Ringeval, B., Spahni, R., Bohn, T., Avis, C. A., Beerling, D. J.,
1137 Chen, G., Eliseev, A. V., Denisov, S. N., Hopcroft, P. O., Lettenmaier, D. P., Riley, W. J., Singarayer, J. S.,
1138 Subin, Z. M., Tian, H., Zürcher, S., & Others. Present state of global wetland extent and wetland methane
1139 modelling: conclusions from a model inter-comparison project (WETCHIMP). *Biogeosciences*, 10(2), 753–
1140 788. <https://doi.org/10.5194/bg-10-753-2013>. 2013.
- 1141 Merbold, Lutz, Corinna Rebmann, & Chiara Corradi. FLUXNET-CH4 RU-Che Cherski. Russian Federation.
1142 <https://doi.org/10.18140/FLX/1669655>. 2020.
- 1143 Meyer, H., & Pebesma, E. Predicting into unknown space? Estimating the area of applicability of spatial prediction
1144 models. *arXiv [stat.ML]*. <http://arxiv.org/abs/2005.07939>. 2020.
- 1145 Mishra, S. R., Pattnaik, P., Sethunathan, N., & Adhya, T. K. Anion-Mediated Salinity Affecting Methane
1146 Production in a Flooded Alluvial Soil. *Geomicrobiol. J.*, 20(6), 579–586. <https://doi.org/10.1080/713851167>.
1147 2003.
- 1148 Moffat, A. M., Papale, D., Reichstein, M., Hollinger, D. Y., Richardson, A. D., Barr, A. G., Beckstein, C., Braswell,
1149 B. H., Churkina, G., Desai, A. R., Falge, E., Gove, J. H., Heimann, M., Hui, D., Jarvis, A. J., Kattge, J.,
1150 Noormets, A., & Stauch, V. J. Comprehensive comparison of gap-filling techniques for eddy covariance net
1151 carbon fluxes. *Agr. Forest Meteorol.*, 147(3), 209–232. <https://doi.org/10.1016/j.agrformet.2007.08.011>. 2007.
- 1152 Myhre, G., D. Shindell, F.-M. Bréon, W. Collins, J. Fuglestedt, J. Huang, D. Koch, J.-F. Lamarque, D. Lee, B.
1153 Mendoza, T. Nakajima, A. Robock, G. Stephens, T. Takemura and H. Zhang. Anthropogenic and Natural
1154 Radiative Forcing Supplementary Material. In Stocker, T.F., D. Qin, G.-K. Plattner, M. Tignor, S.K. Allen, J.
1155 Boschung, A. Nauels, Y. Xia, V. Bex and P.M. Midgley (Ed.), *Climate Change 2013: The Physical Science*



- 1156 Basis. Contribution of Working Group I to the Fifth Assessment Report of the Intergovernmental Panel on
1157 Climate Change. 2013.
- 1158 Nemitz, E., Mammarella, I., Ibrom, A., Aurela, M., Burba, G. G., Dengel, S., Gielen, B., Grelle, A., Heinesch, B.,
1159 Herbst, M., Hörtnagl, L., Klemedtsson, L., Lindroth, A., Lohila, A., McDermitt, D. K., Meier, P., Merbold, L.,
1160 Nelson, D., Nicolini, G., & Others. Standardisation of eddy-covariance flux measurements of methane and
1161 nitrous oxide. *Int. Agrophys.*, 32(4), 517–549. <https://doi.org/10.1515/intag-2017-0042>. 2018.
- 1162 Nielsen, H. B. Damping parameter in Marquardt's method. Department of Mathematical Modeling, IMM, Technical
1163 University of Denmark. Technical Report, IMM-REP-1999-05. 1999.
- 1164 Nilsson, Mats B., & Matthias Peichl. FLUXNET-CH4 SE-Deg Degero. Sweden.
1165 <https://doi.org/10.18140/FLX/1669659>. 2020.
- 1166 Niu, Shuli, & Weinan Chen. FLUXNET-CH4 CN-Hgu Hongyuan. China. <https://doi.org/10.18140/FLX/1669632>. 2020.
- 1167 Noormets, Asko, John King, Bhaskar Mitra, Guofang Miao, Maricar Aguilos, Kevan Minick, Prajaya Prajapati,
1168 Jean-Christophe Domec, Jonathan Furst, & Maxwell Wightman. FLUXNET-CH4 US-NC4
1169 NC_AlligatorRiver. United States. <https://doi.org/10.18140/FLX/1669686>. 2020.
- 1170 Oikawa, P. Y., Jenerette, G. D., Knox, S. H., Sturtevant, C., Verfaillie, J., Dronova, I., Poindexter, C. M.,
1171 Eichelmann, E., & Baldocchi, D. D. Evaluation of a hierarchy of models reveals importance of substrate
1172 limitation for predicting carbon dioxide and methane exchange in restored wetlands. *J. Geophys. Res.-Biogeo.*,
1173 122(1), 145–167. <https://doi.org/10.1002/2016JG003438>. 2017.
- 1174 Oikawa, Patty. FLUXNET-CH4 US-EDN Eden Landing Ecological Reserve. United States.
1175 <https://doi.org/10.18140/FLX/1669673>. 2020.
- 1176 Olefeldt, D., Turetsky, M. R., Crill, P. M., & McGuire, A. D. Environmental and physical controls on northern
1177 terrestrial methane emissions across permafrost zones. *Glob. Change Biol.*, 19(2), 589–603.
1178 <https://doi.org/10.1111/gcb.12071>. 2013.
- 1179 Papale, D., Andrew Black, T., Carvalhais, N., Cescatti, A., Chen, J., Jung, M., Kiely, G., Lasslop, G., Mahecha, M.
1180 D., Margolis, H., Merbold, L., Montagnani, L., Moors, E., Olesen, J. E., Reichstein, M., Tramontana, G., van
1181 Gorsel, E., Wohlfahrt, G., & Ráduly, B. Effect of spatial sampling from European flux towers for estimating
1182 carbon and water fluxes with artificial neural networks. *J. Geophys. Res.-Biogeo.*, 120(10), 1941–1957.
1183 <https://doi.org/10.1002/2015jg002997>. 2015.
- 1184 Parmentier, F. J. W., van Huissteden, J., van der Molen, M. K., Schaepman-Strub, G., Karsanaev, S. A., Maximov,
1185 T. C., & Dolman, A. J. Spatial and temporal dynamics in eddy covariance observations of methane fluxes at a
1186 tundra site in northeastern Siberia. *J. Geophys. Res.*, 116(G3), 1368. <https://doi.org/10.1029/2010JG001637>.
1187 2011.
- 1188 Pastorello, G., Trotta, C., Canfora, E., Chu, H., Christianson, D., Cheah, Y.-W., Poindexter, C., Chen, J.,
1189 Elbashandy, A., Humphrey, M., Isaac, P., Polidori, D., Ribeca, A., van Ingen, C., Zhang, L., Amiro, B.,
1190 Ammann, C., Arain, M. A., Ardö, J., & Others. The FLUXNET2015 dataset and the ONEFlux processing
1191 pipeline for eddy covariance data. *Scientific Data*, 7(1), 225. <https://doi.org/10.1038/s41597-020-0534-3>. 2020.
- 1192 Pattnaik, P., Mishra, S. R., Bharati, K., Mohanty, S. R., Sethunathan, N., & Adhya, T. K. Influence of salinity on
1193 methanogenesis and associated microflora in tropical rice soils. *Microbiol. Res.*, 155(3), 215–220.
1194 [https://doi.org/10.1016/S0944-5013\(00\)80035-X](https://doi.org/10.1016/S0944-5013(00)80035-X). 2000.
- 1195 Poffenbarger, H. J., Needelman, B. A., & Patrick Megonigal, J. Salinity Influence on Methane Emissions from
1196 Tidal Marshes. *Wetlands*, 31(5), 831–842. <https://doi.org/10.1007/s13157-011-0197-0>. 2011.
- 1197 Poulter, B., Bousquet, P., Canadell, J. G., Ciais, P., Peregon, A., Saunois, M., Arora, V. K., Beerling, D. J., Brovkin,
1198 V., Jones, C. D., Joos, F., Gedney, N., Ito, A., Kleinen, T., Koven, C. D., McDonald, K., Melton, J. R., Peng,
1199 C., Peng, S., & Others. Global wetland contribution to 2000–2012 atmospheric methane growth rate dynamics.
1200 *Environ. Res. Lett.*, 12(9), 094013. <https://doi.org/10.1088/1748-9326/aa8391>. 2017.
- 1201 Reba, Michele, Benjamin Runkle, & Kosana Suvocarev. FLUXNET-CH4 US-HRC Humnoke Farm Rice Field –
1202 Field C. United States. <https://doi.org/10.18140/FLX/1669677>. 2020.
- 1203 Reichstein, M., Falge, E., Baldocchi, D., Papale, D., Aubinet, M., Berbigier, P., Bernhofer, C., Buchmann, N.,
1204 Gilmanov, T., Granier, A., Grunwald, T., Havrankova, K., Ilvesniemi, H., Janous, D., Knohl, A., Laurila, T.,
1205 Lohila, A., Loustau, D., Matteucci, G., & Others. On the separation of net ecosystem exchange into
1206 assimilation and ecosystem respiration: review and improved algorithm. *Glob. Change Biol.*, 11(9), 1424–
1207 1439. <https://doi.org/10.1111/j.1365-2486.2005.001002.x>. 2005.
- 1208 Rey-Sanchez, Camilo, Daphne Szutu, Robert Shortt, Samuel D. Chamberlain, Joseph Verfaillie, & Dennis
1209 Baldocchi. FLUXNET-CH4 US-Bi1 Bouldin Island Alfalfa. United States. <https://doi.org/10.18140/FLX/1669666>.
1210 2020a.



- 1211 Rey-Sanchez, Camilo, Daphne Szutu, Kyle Hemes, Joseph Verfaillie, & Dennis Baldocchi. FLUXNET-CH4 US-
1212 Bi2 Bouldin Island corn. United States. <https://doi.org/10.18140/FLX/1669667>. 2020b.
- 1213 Richardson, A. D., Hollinger, D. Y., Burba, G. G., Davis, K. J., Flanagan, L. B., Katul, G. G., William Munger, J.,
1214 Ricciuto, D. M., Stoy, P. C., Suyker, A. E., Verma, S. B., & Wofsy, S. C. A multi-site analysis of random error
1215 in tower-based measurements of carbon and energy fluxes. *Agr. Forest Meteorol.*, 136(1), 1–18.
1216 <https://doi.org/10.1016/j.agrformet.2006.01.007>. 2006.
- 1217 Richardson, A. D., & Hollinger, D. Y. A method to estimate the additional uncertainty in gap-filled NEE resulting
1218 from long gaps in the CO₂ flux record. *Agr. Forest Meteorol.*, 147(3), 199–208.
1219 <https://doi.org/10.1016/j.agrformet.2007.06.004>. 2007.
- 1220 Richardson, A. D., Mahecha, M. D., Falge, E., Kattge, J., Moffat, A. M., Papale, D., Reichstein, M., Stauch, V. J.,
1221 Braswell, B. H., Churkina, G., Kruijt, B., & Hollinger, D. Y. Statistical properties of random CO₂ flux
1222 measurement uncertainty inferred from model residuals. *Agr. Forest Meteorol.*, 148(1), 38–50.
1223 <https://doi.org/10.1016/j.agrformet.2007.09.001>. 2008.
- 1224 Richardson, A. D., Aubinet, M., Barr, A. G., Hollinger, D. Y., Ibrom, A., Lasslop, G., & Reichstein, M. Uncertainty
1225 quantification. *Eddy Covariance: A Practical Guide to Measurement and Data Analysis*. (eds) Aubinet, M.,
1226 Vesala, T., Papale, D. Springer Atmospheric Sciences. 2012.
- 1227 Richardson, Andrew D, & David Y Hollinger. FLUXNET-CH4 US-Ho1 Howland Forest (main tower). United
1228 States. <https://doi.org/10.18140/FLX/1669675>. 2020.
- 1229 Rinne, J., Riutta, T., Pihlatie, M., Aurela, M., Haapanala, S., Tuovinen, J.-P., Tuittila, E.-S., & Vesala, T. Annual
1230 cycle of methane emission from a boreal fen measured by the eddy covariance technique. *Tellus B*, 59(3), 449–
1231 457. <https://doi.org/10.1111/j.1600-0889.2007.00261.x>. 2007.
- 1232 Runkle, B. R. K., Suvočarev, K., Reba, M. L., Reavis, C. W., Smith, S. F., Chiu, Y.-L., & Fong, B. Methane
1233 Emission Reductions from the Alternate Wetting and Drying of Rice Fields Detected Using the Eddy
1234 Covariance Method. *Envir. Sci. Tech.*, 53(2), 671–681. <https://doi.org/10.1021/acs.est.8b05535>. 2019.
- 1235 Runkle, Benjamin, Michele Reba, & Kosana Suvocarev. FLUXNET-CH4 US-HRA Humnoke Farm Rice Field –
1236 Field A. United States. <https://doi.org/10.18140/FLX/1669676>. 2020.
- 1237 Ryu, Youngryel, Minseok Kang, & Jongho Kim. FLUXNET-CH4 KR-CRK Cheorwon Rice paddy. Korea,
1238 Republic of. <https://doi.org/10.18140/FLX/1669649>. 2020.
- 1239 Sachs, T., Giebels, M., Boike, J., & Kutzbach, L. Environmental controls on CH₄ emission from polygonal tundra
1240 on the microsite scale in the Lena river delta, Siberia: CONTROLS ON TUNDRA CH₄ FLUX AND
1241 SCALING. *Glob. Change Biol.*, 16(11) 3096 – 3110. <https://doi.org/10.1111/j.1365-2486.2010.02232.x>. 2010.
- 1242 Sachs, Torsten, Christian Wille, & Eric Larmanou. FLUXNET-CH4 DE-Dgw Dagowsee. Germany.
1243 <https://doi.org/10.18140/FLX/1669633>. 2020a.
- 1244 Sachs, Torsten, Christian Wille, Eric Larmanou, & Daniela Franz. FLUXNET-CH4 DE-Zrk Zarnekow. Germany.
1245 <https://doi.org/10.18140/FLX/1669636>. 2020b.
- 1246 Sakabe, Ayaka, Masayuki Itoh, Takashi Hirano, & Kitso Kusin. FLUXNET-CH4 ID-Pag Palangkaraya undrained
1247 forest. Indonesia. <https://doi.org/10.18140/FLX/1669643>. 2020.
- 1248 Saunio, M., Bousquet, P., Poulter, B., Peregón, A., Ciais, P., Canadell, J. G., Dlugokencky, E. J., Etiope, G.,
1249 Bastviken, D., Houweling, S., Janssens-Maenhout, G., Tubiello, F. N., Castaldi, S., Jackson, R. B., Alexe, M.,
1250 Arora, V. K., Beerling, D. J., Bergamaschi, P., Blake, D. R., & Others. The global methane budget 2000–2012.
1251 *Earth Syst. Sci. Data*, 8, 697–751. <https://doi.org/10.5194/essd-8-697-2016>. 2016.
- 1252 Saunio, M., Stavert, A. R., Poulter, B., Bousquet, P., Canadell, J. G., Jackson, R. B., Raymond, P. A.,
1253 Dlugokencky, E. J., Houweling, S., Patra, P. K., Ciais, P., Arora, V. K., Bastviken, D., Bergamaschi, P., Blake,
1254 D. R., Brailsford, G., Bruhwiler, L., Carlson, K. M., Carrol, M., & Others. The Global Methane Budget 2000–
1255 2017. *Earth Syst. Sci. Data*, 12, 1561–1623. <https://doi.org/10.5194/essd-12-1561-2020>. 2020.
- 1256 Schafer, Karina. FLUXNET-CH4 US-MRM Marsh Resource Meadowlands Mitigation Bank. United States.
1257 <https://doi.org/10.18140/FLX/1669684>. 2020.
- 1258 Schuur, E.A. FLUXNET-CH4 US-EML Eight Mile Lake Permafrost thaw gradient, Healy Alaska. United States.
1259 <https://doi.org/10.18140/FLX/1669674>. 2020.
- 1260 Seyfferth, A. L., Bothfeld, F., Vargas, R., Stuckey, J. W., Wang, J., Kearns, K., Michael, H. A., Guimond, J., Yu,
1261 X., & Sparks, D. L. Spatial and temporal heterogeneity of geochemical controls on carbon cycling in a tidal
1262 salt marsh. *Geochim. Cosmochim. Ac.*, 282, 1–18. <https://doi.org/10.1016/j.gca.2020.05.013>. 2020.
- 1263 Shortt, Robert, Kyle Hemes, Daphne Szutu, Joseph Verfaillie, & Dennis Baldocchi. FLUXNET-CH4 US-Sne
1264 Sherman Island Restored Wetland. United States. <https://doi.org/10.18140/FLX/1669693>. 2020.
- 1265 Sims, D. A., Rahman, A. F., Cordova, V. D., El-Masri, B. Z., Baldocchi, D. D., Flanagan, L. B., Goldstein, A. H.,
1266 Hollinger, D. Y., Misson, L., Monson, R. K., Oechel, W. C., Schmid, H. P., Wofsy, S. C., & Xu, L. On the use



- 1267 of MODIS EVI to assess gross primary productivity of North American ecosystems. *J. Geophys. Res.-Biogeo.*
1268 111(G4). <https://doi.org/10.1029/2006jg000162>. 2006.
- 1269 Sonnentag, Oliver, & Manuel Helbig. FLUXNET-CH4 CA-SCB Scotty Creek Bog. Canada.
1270 <https://doi:10.18140/FLX/1669613>. 2020a.
- 1271 Sonnentag, Oliver, & Manuel Helbig. FLUXNET-CH4 CA-SCC Scotty Creek Landscape. Canada. <https://doi:10.18140/FLX/1669628>. 2020b.
- 1272
- 1273 Spahni, R., Wania, R., Neef, L., van Weele, M., Pison, I., Bousquet, P., Frankenberg, C., Foster, P. N., Joos, F.,
1274 Prentice, I. C., & van Velthoven, P. Constraining global methane emissions and uptake by ecosystems. In
1275 *Biogeosciences*, 8(6), 1643–1665. <https://doi.org/10.5194/bg-8-1643-2011>. 2011.
- 1276 Sparks, Jed P. FLUXNET-CH4 US-MAC MacArthur Agro-Ecology. United States.
1277 <https://doi:10.18140/FLX/1669683>. 2020.
- 1278 Sturtevant, C. S., Ruddell, B. L., Knox, S. H., Verfaillie, J. G., Matthes, J. H., Oikawa, P. Y., & Baldocchi, D. D.
1279 Identifying scale-emergent, nonlinear, asynchronous processes of wetland methane exchange. *J. Geophys.*
1280 *Res.-Biogeo.*, 121, 188–204. <https://doi.org/10.1002/2015JG003054>. 2016.
- 1281 Tagesson, T., Mölder, M., Mastepanov, M., Sigsgaard, C., Tamstorf, M. P., Lund, M., Falk, J. M., Lindroth, A.,
1282 Christensen, T. R., & Ström, L. Land-atmosphere exchange of methane from soil thawing to soil freezing in a
1283 high-Arctic wet tundra ecosystem. *Glob. Change Biol.*, 18(6), 1928–1940. <https://doi.org/10.1111/j.1365-2486.2012.02647.x>. 2012.
- 1284
- 1285 Tang, Angela Che Ing, Guan Xhuan Wong, Lulie Melling, Edward Baran Aeries, Joseph Wenceslaus Waili, Kevin
1286 Kemudang Musin, Kim San Lo, & Frankie Kiew. FLUXNET-CH4 MY-MLM Maludam National Park.
1287 Malaysia. <https://doi:10.18140/FLX/1669650>. 2020.
- 1288 Taoka, T., Iwata, H., Hirata, R., Takahashi, Y., Miyabara, Y., & Itoh, M. Environmental Controls on Diffusive and
1289 Ebullitive Methane Emission at a Sub-Daily Time Scale in the Littoral Zone of a Mid-Latitude Shallow Lake.
1290 *J. Geophys. Res.-Biogeo.*, 125(9), <https://doi.org/10.1029/2020JG005753>. 2020.
- 1291 Torn, Margaret, & Sigrid Dengel. FLUXNET-CH4 US-NGB NGEE Arctic Barrow. United States. <https://doi:10.18140/FLX/1669687>. 2020a.
- 1292
- 1293 Torn, Margaret, & Sigrid Dengel. FLUXNET-CH4 US-NGC NGEE Arctic Council. United States.
1294 <https://doi:10.18140/FLX/1669688>. 2020b.
- 1295 Treat, C. C., Anthony Bloom, A., & Marushchak, M. E. Nongrowing season methane emissions—a significant
1296 component of annual emissions across northern ecosystems. *Glob. Change Biol.*, 24(8), 3331–3343.
1297 <https://doi.org/10.1111/gcb.14137>. 2018.
- 1298 Turetsky, M. R., Kotowska, A., Bubier, J., Dise, N. B., Crill, P., Hornibrook, E. R. C., Minkinen, K., Moore, T. R.,
1299 Myers-Smith, I. H., Nykänen, H., Olefeldt, D., Rinne, J., Saarnio, S., Shurpali, N., Tuittila, E.-S., Waddington,
1300 J. M., White, J. R., Wickland, K. P., & Wilkening, M. A synthesis of methane emissions from 71 northern,
1301 temperate, and subtropical wetlands. *Glob. Change Biol.*, 20(7), 2183–2197.
1302 <https://doi.org/10.1111/gcb.12580>. 2014.
- 1303 Ueyama, Masahito, Takashi Hirano, & Yasuhiro Kominami. FLUXNET-CH4 JP-BBY Bibai bog. Japan.
1304 <https://doi:10.18140/FLX/1669646>. 2020.
- 1305 Valach, Alex, Daphne Szutu, Elke Eichelmann, Sara Knox, Joseph Verfaillie, & Dennis Baldocchi. FLUXNET-CH4
1306 US-Tw1 Twitchell Wetland West Pond. United States. <https://doi:10.18140/FLX/1669696>. 2020a.
- 1307 Valach, Alex, Kuno Kasak, Daphne Szutu, Joseph Verfaillie, & Dennis Baldocchi. FLUXNET-CH4 US-Tw5 East
1308 Pond Wetland. United States. <https://doi:10.18140/FLX/1669699>. 2020b.
- 1309 Varlagin, Andrej. FLUXNET-CH4 RU-Fy2 Fyodorovskoye dry spruce. Russian Federation.
1310 <https://doi:10.18140/FLX/1669657>. 2020.
- 1311 Vazquez-Lule, Alma, & Rodrigo Vargas. FLUXNET-CH4 US-StJ St Jones Reserve. United States.
1312 <https://doi:10.18140/FLX/1669695>. 2020.
- 1313 Verma, S. B., Ullman, F. G., Billesbach, D., Clement, R. J., Kim, J., & Verry, E. S. Eddy correlation measurements
1314 of methane flux in a northern peatland ecosystem. *Bound. Lay. Meteorol.*, 58(3), 289–304.
1315 <https://doi.org/10.1007/BF02033829>. 1992.
- 1316 Vesala, Timo, Eeva-Stiina Tuittila, Ivan Mammarella, & Pavel Alekseychik. FLUXNET-CH4 FI-Si2 Siikaneva-2
1317 Bog. Finland. <https://doi:10.18140/FLX/1669639>. 2020a.
- 1318 Vesala, Timo, Eeva-Stiina Tuittila, Ivan Mammarella, & Janne Rinne. FLUXNET-CH4 FI-Sii Siikaneva. Finland.
1319 <https://doi:10.18140/FLX/1669640>. 2020b.

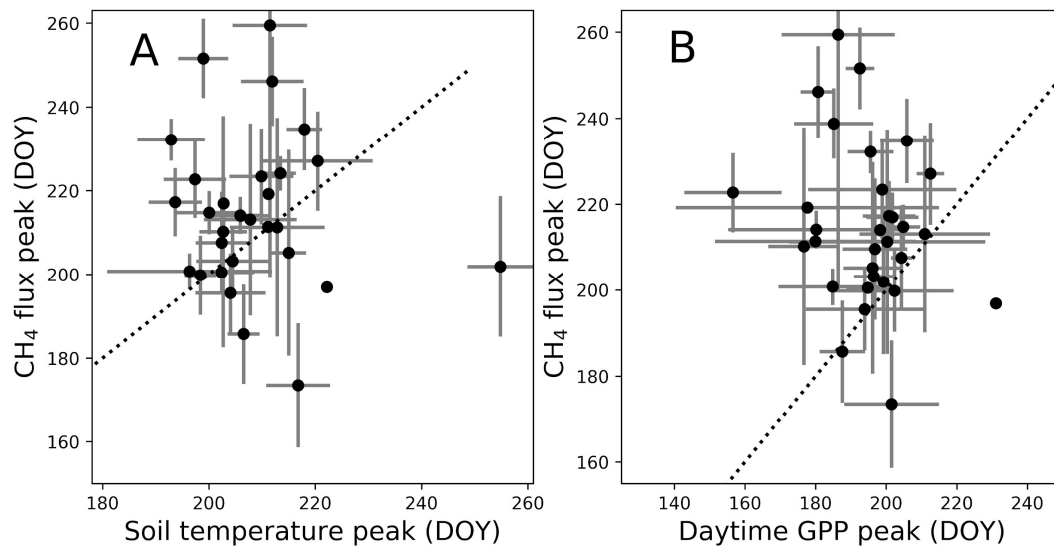


- 1320 Villarreal, S., Guevara, M., Alcaraz-Segura, D., Brunzell, N. A., Hayes, D., Loescher, H. W., & Vargas, R.
1321 Ecosystem functional diversity and the representativeness of environmental networks across the conterminous
1322 United States. *Agr. Forest Meteorol.*, 262, 423–433. <https://doi.org/10.1016/j.agrformet.2018.07.016>. 2018.
- 1323 Villarreal, S., Guevara, M., Alcaraz-Segura, D., & Vargas, R. Optimizing an Environmental Observatory Network
1324 Design Using Publicly Available Data. *J. Geophys. Res.-Biogeo.*, 124(7), 1812–1826.
1325 <https://doi.org/10.1029/2018JG004714>. 2019.
- 1326 Vourlitis, George, Higo Dalmagro, Jose de S. Nogueira, Mark Johnson, & Paulo Arruda. FLUXNET-CH4 BR-Npw
1327 Northern Pantanal Wetland. Brazil. <https://doi.org/10.18140/FLX/1669368>. 2020.
- 1328 Vuichard, N., & Papale, D. Filling the gaps in meteorological continuous data measured at FLUXNET sites with
1329 ERA-Interim reanalysis. *Earth Syst. Sci. Data*, 7(2), 157–171. <https://doi.org/10.5194/essd-7-157-2015>. 2015.
- 1330 Weston, N. B., Dixon, R. E., & Joye, S. B. Ramifications of increased salinity in tidal freshwater sediments:
1331 Geochemistry and microbial pathways of organic matter mineralization. *J. Geophys. Res.*, 111(G1).
1332 <https://doi.org/10.1029/2005jg000071>. 2006.
- 1333 Weston, N. B., Vile, M. A., Neubauer, S. C., & Velinsky, D. J. Accelerated microbial organic matter mineralization
1334 following salt-water intrusion into tidal freshwater marsh soils. *Biogeochemistry*, 102, 135–151.
1335 <https://doi.org/10.1007/s10533-010-9427-4>. 2011.
- 1336 Wik, M., Crill, P. M., Varner, R. K., & Bastviken, D. Multiyear measurements of ebullitive methane flux from three
1337 subarctic lakes. *J. Geophys. Res.-Biogeo.* 118(3), 1307–1321. <https://doi.org/10.1002/jgrg.20103>. 2013.
- 1338 Windham-Myers, Lisamarie, Ellen Stuart-Haëntjens, Brian Bergamaschi, Sara Knox, Frank Anderson, & Kyle
1339 Nakatsuka. FLUXNET-CH4 US-Srr Suisun marsh - Rush Ranch. United States.
1340 <https://doi.org/10.18140/FLX/1669694>. 2020.
- 1341 Wohlfahrt, Georg, Albin Hammerle, & Lukas Hörtnagl. FLUXNET-CH4 AT-Neu Neustift. Austria.
1342 <https://doi.org/10.18140/FLX/1669365>. 2020.
- 1343 Wutzler, T., Lucas-Moffat, A., Migliavacca, M., Knauer, J., Sickel, K., Šigut, L., Menzer, O., & Reichstein, M.
1344 Basic and extensible post-processing of eddy covariance flux data with REdDyProc. *Biogeosciences*, 15, 5015–
1345 5030. <https://doi.org/10.5194/bg-2018-56-sc1>. 2018.
- 1346 Xu, X., Riley, W. J., Koven, C. D., Billesbach, D. P., -W. Chang, R. Y., Commane, R., Euskirchen, E. S., Hartery,
1347 S., Harazono, Y., Iwata, H., McDonald, K. C., Miller, C. E., Oechel, W. C., Poulter, B., Raz-Yaseef, N.,
1348 Sweeney, C., Torn, M., Wofsy, S. C., Zhang, Z., & Zona, D. A multi-scale comparison of modeled and
1349 observed seasonal methane emissions in northern wetlands. *Biogeosciences*, 13(17), 5043–5056.
1350 <https://doi.org/10.5194/bg-13-5043-2016>. 2016.
- 1351 Yvon-Durocher, G., Allen, A. P., Bastviken, D., Conrad, R., Gudas, C., St-Pierre, A., Thanh-Duc, N., & del
1352 Giorgio, P. A. Methane fluxes show consistent temperature dependence across microbial to ecosystem scales.
1353 *Nature*, 507(7493), 488–491. <https://doi.org/10.1038/nature13164>. 2014.
- 1354 Zhang, Z. Fluet-Choinard, E., Jensen, K., McDonald, K., Hugelius, G., Gumbrecht, T., Carrol, M., Prigent, C.,
1355 Bartsch, A., & Poulter, B. Development of a global dataset of Wetland Area and Dynamics for Methane
1356 Modeling (WAD2M). In Review: *Earth Syst. Sci. Data*.
- 1357 Zona, D., Gioli, B., Commane, R., Lindaas, J., Wofsy, S. C., Miller, C. E., Dinardo, S. J., Dengel, S., Sweeney, C.,
1358 Karion, A., Chang, R. Y.-W., Henderson, J. M., Murphy, P. C., Goodrich, J. P., Moreaux, V., Liljedahl, A.,
1359 Watts, J. D., Kimball, J. S., Lipson, D. A., & Oechel, W. C. Cold season emissions dominate the Arctic tundra
1360 methane budget. *P. Natl. A. Sci. USA.*, 113(1), 40–45. <https://doi.org/10.1073/pnas.1516017113>. 2016.
- 1361 Zona, Donatella, & Walter C Oechel. FLUXNET-CH4 US-Atq Atkasuk. United States.
1362 <https://doi.org/10.18140/FLX/1669663>. 2020a.
- 1363 Zona, Donatella, & Walter C Oechel. FLUXNET-CH4 US-Beo Barrow Environmental Observatory (BEO) tower.
1364 United States. <https://doi.org/10.18140/FLX/1669664>. 2020b.
- 1365 Zona, Donatella, & Walter C Oechel. FLUXNET-CH4 US-Bes Barrow-Bes (Biocomplexity Experiment South
1366 tower). United States. <https://doi.org/10.18140/FLX/1669665>. 2020c.
- 1367 Zona, Donatella, & Walter C Oechel. FLUXNET-CH4 US-Ivo Ivotuk. United States.
1368 <https://doi.org/10.18140/FLX/1669679>. 2020d.



1369 APPENDIX A

1370



1371

1372

1373 Figure A1: Peak CH₄ flux timing versus peak GPP timing (A) and peak soil temperature timing (B). Points represent site
1374 average and error bars represent standard deviations.

1375



1376 **APPENDIX B**

1377

1378 **Table B1:** Data variable names, descriptions, and units

1379 **FLUXNET-CH4 Data Variables**

1380 This webpage describes data variables and file formatting for the FLUXNET-CH4 Community
1381 Product.

1382 **1. Data Variable: Base names**

1383 Base names indicate fundamental quantities that are either measured or calculated/derived.
1384 They can also indicate quantified quality information.

1385 Table 1. Base names for data variables

<i>Variable</i>	<i>Description</i>	<i>Units</i>
TIMEKEEPING		
TIMESTAMP_STA RT	ISO timestamp start of averaging period, used in half-hourly data	YYYYMMDDHHMM
TIMESTAMP_END	ISO timestamp end of averaging period, used in half-hourly data	YYYYMMDDHHMM
TIMESTAMP	ISO timestamp used in daily aggregation files	YYYYMMDD
MET_RAD		
SW_IN	Shortwave radiation, incoming	W m ⁻²
SW_OUT	Shortwave radiation, outgoing	W m ⁻²
LW_IN	Longwave radiation, incoming	W m ⁻²
LW_OUT	Longwave radiation, outgoing	W m ⁻²



PPFD_IN	Photosynthetic photon flux density, incoming	$\mu\text{molPhoton m}^{-2} \text{ s}^{-1}$
PPFD_OUT	Photosynthetic photon flux density, outgoing	$\mu\text{molPhoton m}^{-2} \text{ s}^{-1}$
NETRAD	Net radiation	W m^{-2}

MET_WIND

USTAR	Friction velocity	m s^{-1}
WD	Wind direction	Decimal degrees
WS	Wind speed	m s^{-1}

HEAT

H	Sensible heat turbulent flux (with storage term if provided by site PI)	W m^{-2}
LE	Latent heat turbulent flux (with storage term if provided by site PI)	W m^{-2}
G	Soil heat flux	W m^{-2}

MET_ATM

PA	Atmospheric pressure	kPa
TA	Air temperature	deg C



VPD	Vapor Pressure Deficit	hPa
RH	Relative humidity, range 0-100	%
MET_PRECIP		
P	Precipitation	mm
PRODUCTS		
NEE	Net Ecosystem Exchange	$\mu\text{molCO}_2 \text{ m}^{-2} \text{ s}^{-1}$
GPP	Gross primary productivity	$\mu\text{molCO}_2 \text{ m}^{-2} \text{ s}^{-1}$
RECO	Ecosystem respiration	$\mu\text{molCO}_2 \text{ m}^{-2} \text{ s}^{-1}$
GASES		
FCH4	Methane (CH4) turbulent flux (no storage correction)	$\text{nmolCH}_4 \text{ m}^{-2} \text{ s}^{-1}$
MET_SOIL		
TS	Soil temperature	deg C
WTD	Water table depth (negative values indicate below the surface)	m



1387 2. Data Variable: Qualifiers

1388 Qualifiers are suffixes appended to variable base names that provide additional information
1389 about the variable. For example, the `_DT` qualifier in the variable label `GPP_DT` indicates that
1390 gross primary production (GPP) has been partitioned using the flux partitioning method from
1391 Lasslop et al. 2010.

1392 Multiple qualifiers can be added, and they must **follow the order in which they are presented**
1393 **here**.

1394 2.1. Qualifiers: General

1395 General qualifiers indicate additional information about a variable.

1396 · `_F` : Variable has been gap-filled by the FLUXNET-CH4 team. Gaps in meteorological
1397 variables (including air temperature (TA), incoming shortwave (SW_IN) and longwave (LW_IN)
1398 radiation, vapor pressure deficit (VPD), pressure (PA), precipitation (P), and wind speed (WS))
1399 were filled with ERA-Interim (ERA-I) reanalysis data ((Vuichard and Papale 2015)). Other
1400 variables were filled using the MDS approach in REddyProc (see Delwiche et al. 2020 for more
1401 details).

1402 · `_DT` : Variable acquired using the flux partitioning method from (Lasslop et al. 2010), with
1403 values estimated by fitting the light-response curve.

1404 · `_NT` : Variable acquired using the flux partitioning method from (Reichstein et al. 2005), with
1405 values estimated from night-time data and extrapolated to day time.

1406 · `_RANDUNC`: Random uncertainty introduced from several different sources including errors
1407 associated with the flux measurement system (gas analyzer, sonic anemometer, data acquisition
1408 system, flux calculations), errors associated with turbulent transport, and statistical errors relating
1409 to the location and activity of the sites of flux exchange (“footprint heterogeneity”) (Hollinger and
1410 Richardson 2005).

1411 · `_ANNOPTLM` : Gap-filled variable using an artificial neural net routine from Matlab with the
1412 Levenberg-Marquardt algorithm as the training function, and parameters optimized across runs
1413 (more detail in (Sara Helen Knox et al. 2016; Sara H. Knox et al. 2019)).

1414 · `_UNC` : Uncertainty introduced from ANNOPTLM gap-filling routine, as described in Knox et
1415 al. 2016 and Knox et al. 2019.

1416 · `_QC` : Reports quality checks on FCH4 gap-filled data (`_ANNOPTLM`) based on length of
1417 data gap. 1 = data gap shorter than 2 months, 3 = data gap exceeds 2 months which could lead
1418 to poor quality gap-filled data. Nondimensional.

1419

1420 2.2. Qualifiers: Positional (`_V`)

1421 Positional qualifiers are used to indicate relative positions of observations at the site. For
1422 FLUXNET-CH4, positional qualifiers are used to distinguish soil temperature probes for sites with
1423 more than one probe. Probe depths for each positional qualifier per site are included in the



1424 metadata file included with data download and also in Table B6 of Delwiche et al. 2020. For
1425 sites where the original database file release in Ameriflux, AsiaFlux, or EuroFlux contains
1426 multiple probes at the same _V depth, we average values and report only the average for each
1427 _V position. The one exception to this is site US-UAF where the original positional qualifier from
1428 the data we downloaded from Ameriflux had different depths for the same qualifier. We still
1429 averaged the probe data, so _V qualifiers from US-UAF represent an average of more than one
1430 depth.

1431 3.0 Missing data

1432 Missing data are reported using -9999. Data for all days in a leap year are reported.

1433 4.0 References

- 1434 Hollinger, D. Y., and A. D. Richardson. 2005. "Uncertainty in Eddy Covariance Measurements
1435 and Its Application to Physiological Models." *Tree Physiology* 25 (7): 873–85.
- 1436 Knox, Sara Helen, Jaclyn Hatala Matthes, Cove Sturtevant, Patricia Y. Oikawa, Joseph
1437 Verfaillie, and Dennis Baldocchi. 2016. "Biophysical Controls on Interannual Variability in
1438 Ecosystem-Scale CO₂ and CH₄ Exchange in a California Rice Paddy." *Journal of
1439 Geophysical Research: Biogeosciences*. <https://doi.org/10.1002/2015jg003247>.
- 1440 Knox, Sara H., Robert B. Jackson, Benjamin Poulter, Gavin McNicol, Etienne Fluet-Chouinard,
1441 Zhen Zhang, Gustaf Hugelius, et al. 2019. "FLUXNET-CH₄ Synthesis Activity: Objectives,
1442 Observations, and Future Directions." *Bulletin of the American Meteorological Society* 100
1443 (12): 2607–32.
- 1444 Lasslop, Gitta, Markus Reichstein, Dario Papale, Andrew D. Richardson, Almut Arneth, Alan
1445 Barr, Paul Stoy, and Georg Wohlfahrt. 2010. "Separation of Net Ecosystem Exchange into
1446 Assimilation and Respiration Using a Light Response Curve Approach: Critical Issues and
1447 Global Evaluation." *Global Change Biology*. [https://doi.org/10.1111/j.1365-
1448 2486.2009.02041.x](https://doi.org/10.1111/j.1365-2486.2009.02041.x).
- 1449 Reichstein, Markus, Eva Falge, Dennis Baldocchi, Dario Papale, Marc Aubinet, Paul Berbigier,
1450 Christian Bernhofer, et al. 2005. "On the Separation of Net Ecosystem Exchange into
1451 Assimilation and Ecosystem Respiration: Review and Improved Algorithm." *Global Change
1452 Biology*. <https://doi.org/10.1111/j.1365-2486.2005.001002.x>.
- 1453 Vuichard, N., and D. Papale. 2015. "Filling the Gaps in Meteorological Continuous Data
1454 Measured at FLUXNET Sites with ERA-Interim Reanalysis." *Earth System Science Data*.
1455 <https://doi.org/10.5194/essd-7-157-2015>.



Table B2-A: Site metadata, select data, and DOI links

	SITE_ID	SITE_NAME	SITE_PERSONNEL	COUNTRY	LAT	LONG	DATA_DOI	YEAR_S TART	YEAR_ END	UTC_O FFSET	ORIGINAL_D ATA_SOURC E
1	AT-Neu	Neustift	Georg Wohlfahrt	Austria	47.117	11.318	10.18140/FLX/1669365	2010	2012	1	EuroFlux
2	BR-Npw	Northern Pantanal Wetland	George Yourlitis	Brazil	-16.498	-56.412	10.18140/FLX/1669368	2013	2016	-4	AmeriFlux
3	BW-Gum	Guma	Carole Helfter	Botswana	-18.965	22.371	10.18140/FLX/1669370	2018	2018	2	EuroFlux
4	BW-Nxr	Nxaraga	Carole Helfter	Botswana	-19.548	23.179	10.18140/FLX/1669518	2018	2018	2	EuroFlux
5	CA-SCB	Scotty Creek Bog	Oliver Sonnentag, Manuel Helbig	Canada	61.309	-121.298	10.18140/FLX/1669613	2014	2017	-7	AmeriFlux
6	CA-SCC	Scotty Creek Landscape	Oliver Sonnentag, Manuel Helbig	Canada	61.308	-121.299	10.18140/FLX/1669628	2013	2016	-7	AmeriFlux
7	CH-Cha	Chamau	Nina Buchmann	Switzerland	47.210	8.410	10.18140/FLX/1669629	2012	2016	1	EuroFlux
8	CH-Dav	Davos	Nina Buchmann	Switzerland	46.815	9.856	10.18140/FLX/1669630	2016	2017	1	EuroFlux
9	CH-Oe2	Oensingen crop	Nina Buchmann	Switzerland	47.286	7.734	10.18140/FLX/1669631	2018	2018	1	EuroFlux
10	CN-Hgu	Hongyuan	Shuli Niu, Weinan Chen	China	32.845	102.590	10.18140/FLX/1669632	2015	2017	8	EuroFlux
11	DE-Dgw	Dagowsee	Torsten Sachs	Germany	53.151	13.054	10.18140/FLX/1669633	2015	2018	1	EuroFlux
12	DE-Hte	Huetelmoor	Gerald Jurasinski	Germany	54.210	12.176	10.18140/FLX/1669634	2011	2018	1	EuroFlux
13	DE-SFN	Schechenfliz Nord	Hans Peter Schmid	Germany	47.806	11.328	10.18140/FLX/1669635	2012	2014	1	EuroFlux
14	DE-Zrk	Zamekow	Torsten Sachs	Germany	53.876	12.889	10.18140/FLX/1669636	2013	2018	1	EuroFlux
15	FI-Hyy	Hyytiälä	Timo Vesala, Ivan Mammarella	Finland	61.847	24.295	10.18140/FLX/1669637	2016	2016	2	EuroFlux
16	FI-Lom	Lompolojankka	Annalea Lohila Timo Vesala, Ivan Mammarella, Eeva-	Finland	67.997	24.209	10.18140/FLX/1669638	2006	2010	2	EuroFlux
17	FI-Si2	Siikaneva-2 Bog	Stiina Tuittila Timo Vesala, Ivan Mammarella, Eeva-	Finland	61.837	24.197	10.18140/FLX/1669639	2012	2016	2	EuroFlux
18	FI-Sii	Siikaneva	Stiina Tuittila	Finland	61.833	24.193	10.18140/FLX/1669640	2013	2018	2	EuroFlux
19	FR-Lgt	La Guette	Adrien Jacotot, Sébastien Gogo, Fatima Laggoun-Défarge, Laurent Perdereau	France	47.323	2.284	10.18140/FLX/1669641	2017	2018	1	EuroFlux



20	HK-MPM	Mai Po Mangrove	Derrick Lai, Jiangong Liu	Hong Kong	22.498	114.029	10.18140/FLX/1669642	2016	2018	8	EuroFlux
21	ID-Pag	Palangkaraya undrained forest	Takashi Hirano	Indonesia	-2.320	113.900	10.18140/FLX/1669643	2016	2017	7	EuroFlux
22	IT-BCi	Borgo Cioffi	Vincenzo Magliulo	Italy	40.524	14.957	10.18140/FLX/1669644	2017	2018	1	EuroFlux
23	IT-Cas	Castellaro	Giovanni Manca, Ignacio Goded, Carsten Gruening, Ana Meijide	Italy	45.070	8.718	10.18140/FLX/1669645	2009	2010	1	EuroFlux
24	JP-BBY	Bibai bog	Masahito Ueyama	Japan	43.323	141.811	10.18140/FLX/1669646	2015	2018	9	AsiaFlux
25	JP-Mse	Mase rice paddy field	Akira Miyata	Japan	36.054	140.027	10.18140/FLX/1669647	2012	2012	9	AsiaFlux
26	JP-SWL	Suwa Lake	Hiroki Iwata	Japan	36.047	138.108	10.18140/FLX/1669648	2016	2016	9	AsiaFlux
27	KR-CRK	Cheorwon Rice paddy	Youngryel Ryu, Minseok Kang	Korea	38.201	127.251	10.18140/FLX/1669649	2015	2018	9	AsiaFlux
28	MY-MLM	Maludam National Park	Angela C. I. Tang, Guan Xhuan Wong, Lullie Melling	Malaysia	1.454	111.149	10.18140/FLX/1669650	2014	2015	8	AsiaFlux
29	NL-Hor	Horstermeer	Han Dolman	Netherlands	52.240	5.071	10.18140/FLX/1669651	2007	2009	1	EuroFlux
30	NZ-Kop	Kopuatai	Dave Campbell	New Zealand	-37.388	175.554	10.18140/FLX/1669652	2012	2015	13	OzFlux
31	PH-RIF	Philippines Rice Institute flooded	Ma. Carmelita Alberto	Philippines	14.141	121.265	10.18140/FLX/1669653	2012	2014	8	EuroFlux
32	RU-Ch2	Chersky reference	Matthias Goeckede	Russia	68.617	161.351	10.18140/FLX/1669654	2014	2016	11	EuroFlux
33	RU-Che	Cherski	Matthias Goeckede	Russia	68.613	161.341	10.18140/FLX/1669655	2014	2016	11	EuroFlux
34	RU-Cok	Chokurdakh	Han Dolman	Russia	70.829	147.494	10.18140/FLX/1669656	2008	2016	11	EuroFlux
35	RU-Fy2	Fyodorovskoye dry spruce	Andrej Varlagin	Russia	56.448	32.902	10.18140/FLX/1669657	2015	2018	3	EuroFlux
36	SE-Deg	Degero	Matthias Peichi, Mats Nilsson	Sweden	64.182	19.557	10.18140/FLX/1669659	2014	2018	1	EuroFlux
37	UK-LBT	London_BT	Carole Helfter	UK	51.522	-0.139	10.18140/FLX/1670207	2011	2014	0	EuroFlux
38	US-A03	ARM-AMF3-Oliktok	Ryan Sullivan, David Cook, David Billesbach	USA	70.495	-149.882	10.18140/FLX/1669661	2015	2018	-9	AmeriFlux
39	US-A10	ARM-NSA-Barrow	Ryan Sullivan, David Cook, David Billesbach	USA	71.324	-156.615	10.18140/FLX/1669662	2012	2018	-9	AmeriFlux
40	US-Atq	Atqasuk	Donatella Zona	USA	70.470	-157.409	10.18140/FLX/1669663	2013	2016	-9	AmeriFlux



41	US-Beo	Barrow Environmental Observatory (BEO) tower	Donatella Zona	USA	71.281	-156.612	10.18140/FLX/1669664	2013	2014	-8	AmeriFlux
42	US-Bes	Barrow-Bes (Biocomplexity Experiment South tower)	Donatella Zona	USA	71.281	-156.597	10.18140/FLX/1669665	2013	2015	-8	AmeriFlux
43	US-Bi1	Bouldin Island Alfalfa	Dennis Baldocchi	USA	38.099	-121.499	10.18140/FLX/1669666	2016	2018	-8	AmeriFlux
44	US-Bi2	Bouldin Island corn	Dennis Baldocchi	USA	38.109	-121.535	10.18140/FLX/1669667	2017	2018	-8	AmeriFlux
45	US-BZB	Bonanza Creek Thermokarst Bog	Eugenie Euskirchen	USA	64.696	-148.321	10.18140/FLX/1669668	2014	2016	-9	AmeriFlux
46	US-BZF	Bonanza Creek Rich Fen	Eugenie Euskirchen	USA	64.704	-148.313	10.18140/FLX/1669669	2014	2016	-9	AmeriFlux
47	US-BZS	Bonanza Creek Black Spruce	Eugenie Euskirchen	USA	64.696	-148.324	10.18140/FLX/1669670	2015	2016	-9	AmeriFlux
48	US-CRT	Curtice Walter-Berger cropland	Jiquen Chen, Housen Chu	USA	41.628	-83.347	10.18140/FLX/1669671	2011	2012	-5	AmeriFlux
49			Charless Ross Hinkle, Rosvel Bracho, Scott Graham, Brian Benschoter	USA	28.052	-81.436	10.18140/FLX/1669672	2013	2017	-5	AmeriFlux
50	US-DPW	Disney Wilderness Preserve Wetland	Patty Oikawa	USA	37.616	-122.114	10.18140/FLX/1669673	2018	2018	-8	AmeriFlux
51	US-EDN	Eden Landing Ecological Reserve		USA	63.878	-149.254	10.18140/FLX/1669674	2015	2018	-9	AmeriFlux
52	US-EML	Eight Mile Lake Permafrost thaw gradient, Healy Alaska.	Ted Schuur	USA	45.204	-68.740	10.18140/FLX/1669675	2012	2018	-5	AmeriFlux
53	US-Ho1	Howland Forest (main tower)	Andrew Richardson, David Hollinger	USA	34.585	-91.752	10.18140/FLX/1669676	2017	2017	-6	AmeriFlux
54	US-HRA	Humnoke Farm Rice Field – Field A	Benjamin Runkle	USA	34.589	-91.752	10.18140/FLX/1669677	2017	2017	-6	AmeriFlux
55	US-HRC	Humnoke Farm Rice Field – Field C	Benjamin Runkle	USA	68.606	-149.311	10.18140/FLX/1669678	2014	2016	-9	AmeriFlux
56	US-ICs	Innavait Creek Watershed Wet Sedge Tundra	Eugenie Euskirchen	USA	68.487	-155.750	10.18140/FLX/1669679	2013	2016	-9	AmeriFlux
57	US-Ivo	Ivotuk	Donatella Zona	USA	29.501	-90.445	10.18140/FLX/1669680	2011	2012	-6	AmeriFlux
58	US-LA1	Pointe-aux-Chenes Brackish Marsh	Ken Krauss	USA	29.859	-90.287	10.18140/FLX/1669681	2011	2013	-6	AmeriFlux
59	US-LA2	Salvador WMA Freshwater Marsh	Ken Krauss	USA	46.083	-89.979	10.18140/FLX/1669682	2014	2018	-6	AmeriFlux
	US-Los	Lost Creek	Ankur Desai	USA							



60	US-MAC	MacArthur Agro-Ecology	Jed Sparks, Sam Chamberlain	USA	27.163	-81.187	10.18140/FLX/1669683	2013	2015	-5	AmeriFlux
61	US-MRMI	Marsh Resource Meadowlands Mitigation Bank	Karina Schäfer	USA	40.816	-74.044	10.18140/FLX/1669684	2012	2013	5	AmeriFlux
62	US-Myb	Mayberry Wetland	Dennis Baldocchi	USA	38.050	-121.765	10.18140/FLX/1669685	2010	2018	-8	AmeriFlux
63	US-NC4	NC_AlligatorRiver	Asko Noormets	USA	35.788	-75.904	10.18140/FLX/1669686	2012	2016	-5	AmeriFlux
64	US-NGB	NGEE Arctic Barrow	Margaret Torn	USA	71.280	-156.609	10.18140/FLX/1669687	2012	2018	-9	AmeriFlux
65	US-NGC	NGEE Arctic Council	Margaret Torn	USA	64.861	-163.701	10.18140/FLX/1669688	2017	2018	-9	AmeriFlux
66	US-ORv	Olentangy River Wetland Research Park	Gil Bohrer	USA	40.020	-83.018	10.18140/FLX/1669689	2011	2015	-5	AmeriFlux
67	US-OWC	Old Woman Creek	Gil Bohrer	USA	41.380	-82.512	10.18140/FLX/1669690	2015	2016	-5	AmeriFlux
68	US-PFa	Park Falls/WLEF	Ankur Desai	USA	45.946	-90.272	10.18140/FLX/1669691	2010	2018	-6	AmeriFlux
69	US-Snd	Sherman Island	Dennis Baldocchi	USA	38.037	-121.754	10.18140/FLX/1669692	2010	2015	-8	AmeriFlux
70	US-Sne	Sherman Island Restored Wetland	Dennis Baldocchi	USA	38.037	-121.755	10.18140/FLX/1669693	2016	2018	-8	AmeriFlux
71	US-Srr	Suisun marsh - Rush Ranch	Lisamarie Windham-Myers	USA	38.201	-122.026	10.18140/FLX/1669694	2014	2017	-8	AmeriFlux
72	US-SJ	St Jones Reserve	Rodrigo Vargas	USA	39.088	-75.437	10.18140/FLX/1669695	2016	2016	-5	AmeriFlux
73	US-Tw1	Twitchell Wetland West Pond	Dennis Baldocchi	USA	38.107	-121.647	10.18140/FLX/1669696	2011	2018	-8	AmeriFlux
74	US-Tw3	Twitchell Alfalfa	Dennis Baldocchi	USA	38.116	-121.647	10.18140/FLX/1669697	2013	2014	-8	AmeriFlux
75	US-Tw4	Twitchell East End Wetland	Dennis Baldocchi	USA	38.103	-121.641	10.18140/FLX/1669698	2013	2018	-8	AmeriFlux
76	US-Tw5	East Pond Wetland	Dennis Baldocchi	USA	38.107	-121.643	10.18140/FLX/1669699	2018	2018	-8	AmeriFlux
77	US-Twt	Twitchell Island	Dennis Baldocchi	USA	38.109	-121.653	10.18140/FLX/1669700	2009	2017	-8	AmeriFlux
78	US-Uaf	University of Alaska, Fairbanks	Masahito Ueyama	USA	64.866	-147.856	10.18140/FLX/1669701	2011	2018	-9	AmeriFlux
79	US-WPT	Winous Point North Marsh	Jiquen Chen, Housen Chu	USA	41.465	-82.996	10.18140/FLX/1669702	2011	2013	-5	AmeriFlux

Column Descriptions

SITE_ID
 SITE_NAME
 SITE_PERSONNEL
 COUNTRY
 LAT
 LON
 Site identification code as assigned by regional flux data network
 Site name determined by site personnel
 People associated with site FLUXNET-CH4 data
 Site country
 Latitude
 Longitude



DATA_DOI
YEAR_START
YEAR_END
UTC_OFFSET
ORIGINAL_DATA_SOURCE

DOI link for site FLUXNET-CH4 data
Year data begins
Year data ends
Site data offset from Coordinated Universal Time (in hours)
Regional network hosting the site methane data that was incorporated into FLUXNET-CH4



Table B2-B: Site metadata, select data, and DOI links

SITE_ID	SITE_CLASSIFICATION	UPLAND_CLASS	IGBP	KOPPEN	MOSS_BROWN	MOSS_SPHAGNUM	AERENCHYMATOUS	ERI_SHRUB	TREE	DOM_VEG	IN_SEASONALITY_ANALYSIS	
1	AT-Neu	Upland	Alpine meadow	GRA	Dfb	0	0	1	0	0	aerenchymatous	0
2	BR-Npw	Swamp	WSA	Aw	0	0	0	1	0	1	tree	0
3	BW-Glum	Swamp	WET	Bsh	0	0	0	1	0	1	aerenchymatous	0
4	BW-Nxr	Swamp	GRA	Bsh	0	0	0	1	0	1	aerenchymatous	0
5	CA-SCB	Bog	WET	Dfc	0	1	1	1	1	0	moss_sphagnum	1
6	CA-SCC	Upland	Needleleaf forest	ENF	Dfc	0	1	0	1	1	tree	0
7	CH-Cha	Upland	Grassland	GRA	Cfb	0	0	1	0	0	aerenchymatous	0
8	CH-Dav	Upland	Needleleaf forest	ENF	ET	1	0	0	1	1	tree	0
9	CH-Oe2	Upland	Crop - wheat	CRO	Cfb	0	0	1	0	0	aerenchymatous	0
10	CN-Hgu	Upland	Alpine meadow	GRA	Cwc	0	0	1	0	0	aerenchymatous	0
11	DE-Dgw	Lake	WAT	Cfb	0	0	0	0	0	0	no vegetation	0
12	DE-Hte	Fen	WET	Dfb	0	0	0	1	0	0	aerenchymatous	1
13	DE-SFN	Bog	WET	Cfb	0	1	1	1	1	1	tree	1
14	DE-Zrk	Fen	WET	Dfb	0	0	0	1	0	0	aerenchymatous	1
15	FI-Hvy	Upland	Needleleaf forest	ENF	Dfc	1	1	0	1	1	tree	0
16	FI-Lom	Fen	WET	Dfc	1	1	1	1	1	0	aerenchymatous	1
17	FI-SI2	Bog	WET	Dfc	0	1	1	1	1	1	moss_sphagnum	1
18	FI-Sii	Fen	WET	Dfc	0	1	1	1	0	0	moss_sphagnum	1
19	FR-LGt	Fen	WET	Cfb	0	1	1	1	1	0	aerenchymatous	0
20	HK-MPM	Mangrove	EBF	Cfa	0	0	0	1	0	1	aerenchymatous	0
21	ID-Pag	Swamp	EBF	Af	0	0	0	1	0	1	tree	0
22	IT-BCi	Upland	Crop - corn	CRO	Csa	0	0	1	0	0	aerenchymatous	0
23	IT-Cas	Rice	CRO	Cfa	0	0	0	1	0	0	aerenchymatous	0
24	JP-BBY	Bog	WET	Dfb	0	1	1	1	1	0	aerenchymatous	1
25	JP-Mse	Rice	CRO	Cfa	0	0	0	1	0	0	aerenchymatous	0
26	JP-SwL	Lake	WAT	Dfb	0	0	0	1	0	0	aerenchymatous	0
27	KR-CRK	Rice	CRO	Dwa	0	0	0	1	0	0	aerenchymatous	0



ERL_SHRUB	Presence/absence (1/0) ericaceous shrubs. Presence/absence designated by Avni Malhotra using site-literature
TREE	Presence/absence (1/0) trees. Presence/absence designated by Avni Malhotra using site-literature
DOM_VEG	Dominant vegetation type in tower footprint. Dom_veg provided to Avni Malhotra by site personnel via survey, except 15 sites where Pls did not answer and Avni Malhotra estimated dominant vegetation type based on site-literature
IN_SEASONALITY_ANALYSIS	Is site in freshwater wetland seasonality analysis? 1 = yes, 0 = no.



Table B2-C: Site metadata, select data, and DOI links

SITE_ID	Mean_Air_Temp_C	Mean_Air_Temp_stddev_C	Ann_Flux_T g_CH4-C_m-2	Ann_Flux_s tdev_g_CH4-C_m-2	JFM_flux_g_CH4-C_m-2	JFM_flux_s tdev_g_CH4-C_m-2	AMJ_flux_g_CH4-C_m-2	AMJ_flux_s tdev_g_CH4-C_m-2	JAS_flux_g_CH4-C_m-2	JAS_flux_s tdev_g_CH4-C_m-2	OND_flux_g_CH4-C_m-2	OND_flux_s tdev_g_CH4-C_m-2
1	6.60	0.51	0.32	0.09	0.03	0.05	0.04	0.16	0.07	0.09	0.01	0.01
2	25.44	0.73	19.21	2.45	9.68	1.46	8.52	1.15	0.01	0.16	0.15	0.15
3	22.79		51.73				19.32					
4	23.06		47.32				8.88		16.90		18.09	
5	-0.75	1.92	10.67	1.34			2.96	0.70	6.58	0.77	1.16	0.11
6	-0.24	2.04	6.15	1.05			1.79	0.45	3.41	0.67		
7	9.74	0.54	2.95	0.88	0.75	0.18	0.99	0.37	0.60	0.28	0.61	0.25
8	4.37	0.09	1.21		0.28	0.05	0.37	0.21	0.13	0.24	0.24	
9	11.00		0.29					0.14	0.14	0.13	0.13	
10	3.77	1.31	0.82	0.01			0.23	0.04	0.28	0.15	0.15	
11	9.72	0.38	8.97	2.06	0.07	0.06	1.49	0.57	4.15	0.76	2.51	1.05
12	10.04	0.54	48.11	7.41	2.98	0.72	17.18	3.66	24.28	4.07	6.17	1.46
13	8.28	0.72	3.62		0.43	0.10	0.23		1.67	0.43	0.72	0.25
14	9.55	0.51	30.53	0.96	1.18	0.24	12.27	1.55	16.18	1.47	1.51	0.56
15	4.36								-0.02			
16	-0.35	0.78	15.58	1.83	0.93	0.22	3.75	0.51	9.49	1.25	1.68	0.24
17	5.14	0.84	9.74	0.67			2.71	0.59	5.83	1.15	1.19	0.08
18	4.72	0.42	12.43	3.36	0.68	0.11	3.34	0.75	6.79	2.90	1.58	0.42
19	11.07	0.37	2.45		0.02		1.09		0.85		0.29	
20	23.75	0.10	11.09	0.51	0.97	0.15	2.33	0.52	5.56	0.34	2.95	0.26
21	26.57	0.19	0.09	0.00	0.19		0.13		-0.24		0.05	
22	16.69	0.39			-5.18						-2.69	
23	12.58	0.58	21.62	5.40	0.60	0.15	5.59	3.71	15.31	2.24	0.42	0.12
24	7.11	0.44	15.19	5.15	1.60	0.39	2.61	0.97	8.27	2.60	3.67	0.03
25	13.75		9.50				1.59		7.42		0.45	
26	11.67		66.68						39.86		18.53	
27	10.96	0.46	27.92	1.81	0.92	0.15	8.81	0.92	16.69	1.77	1.25	0.11
28	27.09	0.11	9.55		3.28		2.60	0.02	1.62		2.34	
29	10.75	0.60										
30	13.68	0.28	17.34	4.46	3.99	0.84	3.03	1.63	3.63	0.52	5.87	0.30



31	PH-RIF	26.54	0.15	12.41	3.57	1.02	2.58	2.66	5.53	0.01	3.34	0.28
32	RU-Ch2	-9.88	1.26	6.43	0.79	0.29	0.87	0.09	4.65	0.48	1.44	0.04
33	RU-Che	-9.77	1.25	4.09	0.22	0.37	0.47	0.08	2.18	0.12	1.19	
34	RU-Cok	-12.38	0.92	4.45			0.74	0.09	3.42			
35	RU-Fy2	5.80	0.53	3.50	1.88	1.65	-0.27	0.04	-0.39	0.10	2.36	1.32
36	SE-Deg	2.57	0.77	10.74	0.88	0.59	3.30	0.29	5.70	0.78	1.44	0.09
37	UK-LBT	10.62	0.78	46.54	5.61	13.70	12.52		12.26	1.66	14.04	1.87
38	US-A03	-7.15	0.66	5.81	2.06		1.27	0.19	3.25	0.32		
39	US-A10								1.08			
40	US-Atq	-10.88	2.23	1.77	0.03	0.00	0.30	0.07	1.05	0.03	0.55	
41	US-Beo	-9.50	0.20	2.74	0.09	0.09	0.27		1.77		0.69	0.12
42	US-Bes	-10.46	0.21	3.19	0.18	0.09	0.58	0.26	2.20	0.18	0.71	
43	US-Bi1	13.87	1.20	0.69	0.45	0.43	-0.07	0.02	-0.13		0.17	0.05
44	US-Bi2	15.01	0.28	1.28	0.59	0.66	0.30	0.21	0.10	0.06	0.54	0.02
45	US-BZB	-0.62	0.55	9.05	2.23		2.41	0.39	6.06	1.43		
46	US-BZF	-0.31	0.55	8.72	2.98		3.21	2.77	6.35	2.24		
47	US-BZS	0.26	0.68	0.78	0.15		0.23	0.01	0.53	0.11		
48	US-CRT	11.32	0.91	2.21	0.00	0.58			0.26		0.59	
49	US-DPW	22.23	0.41	48.71	8.84	1.53	11.27	2.75	27.64	7.55	12.90	2.54
50	US-EDN	14.99		-0.04			-0.19		0.16			
51	US-EML	-1.72	3.76	0.59	0.39	-0.03	0.06	0.17	0.35	0.12	0.27	
52	US-H01	6.48	1.32	-0.16	0.09	-0.04	-0.03	0.02	-0.02	0.05	-0.07	0.02
53	US-HRA	19.36		-0.24			1.28		6.08			
54	US-HRC	20.23		-0.24			3.07		8.38			
55	US-ICs	-6.02	0.48						1.23	0.30		
56	US-Ivo	-8.27	0.54	4.90	0.95	0.70	0.80	0.05	2.55	0.54	1.26	0.42
57	US-LA1	24.12	0.42	12.68	0.68	0.68	2.27		7.58		1.39	1.08
58	US-LA2	20.34	4.43	34.81	19.34	4.27	14.50	2.18	21.72	2.75	6.96	0.79
59	US-Los	5.01	1.23	6.51	1.28	0.36	1.71	0.46	3.57	0.96	0.81	0.25
60	US-MAC	23.15	0.96	15.82	10.34	1.32	3.71	2.07	14.70	5.53	2.81	0.25
61	US-MRM	13.14	0.88	0.34	0.05	0.09	0.07	0.01	0.11	0.01		
62	US-MYb	15.53	0.58	47.88	14.90	4.51	14.12	5.54	22.04	7.87	6.52	3.17
63	US-NC4	16.74	0.85	33.89	17.41	0.80	5.70	1.62	20.41	9.80	6.77	2.19
64	US-NGB	-9.45	0.92	2.41	0.15		0.26	0.15	2.00	0.26		



65	US-NGC	1.21	0.82	2.52	0.00	0.88	0.10	2.55	0.93	0.86	0.41	0.99	0.17
66	US-ORV	12.20	0.92	7.20	2.51	0.88	0.10	2.55	0.93	3.14	1.16	0.99	0.17
67	US-OWC	13.02	1.72	113.99				31.03		66.03	10.07	9.81	
68	US-PFa	5.42	1.24	0.54	0.25	0.15	0.05	0.39	0.19	0.00	0.00	1.74	1.14
69	US-Snd	14.76	1.16	4.71	1.71	2.00	1.79	1.11	0.74	1.35	0.61	4.71	3.54
70	US-Sne	15.04	0.45	42.80	4.48	2.44	0.71	14.95	5.12	12.61	10.68	4.71	3.54
71	US-Srr	15.93	0.45	0.83	0.08	0.09	0.06	0.31	0.04	0.42	0.09	0.08	0.07
72	US-SU	13.96		9.55				1.40		5.24		2.92	
73	US-Tw1	15.16	0.74	39.51	11.03	4.92	1.91	10.13	3.74	18.02	4.08	7.11	2.49
74	US-Tw3	16.04	0.87									0.29	
75	US-Tw4	15.52	0.56	32.54	11.74	4.39	1.75	9.49	4.83	12.78	6.07	5.89	1.83
76	US-Tw5	15.03		59.72				21.49		29.78		8.45	
77	US-Twt	14.26	1.71	12.07	2.75	3.07	1.10	1.05	0.59	5.49	3.15	1.73	0.40
78	US-Uaf	-2.87	1.03	0.53	0.19			0.07		0.33	0.12		
79	US-WPT	11.40	0.99	49.59	7.48	1.66	0.22	16.31	3.99	28.75	3.05	3.26	0.12

Column Descriptions

SITE_ID	Site identification code as assigned by regional flux data network
Mean_Air_Temp_C	Mean annual air temperature (C)
Ann_Flux_g_CH4-C_m-2	Mean annual methane flux (g CH4-C/m ² /year)
JFM_flux_g_CH4-C_m-2	Mean methane flux in January, February, March (gCH4-C/m ² /year)
AMJ_flux_g_CH4-C_m-2	Mean methane flux in April, May, June (gCH4-C/m ² /year)
JAS_flux_g_CH4-C_m-2	Mean methane flux in July, August, September (gCH4-C/m ² /year)
OND_flux_g_CH4-C_m-2	Mean methane flux in October, November, December (gCH4-C/m ² /year)
Mean_Air_Temp_stddev_C	Standard deviation of annual air temperature (C)
Ann_Flux_stddev_g_CH4-C_m-2	Standard deviation of annual methane flux (gCH4-C/m ² /year)
JFM_flux_stddev_g_CH4-C_m-2	Standard deviation of methane flux in January, February, March (gCH4-C/m ² /year)
AMJ_flux_stddev_g_CH4-C_m-2	Standard deviation of methane flux in April, May, June (gCH4-C/m ² /year)
JAS_flux_stddev_g_CH4-C_m-2	Standard deviation of methane flux in July, August, September (gCH4-C/m ² /year)
OND_flux_stddev_g_CH4-C_m-2	Standard deviation of methane flux in October, November, December (gCH4-C/m ² /year)



Table B2-D: Site metadata, select data, and DOI links

	SITE_ID	SOIL_TEMP_PROBE_DEPTHS
1	AT-Neu	TS_1 = -0.05cm; TS_2 = -0.1cm; TS_3 = -0.2cm;
2	BR-Npw	
3	BW-Gum	
4	BW-Nxr	
5	CA-SCB	TS_1 = 0cm; TS_2 = -0.02cm; TS_3 = -0.04cm; TS_4 = -0.08cm; TS_5 = -0.16cm; TS_6 = -0.32cm; TS_7 = -0.64cm; TS_8 = -1.28cm;
6	CA-SCC	TS_1 = -0.1cm; TS_2 = -0.15cm; TS_3 = -0.2cm; TS_4 = -0.25cm; TS_5 = -0.3cm; TS_6 = -0.5cm; TS_7 = -0.6cm; TS_8 = -0.7cm;
7	CH-Cha	TS_1 = -0.01cm; TS_2 = -0.02cm; TS_3 = -0.04cm; TS_4 = -0.07cm; TS_5 = -0.1cm; TS_6 = -0.15cm; TS_7 = -0.25cm; TS_8 = -0.4cm; TS_9 = -0.95cm;
8	CH-Dav	TS_1 = -0.05cm; TS_2 = -0.15cm; TS_3 = -0.5cm;
9	CH-Oe2	TS_1 = -0.05cm; TS_2 = -0.1cm; TS_3 = -0.15cm; TS_5 = -0.3cm; TS_6 = -0.5cm;
10	CN-Hgu	
11	DE-Dgw	
12	DE-Hte	TS_1 = 0cm; TS_2 = -0.1cm; TS_3 = -0.2cm;
13	DE-SfN	TS_1 = -0.02cm; TS_3 = -0.1cm; TS_4 = -0.2cm; TS_5 = -0.5cm;
14	DE-Zrk	TS_1 = -0.05cm; TS_2 = -0.1cm; TS_3 = -0.2cm; TS_4 = -0.3cm; TS_5 = -0.5cm;
15	FI-HW	TS_1 = -0.02cm; TS_2 = -0.04cm; TS_3 = -0.12cm; TS_4 = -0.25cm; TS_5 = -0.5cm;
16	FI-Lom	TS_1 = -0.07cm; TS_2 = -0.3cm; TS_3 = -0.5cm;
17	FI-Si2	TS_1 = -0.05cm; TS_2 = -0.2cm; TS_3 = -0.35cm; TS_4 = -0.5cm; TS_5 = -0.05cm; TS_6 = -0.2cm; TS_7 = -0.35cm; TS_8 = -0.5cm;
18	FI-Sii	before 2016(TS_1 = -0.05cm; TS_2 = -0.2cm; TS_3 = -0.35cm; TS_4 = -0.5cm; TS_5 = -0.05cm; TS_6 = -0.2cm; TS_7 = -0.35cm; TS_8 = -0.5cm) after 2017 (TS_1 = 0cm; TS_2 = -0.5cm; TS_3 = -0.1cm; TS_4 = -0.15cm; TS_5 = -0.25cm; TS_6 = -0.45cm; TS_7 = -0.95cm)
19	FR-Lgt	TS_1 = -0.02cm; TS_2 = -0.05cm; TS_3 = -0.1cm; TS_4 = -0.2cm; TS_5 = -0.4cm;
20	HK-MPM	
21	ID-Pag	TS_1 = -0.05cm;
22	IT-BCI	TS_1 = -0.05cm; TS_2 = -0.1cm; TS_3 = -0.3cm; TS_4 = -0.5cm; TS_5 = -1cm;
23	IT-Cas	TS_1 = -0.05cm; TS_2 = -0.3cm; TS_3 = -0.5cm;
24	JP-BBY	TS_1 = -0.183cm; TS_2 = -0.233cm; TS_3 = -0.283cm; TS_4 = -0.383cm; TS_5 = -0.483cm;
25	JP-Mse	TS_1 = -0.01cm; TS_2 = -0.025cm; TS_3 = -0.05cm; TS_4 = -0.1cm; TS_5 = -0.2cm; TS_6 = -0.4cm;
26	JP-SwL	
27	KR-CRK	TS_1 = -0.05cm; TS_2 = -0.15cm;
28	MY-MLM	TS_1 = -0.05cm;
29	NL-Hor	
30	NZ-Kop	TS_1 = -0.01cm; TS_2 = -0.02cm; TS_3 = -0.04cm; TS_4 = -0.05cm; TS_5 = -0.1cm; TS_6 = -0.15cm; TS_7 = -0.25cm; TS_8 = -0.4cm; TS_9 = -0.6cm;
31	PH-RIF	TS_1 = -0.5cm; TS_2 = -0.1cm; TS_3 = -0.2cm;



32	RU-Ch2	TS_1 = -0.04cm; TS_2 = -0.08cm; TS_3 = -0.16cm;
33	RU-Che	TS_1 = -0.04cm; TS_2 = -0.08cm; TS_3 = -0.16cm;
34	RU-Cok	
35	RU-Fy2	
36	SE-Deg	TS_1 = -0.02cm; TS_2 = -0.05cm; TS_3 = -0.1cm; TS_4 = -0.15cm; TS_5 = -0.3cm; TS_6 = -0.5cm;
37	UK-LBT	
38	US-A03	TS_1 = -0.025cm; TS_2 = -0.1cm; TS_3 = -0.3cm;
39	US-A10	TS_1 = -0.025cm; TS_2 = -0.1cm; TS_3 = -0.3cm;
40	US-Atq	
41	US-Beo	
42	US-Bes	
43	US-BI1	TS_1 = -0.02cm; TS_2 = -0.04cm; TS_3 = -0.08cm; TS_4 = -0.16cm; TS_5 = -0.32cm;
44	US-BI2	TS_1 = -0.02cm; TS_2 = -0.04cm; TS_3 = -0.08cm; TS_4 = -0.16cm; TS_5 = -0.32cm;
45	US-BZB	TS_1 = -0.075cm; TS_2 = -0.05cm;
46	US-BZF	TS_1 = -0.075cm; TS_2 = -0.05cm;
47	US-BZS	
48	US-CRT	
49	US-DPW	
50	US-EDN	TS_1 = -0.25cm; TS_2 = -0.15cm; TS_3 = -0.05cm; TS_4 = 0cm; TS_5 = 0.05cm; TS_6 = 0.1cm; TS_7 = 0.2cm; TS_8 = 0.3cm;
51	US-EML	TS_1 = -0.05cm; TS_2 = -0.1cm; TS_3 = -0.2cm; TS_4 = -0.4cm;
52	US-Ho1	TS_1 = -0.05cm; TS_2 = -0.1cm;
53	US-HRA	
54	US-HRC	
55	US-ICS	TS_1 = -0.075cm; TS_2 = -0.05cm;
56	US-Ivo	TS_1 = -0.05cm; TS_2 = -0.1cm; TS_3 = -0.15cm; TS_4 = -0.3cm; TS_5 = -0.4cm;
57	US-LA1	TS = -0.1cm;
58	US-LA2	TS = -0.1cm;
59	US-Los	TS_1 = 0cm; TS_2 = -0.05cm; TS_3 = -0.1cm; TS_4 = -0.2cm; TS_5 = -0.5cm;
60	US-IMAC	
61	US-MRM	
62	US-Myb	TS_1 = -0.02cm; TS_2 = -0.04cm; TS_3 = -0.08cm; TS_4 = -0.16cm; TS_5 = -0.32cm;
63	US-NC4	TS_1 = -0.05cm; TS_2 = -0.2cm;
64	US-NGB	
65	US-NGC	



66	US-ORV	TS_1 = -0.08cm;
67	US-OWC	TS_1 = -0.05cm; TS_2 = -0.3cm;
68	US-PFa	
69	US-Snd	TS_1 = -0.08cm; TS_2 = -0.16cm; TS_3 = nancm; TS_4 = nancm; TS_5 = nancm; TS_6 = nancm;
70	US-Sne	TS_1 = -0.01cm; TS_2 = -0.02cm; TS_3 = -0.08cm; TS_4 = -0.16cm; TS_5 = -0.32cm;
71	US-Srr	
72	US-SU	TS_2 = -0.05cm; TS_3 = -0.1cm;
73	US-Tw1	TS_1 = -0.02cm; TS_2 = -0.04cm; TS_3 = -0.08cm; TS_4 = -0.16cm; TS_5 = -0.32cm;
74	US-Tw3	TS_1 = -0.02cm; TS_2 = -0.04cm; TS_3 = -0.08cm; TS_4 = -0.16cm; TS_5 = -0.32cm;
75	US-Tw4	TS_1 = -0.02cm; TS_2 = -0.04cm; TS_3 = -0.08cm; TS_4 = -0.16cm; TS_5 = -0.32cm;
76	US-Tw5	TS_1 = -0.02cm; TS_2 = -0.1cm; TS_3 = -0.02cm; TS_4 = -0.08cm; TS_5 = -0.16cm;
77	US-Twt	TS_1 = -0.02cm; TS_2 = -0.04cm; TS_3 = -0.08cm; TS_4 = -0.16cm; TS_5 = -0.32cm;
78		
	US-Uaf	TS_1 = -0.09cm; TS_2 = -0.183cm; TS_3 = -0.283cm; TS_4 = -0.367cm; TS_5 = -0.5cm; TS_6 = -0.6cm; TS_7 = -0.75cm; TS_8 = -0.925cm; TS_9 = -1cm;
79	US-WPT	TS_1 = -0.1cm; TS_2 = -0.3cm;

Column Descriptions

SITE_ID Site identification code as assigned by regional flux data network

SOIL_TEMP_PROBE_

DEPTHS Depth of soil temperature probe (m), with negative values being under the surface



Table B3: Bio-climatic data for representativeness analysis.

Bioclimatic predictor	Source	Units	Original temporal resolution
Latent Heat (LE)	FLUXCOM (Jung et al., 2019)	W m ⁻²	Monthly 2003-2013
Wong Simple Ratio Water Index (SRWI)	MOD09A1 (Vermote 2015)	Unitless	Monthly ~2001-2018
Enhanced Vegetation Index (EVI)	MOD13A3 (Didan 2015)	Unitless	Monthly 2001-2018
Mean Annual Temperature (MAT)	BioClim (Fick & Hijman 2017)	Degrees Celsius	Monthly 2001-2018

Supplementary References

- Didan, K. *MOD13A3 MODIS/Terra vegetation Indices Monthly L3 Global 1km SIN Grid V006* [Data set]. NASA EOSDIS Land Processes DAAC. 2015.
- Fick, S.E. & R.J. Hijmans. WorldClim 2: new 1km spatial resolution climate surfaces for global land areas. *International Journal of Climatology*, 37(12): 4302-4315. 2017.
- Jung, M., Koirala, S., Weber, U., Ichii, K., Gans, F., Camps-Valls, G., Papale, D., Schwalm, C., Tramontana, G., & Reichstein, M. The FLUXCOM ensemble of global land-atmosphere energy fluxes. *Scientific Data*, 6(74). doi:10.1038/s41597-019-0076-8. 2019.
- Vermote, E. MOD09A1 MODIS Surface Reflectance 8-Day L3 Global 500m SIN Grid V006. NASA EOSDIS Land Processes DAAC. <http://doi.org/10.5067/MODIS/MOD09A1.006> (Terra). 2015.



Table B4-A Timesat output for FCH4, GPP_DT, TA, and TS (TS from shallowest probe at each site)

	Site	Year	Start_FCH4_(DOY)	End_FCH4_(DOY)	Base_value_FCH4_(nmolC H4/m2/s)	Ampl_FCH4_(nmolCH4/m2/s)	Peak_FCH4_(DOY)	Peak_value_FCH4_(nmolCH4/m2/s)
1	AT-Neu	2010	NaN	NaN	NaN	NaN	NaN	NaN
2	AT-Neu	2011	NaN	NaN	NaN	NaN	NaN	NaN
3	AT-Neu	2012	NaN	NaN	NaN	NaN	NaN	NaN
4	BR-Npw	2014	NaN	NaN	NaN	NaN	NaN	NaN
5	BR-Npw	2015	NaN	NaN	NaN	NaN	NaN	NaN
6	BR-Npw	2016	192.7	345.8	-2.0	154.8	270.0	152.8
7	BW-Gum	2018	34.1	151.1	132.9	186.2	89.0	319.1
8	BW-Gum	2019	230.4	NaN	134.2	202.1	281.9	336.3
9	BW-Nxr	2018	65.1	NaN	29.2	208.7	287.5	237.9
10	CA-SCB	2014	138.8	299.1	17.5	72.3	222.4	89.8
11	CA-SCB	2015	NaN	NaN	NaN	NaN	NaN	NaN
12	CA-SCB	2016	109.2	290.4	11.8	82.0	207.9	93.8
13	CA-SCB	2017	119.0	300.4	14.0	58.9	221.5	72.9
14	CA-SCC	2013	NaN	NaN	NaN	NaN	203.4	44.8
15	CA-SCC	2014	128.4	313.1	3.1	40.1	215.0	43.3
16	CA-SCC	2015	98.0	303.9	1.7	54.6	210.9	56.3
17	CA-SCC	2016	102.7	NaN	1.7	NaN	208.0	59.6
18	DE-Dgw	2015	NaN	NaN	NaN	NaN	NaN	NaN
19	DE-Dgw	2016	NaN	NaN	NaN	NaN	NaN	NaN
20	DE-Dgw	2017	NaN	NaN	NaN	NaN	NaN	NaN
21	DE-Hte	2011	NaN	NaN	NaN	NaN	NaN	NaN
22	DE-Hte	2012	82.6	330.1	20.3	201.8	205.5	222.1
23	DE-Hte	2013	101.9	NaN	29.9	NaN	201.1	378.7
24	DE-Hte	2014	NaN	338.5	38.3	NaN	204.8	314.1
25	DE-Hte	2015	75.1	322.4	29.2	277.7	202.0	306.9
26	DE-Hte	2016	83.9	289.7	21.5	347.8	202.0	369.3
27	DE-Hte	2017	90.0	304.5	18.3	272.7	194.0	290.9
28	DE-Hte	2018	85.6	258.1	21.0	322.0	196.0	343.0



29	DE-Sfn	2012	79.6	340.7	4.3	10.2	217.0	14.5
30	DE-Sfn	2013	NaN	NaN	2.7	3.0	301.9	5.7
31	DE-Sfn	2014	NaN	NaN	NaN	NaN	NaN	NaN
32	DE-Zrk	2013	NaN	NaN	NaN	NaN	NaN	NaN
33	DE-Zrk	2014	NaN	NaN	NaN	NaN	NaN	NaN
34	DE-Zrk	2015	87.0	273.0	9.3	242.5	208.7	251.9
35	DE-Zrk	2016	107.9	274.0	9.9	224.2	187.3	234.2
36	DE-Zrk	2017	110.0	270.1	11.2	203.6	190.0	214.8
37	DE-Zrk	2018	88.1	261.0	8.5	250.8	196.0	259.2
38	FI-Lom	2006	142.8	288.8	7.8	111.0	215.1	118.9
39	FI-Lom	2007	139.3	270.6	10.9	165.0	214.5	175.9
40	FI-Lom	2008	134.0	284.8	10.8	127.7	211.5	138.5
41	FI-Lom	2009	121.5	291.0	12.1	132.3	215.0	144.4
42	FI-Lom	2010	137.1	282.8	13.4	101.6	214.0	115.0
43	FI-Si2	2012	NaN	NaN	NaN	NaN	220.6	80.0
44	FI-Si2	2013	NaN	NaN	NaN	NaN	211.1	77.4
45	FI-Si2	2014	NaN	280.7	7.2	NaN	212.8	111.1
46	FI-Si2	2015	NaN	309.5	9.5	NaN	212.0	72.2
47	FI-Si2	2016	NaN	NaN	NaN	NaN	NaN	NaN
48	FI-Sii	2013	123.8	307.6	7.2	104.3	202.5	111.5
49	FI-Sii	2014	118.8	NaN	2.3	NaN	215.1	112.7
50	FI-Sii	2015	NaN	NaN	NaN	NaN	236.0	112.7
51	FI-Sii	2016	114.5	311.3	8.9	121.1	214.0	130.0
52	FI-Sii	2017	118.9	300.4	6.5	57.1	203.0	63.6
53	FI-Sii	2018	116.3	295.1	7.5	53.8	187.0	61.3
54	HK-MPM	2016	NaN	NaN	NaN	NaN	NaN	NaN
55	HK-MPM	2017	NaN	NaN	NaN	NaN	NaN	NaN
56	HK-MPM	2018	NaN	NaN	NaN	NaN	NaN	NaN
57	ID-Pag	2016	274.1	NaN	-2.8	5.1	NaN	2.3
58	JP-BBY	2015	166.7	NaN	18.3	NaN	237.7	71.4
59	JP-BBY	2016	NaN	324.9	18.3	105.7	244.3	124.0
60	JP-BBY	2017	138.5	323.1	15.2	130.1	236.0	145.3
61	JP-BBY	2018	NaN	332.1	17.8	74.7	221.0	92.6
62	JP-Mse	2012	NaN	NaN	NaN	NaN	NaN	NaN



63	KR-CRK	2015	NaN	NaN	NaN	NaN	NaN	NaN	NaN	NaN	NaN	NaN
64	KR-CRK	2016	NaN	NaN	NaN	NaN	NaN	NaN	NaN	NaN	NaN	NaN
65	KR-CRK	2017	NaN	NaN	NaN	NaN	NaN	NaN	NaN	NaN	NaN	NaN
66	KR-CRK	2018	NaN	NaN	NaN	NaN	NaN	NaN	NaN	NaN	NaN	NaN
67	MY-MLM	2014	229.6	562.4	15.5	19.8	64.2	35.3	NaN	NaN	NaN	NaN
68	MY-MLM	2015	NaN	NaN	NaN	NaN	NaN	NaN	NaN	NaN	NaN	NaN
69	NZ-Kop	2012	-94.5	227.6	36.9	28.3	176.2	65.2	NaN	NaN	NaN	NaN
70	NZ-Kop	2013	7.2	251.5	21.1	61.7	182.0	82.8	NaN	NaN	NaN	NaN
71	NZ-Kop	2014	10.0	228.4	22.6	42.7	161.0	65.2	NaN	NaN	NaN	NaN
72	NZ-Kop	2015	-8.5	NaN	23.0	34.7	150.0	57.8	NaN	NaN	NaN	NaN
73	PH-RiF	2012	154.2	303.9	4.0	62.9	239.1	66.9	NaN	NaN	NaN	NaN
74	PH-RiF	2013	304.1	455.0	5.3	54.0	380.3	59.3	NaN	NaN	NaN	NaN
75	PH-RiF	2014	133.9	265.7	6.1	121.8	178.3	127.9	NaN	NaN	NaN	NaN
76	PH-RiF	2015	NaN	NaN	3.8	56.3	NaN	60.1	NaN	NaN	NaN	NaN
77	RU-Ch2	2014	150.8	312.2	0.7	70.2	216.5	70.9	NaN	NaN	NaN	NaN
78	RU-Ch2	2015	153.3	NaN	8.0	NaN	209.0	56.1	NaN	NaN	NaN	NaN
79	RU-Ch2	2016	NaN	NaN	NaN	NaN	218.8	68.3	NaN	NaN	NaN	NaN
80	RU-Che	2014	NaN	NaN	NaN	NaN	NaN	NaN	NaN	NaN	NaN	NaN
81	RU-Che	2015	NaN	NaN	NaN	NaN	NaN	NaN	NaN	NaN	NaN	NaN
82	RU-Che	2016	NaN	NaN	NaN	NaN	NaN	NaN	NaN	NaN	NaN	NaN
83	SE-Deg	2014	NaN	NaN	NaN	80.8	204.2	91.7	NaN	NaN	NaN	NaN
84	SE-Deg	2015	103.3	318.7	5.1	73.7	211.3	78.8	NaN	NaN	NaN	NaN
85	SE-Deg	2016	102.5	324.1	4.3	74.3	205.3	78.7	NaN	NaN	NaN	NaN
86	SE-Deg	2017	NaN	NaN	NaN	NaN	NaN	NaN	NaN	NaN	NaN	NaN
87	SE-Deg	2018	117.2	327.6	6.9	50.9	192.0	57.8	NaN	NaN	NaN	NaN
88	US-Atq	2013	NaN	NaN	NaN	NaN	NaN	NaN	NaN	NaN	NaN	NaN
89	US-Atq	2014	145.7	328.7	0.9	13.2	215.0	14.1	NaN	NaN	NaN	NaN
90	US-Atq	2015	153.3	264.0	1.0	18.6	193.2	19.6	NaN	NaN	NaN	NaN
91	US-Beo	2013	NaN	NaN	NaN	NaN	NaN	NaN	NaN	NaN	NaN	NaN
92	US-Beo	2014	157.0	356.3	0.4	23.0	211.4	23.4	NaN	NaN	NaN	NaN
93	US-Bes	2013	NaN	NaN	NaN	NaN	NaN	NaN	NaN	NaN	NaN	NaN
94	US-Bes	2014	157.3	312.6	0.6	34.3	206.5	34.9	NaN	NaN	NaN	NaN
95	US-Bes	2015	146.8	283.8	0.6	35.0	193.1	35.7	NaN	NaN	NaN	NaN
96	US-BZB	2014	NaN	NaN	NaN	NaN	226.9	67.5	NaN	NaN	NaN	NaN



97	US-BZB	2015	NaN	NaN	NaN	NaN	NaN	NaN	NaN	219.4	68.4
98	US-BZB	2016	NaN	NaN	NaN	NaN	NaN	NaN	NaN	226.1	98.4
99	US-BZF	2014	NaN	NaN	NaN	NaN	NaN	NaN	NaN	231.6	57.7
100	US-BZF	2015	NaN	NaN	NaN	NaN	NaN	NaN	NaN	179.0	87.0
101	US-BZF	2016	NaN	NaN	NaN	NaN	NaN	NaN	NaN	220.1	119.1
102	US-BZS	2015	NaN	NaN	NaN	NaN	NaN	NaN	NaN	NaN	NaN
103	US-BZS	2016	NaN	NaN	NaN	NaN	NaN	NaN	NaN	NaN	NaN
104	US-DPW	2013	151.7	364.0	16.4	395.0	240.7	411.4	NaN	NaN	NaN
105	US-DPW	2014	98.9	332.5	34.5	338.0	228.9	372.4	NaN	NaN	NaN
106	US-DPW	2015	NaN	376.3	25.0	NaN	248.6	247.3	NaN	NaN	NaN
107	US-DPW	2016	84.2	389.2	23.5	184.3	237.0	207.8	NaN	NaN	NaN
108	US-HRA	2017	NaN	NaN	NaN	NaN	NaN	NaN	NaN	NaN	NaN
109	US-HRC	2018	NaN	NaN	NaN	NaN	NaN	NaN	NaN	NaN	NaN
110	US-ICs	2014	NaN	NaN	NaN	NaN	NaN	NaN	NaN	NaN	NaN
111	US-ICs	2015	NaN	NaN	NaN	NaN	NaN	NaN	NaN	NaN	NaN
112	US-ICs	2016	138.2	302.1	0.2	18.0	200.5	18.2	NaN	NaN	NaN
113	US-Ivo	2013	NaN	400.0	1.9	29.9	238.9	31.9	NaN	NaN	NaN
114	US-Ivo	2014	158.5	301.8	6.7	30.0	226.8	36.7	NaN	NaN	NaN
115	US-Ivo	2015	156.8	278.0	6.9	19.4	231.1	26.3	NaN	NaN	NaN
116	US-Ivo	2016	164.7	352.4	6.1	32.5	232.0	38.7	NaN	NaN	NaN
117	US-LA1	2012	NaN	NaN	NaN	NaN	NaN	NaN	NaN	NaN	NaN
118	US-LA2	2012	62.8	NaN	38.8	225.7	229.2	264.5	NaN	NaN	NaN
119	US-LA2	2013	NaN	NaN	25.1	193.2	216.2	218.3	NaN	NaN	NaN
120	US-Los	2014	127.1	309.8	4.0	35.1	219.3	39.1	NaN	NaN	NaN
121	US-Los	2015	143.4	324.4	3.2	34.6	220.7	37.8	NaN	NaN	NaN
122	US-Los	2016	143.8	310.1	3.3	75.8	193.6	79.1	NaN	NaN	NaN
123	US-Los	2017	134.1	255.2	3.6	58.3	185.0	61.9	NaN	NaN	NaN
124	US-Los	2018	143.0	288.8	3.0	52.4	191.0	55.4	NaN	NaN	NaN
125	US-MAC	2013	NaN	NaN	NaN	NaN	NaN	NaN	NaN	NaN	NaN
126	US-MAC	2014	NaN	NaN	NaN	NaN	NaN	NaN	NaN	NaN	NaN
127	US-MAC	2015	NaN	NaN	NaN	NaN	NaN	NaN	NaN	NaN	NaN
128	US-Myb	2010	NaN	NaN	NaN	NaN	NaN	NaN	NaN	NaN	NaN
129	US-Myb	2011	72.4	369.3	18.3	174.2	253.5	192.5	NaN	NaN	NaN
130	US-Myb	2012	97.2	345.3	18.9	366.6	214.7	385.5	NaN	NaN	NaN



131	US-Myb	2013	46.8	336.3	39.0	265.4	220.2	304.3
132	US-Myb	2014	57.4	334.7	37.1	276.9	206.0	314.0
133	US-Myb	2015	23.7	330.0	21.6	285.7	201.0	307.3
134	US-Myb	2016	36.9	306.0	21.9	216.0	191.0	237.9
135	US-Myb	2017	175.8	332.2	30.5	191.7	235.0	222.2
136	US-Myb	2018	33.1	322.6	28.8	99.3	169.0	128.1
137	US-NC4	2012	132.9	307.9	9.5	323.8	232.2	333.3
138	US-NC4	2013	97.2	365.1	4.3	113.3	240.7	117.5
139	US-NC4	2014	110.6	332.3	-0.1	181.8	253.9	181.6
140	US-NC4	2015	68.4	414.1	-0.8	122.5	245.0	121.7
141	US-NC4	2016	128.4	350.6	2.7	373.6	259.0	376.2
142	US-ORV	2011	NaN	297.3	7.3	15.2	178.5	22.4
143	US-ORV	2012	120.1	269.1	8.3	65.2	189.7	73.4
144	US-ORV	2013	72.4	308.4	9.0	27.4	189.4	36.4
145	US-ORV	2014	87.6	292.2	9.1	32.4	201.0	41.5
146	US-ORV	2015	86.0	NaN	8.9	38.5	170.0	47.4
147	US-OWC	2015	NaN	NaN	NaN	NaN	NaN	NaN
148	US-OWC	2016	NaN	NaN	NaN	NaN	219.2	882.8
149	US-Sne	2016	NaN	NaN	NaN	NaN	NaN	NaN
150	US-Sne	2017	76.2	337.1	14.9	244.2	187.8	259.0
151	US-Sne	2018	60.6	341.6	21.4	168.3	222.6	189.8
152	US-Srr	2014	NaN	NaN	NaN	NaN	NaN	NaN
153	US-Srr	2015	NaN	NaN	NaN	NaN	NaN	NaN
154	US-Srr	2016	NaN	NaN	NaN	NaN	NaN	NaN
155	US-Srr	2017	NaN	NaN	NaN	NaN	NaN	NaN
156	US-StJ	2016	NaN	NaN	NaN	NaN	NaN	NaN
157	US-Tw1	2011	140.5	352.4	36.3	104.5	233.8	140.8
158	US-Tw1	2012	NaN	309.6	28.1	243.5	242.9	271.6
159	US-Tw1	2013	33.4	307.1	42.2	114.3	218.0	156.5
160	US-Tw1	2014	174.6	331.5	65.3	253.2	240.0	318.5
161	US-Tw1	2015	62.3	330.3	63.8	204.1	207.0	267.9
162	US-Tw1	2016	32.3	323.8	48.5	160.0	221.0	208.5
163	US-Tw1	2017	27.8	305.0	43.1	138.1	226.0	181.1
164	US-Tw1	2018	155.0	314.9	38.7	127.5	228.0	166.3



165	US-Tw4	2014	93.8	461.3	27.4	36.5	226.8	63.8
166	US-Tw4	2015	114.5	334.1	39.8	86.5	228.2	126.3
167	US-Tw4	2016	42.8	357.1	43.2	101.8	215.6	144.9
168	US-Tw4	2017	110.7	318.8	55.1	201.2	222.0	256.3
169	US-Tw4	2018	63.0	237.3	53.0	165.1	173.0	218.1
170	US-Tw5	2018	NaN	331.9	26.5	339.3	196.9	365.8
171	US-Twt	2009	NaN	NaN	NaN	NaN	NaN	NaN
172	US-Twt	2010	NaN	NaN	NaN	NaN	NaN	NaN
173	US-Twt	2011	NaN	NaN	NaN	NaN	NaN	NaN
174	US-Twt	2012	NaN	NaN	NaN	NaN	NaN	NaN
175	US-Twt	2013	NaN	NaN	NaN	NaN	NaN	NaN
176	US-Twt	2014	NaN	NaN	NaN	NaN	NaN	NaN
177	US-Twt	2015	NaN	NaN	NaN	NaN	NaN	NaN
178	US-Twt	2016	NaN	NaN	NaN	NaN	NaN	NaN
179	US-Uaf	2011	157.6	NaN	0.8	2.1	242.0	2.8
180	US-Uaf	2012	151.8	NaN	0.7	1.6	265.9	2.3
181	US-Uaf	2013	167.0	NaN	0.8	1.4	267.0	2.2
182	US-Uaf	2014	182.2	NaN	0.9	3.2	247.0	4.1
183	US-Uaf	2015	176.0	NaN	0.8	3.5	245.0	4.3
184	US-Uaf	2016	184.7	NaN	0.9	7.3	248.0	8.2
185	US-Uaf	2017	182.0	NaN	0.9	6.0	248.0	6.8
186	US-Uaf	2018	158.5	NaN	0.9	4.9	250.0	5.8
187	US-WPT	2011	103.5	294.1	5.6	355.3	207.1	360.9
188	US-WPT	2012	90.0	296.5	9.0	380.5	195.6	389.5
189	US-WPT	2013	72.5	297.0	7.5	343.3	220.0	350.8

Column Descriptions

Site	Site name
Year	Data year
Start_FCH4_(DOY)	Season start for elevated methane fluxes (DOY), point "f" in Figure 1
End_FCH4_(DOY)	Season end for elevated methane fluxes (DOY), point "h" in Figure 1



Base_value_FCH4_(nmolCH4/m2/s)
Ampl_FCH4_(nmolCH4/m2/s)
Peak_FCH4_(DOY)
Peak_value_FCH4_(nmolCH4/m2/s)

Baseline methane flux during non-elevated season (nmol CH4 /m2/ s), average of points "a" and "b" in Figure 1
Amplitude of methane flux during elevated flux season (nmol CH4/m2/s), difference between point "e" in Figure 1 and Base_value_FCH4
Day of maximum elevated methane flux (DOY), point "g" in Figure 1
Maximum value of methane flux (nmol CH4/m2/s), point "e" in Figure 1



Table B4-B Timesat output for FCH4, GPP_DT, TA, and TS (TS from shallowest probe at each site)

	Site	Year	Start_GPP_D T_(DOY)	End_GPP_ DT_(DOY)	Base_value_G PP_DT_(μmol CO2/m2/s)	Ampl_GPP_D T_(μmolCO2/ m2/s)	Peak_GPP_D T_(DOY)	Peak_value_G PP_DT_(μmol CO2/m2/s)
1	AT-Neu	2010	61.39	332.24	-0.22	9.75	175.90	9.53
2	AT-Neu	2011	76.71	303.74	0.18	11.36	167.90	11.54
3	AT-Neu	2012	84.67	305.48	0.29	9.75	179.00	10.04
4	BR-Npw	2014	59.47	367.83	2.03	5.10	242.90	7.13
5	BR-Npw	2015	61.54	385.15	2.05	5.15	228.00	7.20
6	BR-Npw	2016	83.78	375.61	2.44	4.74	203.00	7.19
7	BW-Gum	2018	NaN	NaN	NaN	NaN	NaN	NaN
8	BW-Gum	2019	NaN	NaN	NaN	NaN	NaN	NaN
9	BW-Nxr	2018	NaN	NaN	NaN	NaN	NaN	NaN
10	CA-SCB	2014	127.53	266.07	0.10	2.69	210.00	2.79
11	CA-SCB	2015	60.15	275.15	0.10	3.35	199.40	3.45
12	CA-SCB	2016	123.04	277.07	0.05	3.66	191.90	3.71
13	CA-SCB	2017	113.78	274.63	0.04	2.99	202.00	3.02
14	CA-SCC	2013	126.43	273.72	0.20	3.21	198.80	3.41
15	CA-SCC	2014	130.06	269.31	0.30	3.22	194.30	3.52
16	CA-SCC	2015	104.41	269.97	0.28	4.54	196.90	4.82
17	CA-SCC	2016	106.89	284.75	0.09	3.67	191.00	3.76
18	DE-Dgw	2015	13.43	348.62	0.04	0.40	227.30	0.44
19	DE-Dgw	2016	31.35	294.27	0.04	0.49	167.60	0.52
20	DE-Dgw	2017	80.56	293.50	0.04	0.46	191.00	0.50
21	DE-Hte	2011	111.70	280.46	0.05	6.87	170.10	6.92
22	DE-Hte	2012	122.64	296.52	0.31	7.11	200.10	7.42
23	DE-Hte	2013	133.51	293.97	0.29	6.10	206.40	6.39
24	DE-Hte	2014	37.51	277.70	0.27	5.50	160.00	5.77
25	DE-Hte	2015	127.82	303.30	0.27	5.35	191.00	5.61
26	DE-Hte	2016	117.96	328.49	0.16	5.39	184.00	5.55
27	DE-Hte	2017	123.83	301.59	0.11	5.71	177.00	5.82
28	DE-Hte	2018	121.03	334.06	0.06	6.99	190.00	7.05



29	DE-Sfn	2012	-13.79	320.94	0.37	4.34	168.10	4.71
30	DE-Sfn	2013	64.35	316.65	0.31	3.96	198.00	4.27
31	DE-Sfn	2014	43.97	335.84	0.41	4.10	193.00	4.51
32	DE-Zrk	2013	110.23	283.50	0.09	4.30	186.30	4.39
33	DE-Zrk	2014	86.61	309.76	0.06	3.56	180.40	3.62
34	DE-Zrk	2015	99.44	264.19	0.10	3.54	186.60	3.64
35	DE-Zrk	2016	90.31	301.90	0.13	4.38	218.00	4.51
36	DE-Zrk	2017	92.93	303.86	0.11	4.07	180.00	4.18
37	DE-Zrk	2018	105.21	314.58	0.06	6.90	212.00	6.96
38	FI-Lom	2006	147.75	261.40	0.06	5.89	197.40	5.95
39	FI-Lom	2007	145.82	257.55	0.06	6.36	197.90	6.43
40	FI-Lom	2008	151.61	258.87	0.06	7.24	200.00	7.30
41	FI-Lom	2009	147.57	262.55	0.02	6.55	197.00	6.57
42	FI-Lom	2010	153.94	262.64	0.03	6.39	199.00	6.41
43	FI-Si2	2012	33.66	276.85	0.07	1.52	209.00	1.59
44	FI-Si2	2013	106.78	338.07	0.13	1.63	182.90	1.76
45	FI-Si2	2014	40.93	290.00	0.13	2.19	146.00	2.32
46	FI-Si2	2015	113.24	267.77	0.13	1.93	197.00	2.06
47	FI-Si2	2016	43.90	284.85	0.13	1.85	166.00	1.98
48	FI-Sii	2013	118.98	282.46	-0.03	3.70	185.70	3.67
49	FI-Sii	2014	100.30	294.41	0.00	2.43	199.70	2.44
50	FI-Sii	2015	84.64	321.89	0.06	2.63	204.30	2.69
51	FI-Sii	2016	118.70	284.09	0.09	3.43	200.00	3.52
52	FI-Sii	2017	117.46	290.52	0.05	3.04	206.00	3.09
53	FI-Sii	2018	113.63	295.59	0.04	2.32	185.00	2.36
54	HK-MPM	2016	NaN	NaN	NaN	NaN	NaN	NaN
55	HK-MPM	2017	NaN	NaN	NaN	NaN	NaN	NaN
56	HK-MPM	2018	NaN	NaN	NaN	NaN	NaN	NaN
57	ID-Pag	2016	NaN	NaN	NaN	NaN	NaN	NaN
58	JP-BBY	2015	123.64	304.32	0.23	5.32	203.40	5.56
59	JP-BBY	2016	114.13	302.43	0.03	7.94	203.20	7.98
60	JP-BBY	2017	119.90	300.38	0.03	7.58	199.80	7.61
61	JP-BBY	2018	96.26	311.58	0.01	5.44	217.00	5.45
62	JP-Mse	2012	144.63	266.88	0.63	9.81	209.70	10.44



63	KR-CRK	2015	134.99	267.83	0.10	10.68	202.10	10.78
64	KR-CRK	2016	137.21	262.37	0.06	12.44	198.80	12.50
65	KR-CRK	2017	143.28	266.25	0.13	12.20	193.50	12.33
66	KR-CRK	2018	138.97	263.80	0.17	10.96	198.00	11.13
67	MY-MLM	2014	179.97	437.86	8.48	2.67	272.60	11.16
68	MY-MLM	2015	194.24	NaN	8.76	8.31	271.10	17.07
69	NZ-Kop	2012	38.67	334.88	1.33	2.50	194.80	3.83
70	NZ-Kop	2013	58.12	351.65	1.50	2.61	190.00	4.10
71	NZ-Kop	2014	42.25	355.00	1.41	2.78	209.00	4.18
72	NZ-Kop	2015	44.32	366.21	1.19	3.28	193.00	4.47
73	PH-Rif	2012	NaN	NaN	NaN	NaN	NaN	NaN
74	PH-Rif	2013	NaN	NaN	NaN	NaN	NaN	NaN
75	PH-Rif	2014	NaN	NaN	NaN	NaN	NaN	NaN
76	PH-Rif	2015	NaN	NaN	NaN	NaN	NaN	NaN
77	RU-Ch2	2014	142.91	252.79	0.02	5.10	210.30	5.11
78	RU-Ch2	2015	157.47	247.95	-0.02	5.00	202.60	4.97
79	RU-Ch2	2016	145.27	257.90	-0.04	4.15	201.50	4.11
80	RU-Che	2014	161.74	258.77	0.14	5.51	206.90	5.65
81	RU-Che	2015	157.04	250.25	0.01	5.39	203.30	5.40
82	RU-Che	2016	140.55	258.30	-0.10	6.94	188.60	6.84
83	SE-Deg	2014	115.38	285.94	0.02	2.78	196.30	2.79
84	SE-Deg	2015	113.50	278.71	0.02	2.69	203.40	2.70
85	SE-Deg	2016	118.80	290.27	0.02	2.32	195.50	2.35
86	SE-Deg	2017	121.86	276.14	0.02	2.45	199.00	2.47
87	SE-Deg	2018	118.54	276.63	0.00	1.72	188.00	1.72
88	US-Atq	2013	33.24	256.46	0.03	3.05	161.70	3.09
89	US-Atq	2014	139.11	244.88	0.09	1.77	194.30	1.86
90	US-Atq	2015	132.75	243.97	0.08	3.41	191.00	3.48
91	US-Beo	2013	39.33	285.28	0.01	0.88	159.80	0.88
92	US-Beo	2014	88.23	261.54	0.02	1.99	200.00	2.02
93	US-Bes	2013	49.45	269.44	0.04	0.84	187.90	0.87
94	US-Bes	2014	174.64	262.25	0.04	1.60	220.70	1.64
95	US-Bes	2015	160.53	248.82	0.04	2.53	198.40	2.57
96	US-BZB	2014	NaN	NaN	NaN	NaN	NaN	NaN



97	US-BZB	2015	NaN	NaN	NaN	NaN	NaN	NaN	NaN	NaN	NaN	NaN
98	US-BZB	2016	NaN	NaN	NaN	NaN	NaN	NaN	NaN	NaN	NaN	NaN
99	US-BZF	2014	132.71	201.27	0.18	5.84	167.50	6.01	6.01	6.01	6.01	6.01
100	US-BZF	2015	129.12	258.65	0.16	6.93	187.50	7.10	7.10	7.10	7.10	7.10
101	US-BZF	2016	128.63	227.99	0.18	9.14	175.00	9.32	9.32	9.32	9.32	9.32
102	US-BZS	2015	NaN	NaN	NaN	NaN	NaN	NaN	NaN	NaN	NaN	NaN
103	US-BZS	2016	NaN	NaN	NaN	NaN	NaN	NaN	NaN	NaN	NaN	NaN
104	US-DPW	2013	NaN	NaN	NaN	NaN	NaN	NaN	NaN	NaN	NaN	NaN
105	US-DPW	2014	55.72	332.08	0.65	4.60	183.50	5.24	5.24	5.24	5.24	5.24
106	US-DPW	2015	53.69	372.93	0.73	4.77	174.80	5.50	5.50	5.50	5.50	5.50
107	US-DPW	2016	71.21	343.87	0.85	4.83	197.00	5.68	5.68	5.68	5.68	5.68
108	US-HRA	2017	131.27	244.82	0.39	20.14	183.10	20.53	20.53	20.53	20.53	20.53
109	US-HRC	2018	135.69	237.65	1.34	18.79	182.20	20.13	20.13	20.13	20.13	20.13
110	US-ICS	2014	150.35	253.40	0.21	3.46	201.60	3.66	3.66	3.66	3.66	3.66
111	US-ICS	2015	142.83	263.16	0.15	4.42	189.90	4.57	4.57	4.57	4.57	4.57
112	US-ICS	2016	154.39	245.71	0.12	3.22	192.80	3.34	3.34	3.34	3.34	3.34
113	US-Ivo	2013	149.10	257.98	0.06	3.85	201.90	3.91	3.91	3.91	3.91	3.91
114	US-Ivo	2014	151.63	257.85	0.11	3.63	199.10	3.73	3.73	3.73	3.73	3.73
115	US-Ivo	2015	121.66	248.35	0.07	3.97	187.10	4.03	4.03	4.03	4.03	4.03
116	US-Ivo	2016	154.70	254.51	0.09	5.30	194.00	5.39	5.39	5.39	5.39	5.39
117	US-LA1	2012	-7.96	216.91	0.49	2.29	142.80	2.78	2.78	2.78	2.78	2.78
118	US-LA2	2012	46.97	334.04	0.34	5.64	146.80	5.98	5.98	5.98	5.98	5.98
119	US-LA2	2013	93.73	335.84	0.31	6.94	166.30	7.25	7.25	7.25	7.25	7.25
120	US-Los	2014	131.45	288.06	-0.01	6.65	198.20	6.64	6.64	6.64	6.64	6.64
121	US-Los	2015	130.36	288.12	0.11	6.26	201.50	6.37	6.37	6.37	6.37	6.37
122	US-Los	2016	130.87	291.48	0.17	7.17	198.20	7.33	7.33	7.33	7.33	7.33
123	US-Los	2017	136.00	292.41	0.13	7.38	199.00	7.51	7.51	7.51	7.51	7.51
124	US-Los	2018	134.97	285.61	0.13	7.17	199.00	7.29	7.29	7.29	7.29	7.29
125	US-MAC	2013	NaN	378.12	2.50	5.43	222.70	9.45	9.45	9.45	9.45	9.45
126	US-MAC	2014	47.02	334.19	2.51	9.17	180.70	11.68	11.68	11.68	11.68	11.68
127	US-MAC	2015	46.53	356.65	2.92	5.92	154.10	8.84	8.84	8.84	8.84	8.84
128	US-Myb	2010	28.65	305.24	0.56	1.41	183.40	1.97	1.97	1.97	1.97	1.97
129	US-Myb	2011	200.41	367.27	0.28	3.62	265.50	3.89	3.89	3.89	3.89	3.89
130	US-Myb	2012	88.45	331.93	-0.06	13.68	204.50	13.62	13.62	13.62	13.62	13.62



131	US-Myb	2013	47.39	341.89	-0.12	7.95	200.00	7.83
132	US-Myb	2014	86.80	310.73	0.16	8.20	168.00	8.36
133	US-Myb	2015	76.10	323.19	0.17	7.31	202.00	7.47
134	US-Myb	2016	24.11	328.43	0.00	4.03	176.00	4.03
135	US-Myb	2017	67.46	395.16	-0.24	5.79	202.00	5.55
136	US-Myb	2018	83.66	331.31	-0.25	10.50	201.00	10.25
137	US-NC4	2012	NaN	NaN	NaN	NaN	NaN	NaN
138	US-NC4	2013	94.35	304.81	0.78	6.97	181.00	7.75
139	US-NC4	2014	97.51	354.46	0.64	6.09	173.70	6.73
140	US-NC4	2015	92.03	315.08	0.74	9.73	185.00	10.47
141	US-NC4	2016	99.57	326.98	0.92	8.22	183.00	9.14
142	US-ORV	2011	88.77	316.45	-0.06	7.39	180.40	7.33
143	US-ORV	2012	93.50	303.39	0.27	9.29	181.00	9.55
144	US-ORV	2013	107.62	305.23	0.36	10.11	192.40	10.46
145	US-ORV	2014	109.31	299.17	0.24	10.14	190.00	10.38
146	US-ORV	2015	105.01	301.56	0.27	9.64	194.00	9.91
147	US-OWC	2015	NaN	301.35	0.26	6.72	151.30	6.98
148	US-OWC	2016	116.05	309.20	0.30	6.44	204.00	6.73
149	US-Sne	2016	-21.79	306.16	0.34	7.99	190.30	8.34
150	US-Sne	2017	NaN	NaN	NaN	NaN	NaN	NaN
151	US-Sne	2018	84.63	370.31	0.32	2.43	202.00	2.75
152	US-Srr	2014	47.02	307.53	0.78	6.04	175.60	6.83
153	US-Srr	2015	35.50	320.88	0.33	7.96	158.60	8.29
154	US-Srr	2016	44.76	318.87	0.38	8.86	170.80	9.24
155	US-Srr	2017	56.75	309.79	0.30	10.46	185.00	10.76
156	US-StJ	2016	120.72	280.75	1.30	12.01	193.80	13.31
157	US-Tw1	2011	NaN	NaN	NaN	NaN	NaN	NaN
158	US-Tw1	2012	102.12	325.54	0.00	12.83	216.10	12.83
159	US-Tw1	2013	98.35	338.02	-0.18	13.11	208.40	12.93
160	US-Tw1	2014	95.66	326.27	0.12	10.46	208.00	10.58
161	US-Tw1	2015	105.53	344.13	0.26	9.88	215.00	10.13
162	US-Tw1	2016	91.82	313.13	-0.01	10.10	209.00	10.09
163	US-Tw1	2017	93.36	329.76	-0.04	11.26	214.00	11.22
164	US-Tw1	2018	119.04	363.78	-0.02	12.73	217.00	12.70



165	US-Tw4	2014	160.04	363.23	0.00	4.70	236.60	4.70
166	US-Tw4	2015	57.22	335.89	0.01	8.11	213.00	8.13
167	US-Tw4	2016	76.15	311.33	0.17	8.22	185.00	8.39
168	US-Tw4	2017	100.19	332.90	0.14	8.76	214.00	8.90
169	US-Tw4	2018	98.39	337.78	0.04	11.84	206.00	11.88
170	US-Tw5	2018	115.94	321.33	1.77	6.68	231.10	8.45
171	US-Twt	2009	149.98	293.01	0.20	12.46	212.00	12.66
172	US-Twt	2010	141.10	311.91	0.10	13.71	224.40	13.81
173	US-Twt	2011	158.51	288.69	0.12	14.22	215.90	14.34
174	US-Twt	2012	166.84	308.78	0.21	12.31	233.00	12.52
175	US-Twt	2013	138.24	272.38	0.27	16.71	202.00	16.98
176	US-Twt	2014	148.14	281.40	0.16	15.01	205.00	15.17
177	US-Twt	2015	137.11	277.23	0.17	11.52	218.00	11.68
178	US-Twt	2016	169.14	289.90	0.29	13.80	224.00	14.08
179	US-Uaf	2011	114.56	283.49	0.12	6.04	196.90	6.17
180	US-Uaf	2012	88.03	271.24	0.18	6.58	187.30	6.76
181	US-Uaf	2013	124.13	271.61	0.22	5.79	192.10	6.01
182	US-Uaf	2014	84.63	269.30	0.14	5.32	188.00	5.46
183	US-Uaf	2015	90.52	264.29	0.09	5.17	196.00	5.25
184	US-Uaf	2016	103.06	270.75	0.14	4.66	192.00	4.80
185	US-Uaf	2017	102.29	275.58	0.14	6.10	198.00	6.25
186	US-Uaf	2018	111.65	291.46	0.04	5.60	190.00	5.64
187	US-WPT	2011	134.98	285.59	0.24	7.43	206.10	7.67
188	US-WPT	2012	129.04	293.67	0.06	6.97	205.90	7.03
189	US-WPT	2013	134.87	278.12	0.05	6.20	200.90	6.24

Column Descriptions

Site	Site name
Year	Data year
Start_GPP_DT_(DOY)	Season start for elevated GPP_DT (DOY), point "f" in Figure 1
End_GPP_DT_(DOY)	Season end for elevated GPP_DT fluxes (DOY), point "h" in Figure 1



Baseline GPP_DT flux during non-elevated season ($\mu\text{mol CO}_2/\text{m}^2/\text{s}$), average of points "a" and "b" in Figure 1

Amplitude of GPP_DT flux during elevated flux season ($\mu\text{mol CO}_2/\text{m}^2/\text{s}$), difference between point "e" in Figure 1 and Base_value_GPP_DT

Day of maximum elevated GPP_DT flux (DOY), point "g" in Figure 1

Maximum value of GPP_DT flux ($\mu\text{mol CO}_2/\text{m}^2/\text{s}$), point "e" in Figure 1

Base_value_GPP_DT_ ($\mu\text{molCO}_2/\text{m}^2/\text{s}$)

Ampl_GPP_DT_ ($\mu\text{molCO}_2/\text{m}^2/\text{s}$)

Peak_GPP_DT_(DOY)

Peak_value_GPP_DT_ ($\mu\text{molCO}_2/\text{m}^2/\text{s}$)



Table B4-C Timesat output for FCH4, GPP_DT, TA, and TS (TS from shallowest probe at each site)

	Site	Year	Start_TA_ (DOY)	End_TA_ (DOY)	Base_value_ TA_(C)	Ampl_TA_ (C)	Peak_TA_ (DOY)	Peak_value_ TA_(C)
1	AT-Neu	2010	43.17	351.66	-4.84	20.94	195.90	16.10
2	AT-Neu	2011	18.47	359.91	-5.08	20.55	198.50	15.47
3	AT-Neu	2012	38.03	366.62	-5.57	22.35	197.20	16.78
4	BR-Npw	2014	NaN	NaN	NaN	NaN	NaN	NaN
5	BR-Npw	2015	NaN	NaN	NaN	NaN	NaN	NaN
6	BR-Npw	2016	7.49	348.67	19.56	7.53	211.00	27.10
7	BW-Gum	2018	NaN	NaN	NaN	NaN	NaN	NaN
8	BW-Gum	2019	NaN	NaN	NaN	NaN	NaN	NaN
9	BW-Nxr	2018	NaN	NaN	NaN	NaN	NaN	NaN
10	CA-SCB	2014	60.23	335.31	-23.33	41.29	197.40	17.96
11	CA-SCB	2015	45.11	360.83	-21.75	39.11	186.40	17.37
12	CA-SCB	2016	49.77	335.79	-18.88	37.28	193.90	18.40
13	CA-SCB	2017	64.68	327.30	-18.45	35.95	201.00	17.50
14	CA-SCC	2013	67.57	338.23	-21.08	39.13	203.80	18.05
15	CA-SCC	2014	54.14	337.83	-22.27	40.98	196.70	18.72
16	CA-SCC	2015	46.41	359.38	-20.09	37.86	187.10	17.77
17	CA-SCC	2016	47.31	350.23	-18.76	37.65	194.00	18.89
18	DE-Dgw	2015	72.47	347.56	2.18	16.25	203.80	18.42
19	DE-Dgw	2016	64.46	324.69	1.34	17.37	205.40	18.71
20	DE-Dgw	2017	43.79	375.32	-0.17	18.47	202.20	18.30
21	DE-Hte	2011	NaN	NaN	NaN	NaN	NaN	NaN
22	DE-Hte	2012	50.34	352.49	0.77	17.03	207.60	17.80
23	DE-Hte	2013	83.53	365.30	1.64	17.09	202.50	18.73
24	DE-Hte	2014	48.71	352.47	2.86	15.82	213.00	18.68
25	DE-Hte	2015	57.62	366.35	2.59	15.33	211.00	17.92
26	DE-Hte	2016	67.53	323.10	2.75	16.01	211.00	18.76
27	DE-Hte	2017	58.94	370.07	1.81	16.22	212.00	18.02
28	DE-Hte	2018	74.55	368.02	0.91	19.14	203.00	20.05
29	DE-Sfn	2012	54.86	355.18	-2.09	20.25	196.30	18.16
30	DE-Sfn	2013	64.64	344.04	-0.35	18.57	202.80	18.22



31	DE-Sfn	2014	NaN	NaN	NaN	NaN	NaN	NaN	NaN	NaN	NaN	NaN	NaN
32	DE-Zrk	2013	NaN	NaN	NaN	NaN	NaN	NaN	NaN	NaN	NaN	NaN	NaN
33	DE-Zrk	2014	NaN	NaN	NaN	NaN	NaN	NaN	NaN	NaN	NaN	NaN	NaN
34	DE-Zrk	2015	49.71	355.39	2.13	15.33	203.40	17.46	NaN	NaN	NaN	NaN	NaN
35	DE-Zrk	2016	63.30	323.76	1.85	16.45	204.00	18.31	NaN	NaN	NaN	NaN	NaN
36	DE-Zrk	2017	45.25	372.48	0.47	17.44	205.00	17.91	NaN	NaN	NaN	NaN	NaN
37	DE-Zrk	2018	75.77	358.90	-0.10	18.78	190.00	18.68	NaN	NaN	NaN	NaN	NaN
38	FI-Lom	2006	72.49	355.63	-12.19	26.67	195.00	14.48	NaN	NaN	NaN	NaN	NaN
39	FI-Lom	2007	56.24	372.50	-11.01	22.60	193.40	11.59	NaN	NaN	NaN	NaN	NaN
40	FI-Lom	2008	73.45	348.05	-10.36	22.30	200.40	11.95	NaN	NaN	NaN	NaN	NaN
41	FI-Lom	2009	56.72	356.29	-13.61	27.09	205.00	13.48	NaN	NaN	NaN	NaN	NaN
42	FI-Lom	2010	54.81	346.00	-16.10	27.81	200.00	11.71	NaN	NaN	NaN	NaN	NaN
43	FI-Si2	2012	70.38	349.74	-6.91	22.72	199.10	15.81	NaN	NaN	NaN	NaN	NaN
44	FI-Si2	2013	88.15	369.48	-5.99	23.74	188.60	17.76	NaN	NaN	NaN	NaN	NaN
45	FI-Si2	2014	53.29	350.42	-4.39	21.50	200.30	17.11	NaN	NaN	NaN	NaN	NaN
46	FI-Si2	2015	39.64	359.19	-5.00	19.39	212.00	14.39	NaN	NaN	NaN	NaN	NaN
47	FI-Si2	2016	42.62	345.02	-6.72	23.17	199.00	16.45	NaN	NaN	NaN	NaN	NaN
48	FI-Sii	2013	89.28	363.91	-5.74	22.24	189.10	16.50	NaN	NaN	NaN	NaN	NaN
49	FI-Sii	2014	52.05	339.85	-4.36	21.52	200.90	17.15	NaN	NaN	NaN	NaN	NaN
50	FI-Sii	2015	34.40	357.72	-5.42	19.66	209.50	14.25	NaN	NaN	NaN	NaN	NaN
51	FI-Sii	2016	55.00	320.65	-5.24	20.90	195.00	15.66	NaN	NaN	NaN	NaN	NaN
52	FI-Sii	2017	61.62	377.27	-6.32	20.93	208.00	14.61	NaN	NaN	NaN	NaN	NaN
53	FI-Sii	2018	74.22	378.66	-8.98	27.37	195.00	18.39	NaN	NaN	NaN	NaN	NaN
54	HK-MPM	2016	53.59	378.86	15.97	13.27	198.10	29.24	NaN	NaN	NaN	NaN	NaN
55	HK-MPM	2017	49.13	357.32	16.27	13.07	215.60	29.34	NaN	NaN	NaN	NaN	NaN
56	HK-MPM	2018	42.11	383.02	15.25	14.05	199.00	29.30	NaN	NaN	NaN	NaN	NaN
57	ID-Pag	2016	NaN	NaN	NaN	NaN	NaN	NaN	NaN	NaN	NaN	NaN	NaN
58	JP-BBY	2015	56.18	355.66	-5.30	25.89	209.50	20.58	NaN	NaN	NaN	NaN	NaN
59	JP-BBY	2016	46.06	348.04	-7.13	28.01	212.00	20.89	NaN	NaN	NaN	NaN	NaN
60	JP-BBY	2017	44.65	361.65	-7.47	28.20	208.70	20.73	NaN	NaN	NaN	NaN	NaN
61	JP-BBY	2018	45.63	367.94	-7.55	27.12	210.00	19.57	NaN	NaN	NaN	NaN	NaN
62	JP-Mse	2012	54.48	351.81	1.48	24.59	219.90	26.08	NaN	NaN	NaN	NaN	NaN
63	KR-CRK	2015	NaN	NaN	NaN	NaN	NaN	NaN	NaN	NaN	NaN	NaN	NaN
64	KR-CRK	2016	NaN	NaN	NaN	NaN	NaN	NaN	NaN	NaN	NaN	NaN	NaN



65	KR-CRK	2017	NaN	NaN	NaN	NaN	NaN	NaN	NaN	NaN	NaN	NaN	NaN
66	KR-CRK	2018	NaN	NaN	NaN	NaN	NaN	NaN	NaN	NaN	NaN	NaN	NaN
67	MY-MLM	2014	17.51	365.80	25.97	1.95	179.40	27.91	NaN	NaN	NaN	NaN	NaN
68	MY-MLM	2015	NaN	NaN	NaN	NaN	NaN	NaN	NaN	NaN	NaN	NaN	NaN
69	NZ-Kop	2012	50.84	347.05	9.12	9.72	219.90	18.84	NaN	NaN	NaN	NaN	NaN
70	NZ-Kop	2013	39.31	352.93	9.31	8.28	209.60	17.60	NaN	NaN	NaN	NaN	NaN
71	NZ-Kop	2014	53.45	352.71	9.08	9.68	215.00	18.76	NaN	NaN	NaN	NaN	NaN
72	NZ-Kop	2015	51.01	357.77	8.55	10.41	212.00	18.96	NaN	NaN	NaN	NaN	NaN
73	PH-Rif	2012	NaN	NaN	NaN	NaN	NaN	NaN	NaN	NaN	NaN	NaN	NaN
74	PH-Rif	2013	NaN	NaN	NaN	NaN	NaN	NaN	NaN	NaN	NaN	NaN	NaN
75	PH-Rif	2014	NaN	NaN	NaN	NaN	NaN	NaN	NaN	NaN	NaN	NaN	NaN
76	PH-Rif	2015	NaN	NaN	NaN	NaN	NaN	NaN	NaN	NaN	NaN	NaN	NaN
77	RU-Ch2	2014	62.07	339.91	-31.58	46.02	208.40	14.44	NaN	NaN	NaN	NaN	NaN
78	RU-Ch2	2015	54.09	340.02	-34.37	47.59	204.40	13.23	NaN	NaN	NaN	NaN	NaN
79	RU-Ch2	2016	56.44	373.19	-34.38	48.39	201.90	14.00	NaN	NaN	NaN	NaN	NaN
80	RU-Che	2014	61.35	339.96	-31.54	45.92	208.00	14.37	NaN	NaN	NaN	NaN	NaN
81	RU-Che	2015	53.19	340.10	-34.28	47.55	204.30	13.26	NaN	NaN	NaN	NaN	NaN
82	RU-Che	2016	55.88	372.30	-34.29	48.37	201.70	14.08	NaN	NaN	NaN	NaN	NaN
83	SE-Deg	2014	69.57	327.67	-5.24	21.42	201.00	16.18	NaN	NaN	NaN	NaN	NaN
84	SE-Deg	2015	29.69	352.18	-7.38	19.31	213.90	11.93	NaN	NaN	NaN	NaN	NaN
85	SE-Deg	2016	54.69	331.26	-7.34	20.99	197.10	13.65	NaN	NaN	NaN	NaN	NaN
86	SE-Deg	2017	61.87	353.17	-8.35	21.32	210.00	12.98	NaN	NaN	NaN	NaN	NaN
87	SE-Deg	2018	74.36	373.70	-11.34	26.53	193.00	15.18	NaN	NaN	NaN	NaN	NaN
88	US-Atq	2013	NaN	NaN	NaN	NaN	NaN	NaN	NaN	NaN	NaN	NaN	NaN
89	US-Atq	2014	70.05	360.75	-25.81	32.20	203.40	6.38	NaN	NaN	NaN	NaN	NaN
90	US-Atq	2015	84.07	347.24	-26.07	34.70	196.70	8.63	NaN	NaN	NaN	NaN	NaN
91	US-Beo	2013	NaN	NaN	NaN	NaN	NaN	NaN	NaN	NaN	NaN	NaN	NaN
92	US-Beo	2014	63.26	351.27	-22.70	25.61	203.20	2.91	NaN	NaN	NaN	NaN	NaN
93	US-Bes	2013	NaN	NaN	NaN	NaN	NaN	NaN	NaN	NaN	NaN	NaN	NaN
94	US-Bes	2014	76.62	357.34	-24.74	26.57	208.30	1.83	NaN	NaN	NaN	NaN	NaN
95	US-Bes	2015	82.66	344.05	-25.16	29.49	203.30	4.32	NaN	NaN	NaN	NaN	NaN
96	US-BZB	2014	65.05	339.25	-17.12	32.08	189.60	14.95	NaN	NaN	NaN	NaN	NaN
97	US-BZB	2015	52.17	340.04	-17.27	33.86	181.60	16.58	NaN	NaN	NaN	NaN	NaN
98	US-BZB	2016	35.70	321.04	-16.88	33.52	192.50	16.64	NaN	NaN	NaN	NaN	NaN



99	US-BZF	2014	64.65	341.50	-16.78	31.98	190.50	15.20
100	US-BZF	2015	52.19	340.98	-16.93	33.41	181.50	16.48
101	US-BZF	2016	34.60	321.31	-16.57	33.21	194.00	16.63
102	US-BZS	2015	46.24	343.61	-17.41	34.59	180.20	17.18
103	US-BZS	2016	32.55	320.26	-15.91	33.02	193.80	17.11
104	US-DPW	2013	59.45	361.72	16.30	10.86	220.80	27.16
105	US-DPW	2014	38.66	326.75	15.99	11.79	210.30	27.78
106	US-DPW	2015	33.62	381.23	15.93	9.98	211.80	25.91
107	US-DPW	2016	45.53	367.09	15.72	12.81	203.00	28.53
108	US-HRA	2017	NaN	NaN	NaN	NaN	NaN	NaN
109	US-HRC	2018	NaN	NaN	NaN	NaN	NaN	NaN
110	US-ICS	2014	NaN	NaN	NaN	NaN	NaN	NaN
111	US-ICS	2015	NaN	NaN	NaN	NaN	NaN	NaN
112	US-ICS	2016	68.13	328.76	-16.90	26.34	196.80	9.44
113	US-Ivo	2013	93.13	360.42	-23.36	36.20	193.60	12.84
114	US-Ivo	2014	69.00	341.89	-21.44	30.70	193.50	9.26
115	US-Ivo	2015	90.83	326.77	-21.52	31.94	188.60	10.42
116	US-Ivo	2016	90.00	339.98	-21.61	31.33	197.00	9.72
117	US-LA1	2012	31.05	302.54	19.07	8.85	177.60	27.92
118	US-LA2	2012	35.18	316.87	16.70	11.55	197.40	28.25
119	US-LA2	2013	71.41	321.17	15.91	13.32	210.60	29.23
120	US-Los	2014	58.01	365.46	-14.20	33.10	195.40	18.89
121	US-Los	2015	50.36	367.57	-10.76	29.37	203.50	18.60
122	US-Los	2016	39.16	356.37	-9.11	29.07	209.40	19.96
123	US-Los	2017	30.73	345.36	-9.80	28.09	212.00	18.29
124	US-Los	2018	69.61	336.03	-9.75	29.76	197.00	20.02
125	US-MAC	2013	NaN	NaN	NaN	NaN	NaN	NaN
126	US-MAC	2014	42.39	323.96	17.10	9.77	211.20	26.87
127	US-MAC	2015	39.48	328.01	16.94	9.62	200.60	26.56
128	US-Myb	2010	NaN	NaN	NaN	NaN	NaN	NaN
129	US-Myb	2011	31.10	331.80	8.15	12.63	223.60	20.78
130	US-Myb	2012	16.54	358.52	7.18	13.47	214.90	20.66
131	US-Myb	2013	24.44	342.29	7.26	13.44	197.00	20.70
132	US-Myb	2014	11.52	353.52	8.78	12.76	211.00	21.54



133	US-Myb	2015	-0.97	325.62	8.88	13.12	228.00	21.99
134	US-Myb	2016	-3.34	351.73	7.96	12.97	208.00	20.93
135	US-Myb	2017	27.35	345.82	8.30	13.88	214.00	22.19
136	US-Myb	2018	44.40	332.57	9.03	11.46	218.00	20.49
137	US-NC4	2012	57.32	339.28	9.01	17.49	208.70	26.50
138	US-NC4	2013	69.27	352.37	6.79	19.01	204.60	25.79
139	US-NC4	2014	49.17	367.68	5.41	18.30	206.30	23.71
140	US-NC4	2015	64.43	392.18	6.92	19.42	202.00	26.33
141	US-NC4	2016	53.97	350.61	8.14	19.07	215.00	27.21
142	US-ORv	2011	63.96	358.28	0.50	25.07	195.20	25.57
143	US-ORv	2012	32.88	351.31	0.84	24.92	195.90	25.76
144	US-ORv	2013	51.21	355.78	-2.44	25.94	203.60	23.50
145	US-ORv	2014	51.30	370.00	-4.35	27.96	196.00	23.61
146	US-ORv	2015	62.52	393.56	-4.58	27.87	199.00	23.29
147	US-OWC	2015	NaN	NaN	NaN	NaN	NaN	NaN
148	US-OWC	2016	56.19	365.00	2.20	22.65	211.80	24.85
149	US-Sne	2016	NaN	NaN	NaN	NaN	NaN	NaN
150	US-Sne	2017	9.23	344.35	7.29	14.52	217.90	21.80
151	US-Sne	2018	49.63	357.43	7.14	13.97	220.90	21.11
152	US-Srr	2014	50.56	337.45	10.74	10.06	217.30	20.80
153	US-Srr	2015	4.98	323.35	9.49	12.20	235.30	21.69
154	US-Srr	2016	-6.23	346.21	8.26	11.70	211.90	19.96
155	US-Srr	2017	17.23	346.39	7.94	13.42	216.00	21.36
156	US-StJ	2016	67.33	347.07	3.01	23.37	214.00	26.37
157	US-Tw1	2011	59.53	328.03	7.82	13.46	222.10	21.28
158	US-Tw1	2012	18.52	356.80	6.67	14.88	216.30	21.56
159	US-Tw1	2013	29.27	344.79	7.09	14.34	196.80	21.43
160	US-Tw1	2014	14.74	349.77	8.52	13.61	204.00	22.13
161	US-Tw1	2015	7.05	324.07	8.19	13.45	222.00	21.63
162	US-Tw1	2016	4.40	350.56	7.22	13.89	203.00	21.11
163	US-Tw1	2017	25.14	343.29	7.24	15.12	206.00	22.36
164	US-Tw1	2018	50.84	337.80	7.43	13.37	211.00	20.80
165	US-Tw4	2014	15.67	348.81	8.65	13.44	206.80	22.09
166	US-Tw4	2015	5.29	324.60	8.49	13.42	224.80	21.90



167	US-Tw4	2016	2.66	347.62	7.58	14.06	201.00	21.64
168	US-Tw4	2017	30.79	337.78	7.88	15.11	208.00	22.99
169	US-Tw4	2018	44.48	331.60	8.26	13.08	213.00	21.33
170	US-Tw5	2018	76.28	338.55	9.15	12.61	208.50	21.76
171	US-Twt	2009	NaN	NaN	NaN	NaN	NaN	NaN
172	US-Twt	2010	NaN	NaN	NaN	NaN	NaN	NaN
173	US-Twt	2011	NaN	NaN	NaN	NaN	NaN	NaN
174	US-Twt	2012	NaN	NaN	NaN	NaN	NaN	NaN
175	US-Twt	2013	NaN	NaN	NaN	NaN	NaN	NaN
176	US-Twt	2014	NaN	NaN	NaN	NaN	NaN	NaN
177	US-Twt	2015	NaN	NaN	NaN	NaN	NaN	NaN
178	US-Twt	2016	NaN	NaN	NaN	NaN	NaN	NaN
179	US-Uaf	2011	59.01	330.80	-23.42	38.45	191.90	15.02
180	US-Uaf	2012	43.13	317.75	-23.94	38.57	192.30	14.63
181	US-Uaf	2013	64.43	344.15	-22.12	39.63	195.90	17.51
182	US-Uaf	2014	49.85	342.99	-20.55	34.19	190.00	13.65
183	US-Uaf	2015	51.31	346.65	-19.52	34.90	182.00	15.38
184	US-Uaf	2016	27.33	325.47	-20.83	36.13	193.00	15.31
185	US-Uaf	2017	59.18	357.64	-22.10	38.30	191.00	16.20
186	US-Uaf	2018	35.38	354.57	-21.58	36.74	196.00	15.16
187	US-WPT	2011	62.29	362.57	-1.13	26.31	199.10	25.18
188	US-WPT	2012	34.86	355.23	-0.44	25.53	198.40	25.09
189	US-WPT	2013	64.19	341.07	-1.92	24.49	205.00	22.57

Column Description

Site	Site name
Year	Data year
Start_TA_(DOY)	Season start for elevated TA (DOY), point "f" in Figure 1
End_TA_(DOY)	Season end for elevated TA (DOY), point "h" in Figure 1
Base_value_TA_(C)	Baseline TA during non-elevated season (C), average of points "a" and "b" in Figure 1
Ampl_TA_(C)	Amplitude of TAduring elevated temperature season (C), difference between point "e" in Figure 1 and Base_value_TA
Peak_TA_(DOY)	Day of maximum elevated TA (DOY), point "g" in Figure 1
Peak_value_TA_(C)	Maximum value of TA (C) point "e" in Figure 1



Table B4-D Timesat output for FCH4, GPP_DT, TA, and TS (TS from shallowest probe at each site)

	Site	Year	Probe_name	Soil_temp_depth_m	Start_TS_(DOY)	End_TS_(DOY)	Base_value_TS_(C)	Ampl_TS_(C)	Peak_TS_(DOY)	Peak_value_TS_(C)
1	AT-Neu	2010	TS_1	-0.05	61.32	339.44	0.15	17.54	200.90	17.70
2	AT-Neu	2011	TS_1	-0.05	51.04	328.84	0.40	16.37	201.00	16.77
3	AT-Neu	2012	TS_1	-0.05	61.12	341.88	0.73	17.57	202.90	18.30
4	BR-Npw	2014	NaN	NaN	NaN	NaN	NaN	NaN	NaN	NaN
5	BR-Npw	2015	NaN	NaN	NaN	NaN	NaN	NaN	NaN	NaN
6	BR-Npw	2016	TS_1	NaN	18.41	343.22	22.41	5.98	188.00	28.40
7	BW-Gum	2018	NaN	NaN	NaN	NaN	NaN	NaN	NaN	NaN
8	BW-Gum	2019	NaN	NaN	NaN	NaN	NaN	NaN	NaN	NaN
9	BW-Nxr	2018	NaN	NaN	NaN	NaN	NaN	NaN	NaN	NaN
10	CA-SCB	2014	TS_1	0.00	105.94	292.18	-0.63	20.62	196.60	19.99
11	CA-SCB	2015	TS_1	0.00	106.92	287.14	-0.39	17.23	186.80	16.84
12	CA-SCB	2016	TS_1	0.00	101.64	284.09	-0.31	19.07	193.20	18.77
13	CA-SCB	2017	TS_1	0.00	107.44	289.72	-0.25	17.67	198.00	17.42
14	CA-SCC	2013	NaN	NaN	NaN	NaN	NaN	NaN	NaN	NaN
15	CA-SCC	2014	TS_1	-0.10	123.36	287.06	-0.55	15.64	203.00	15.09
16	CA-SCC	2015	TS_1	-0.10	113.88	285.22	-0.28	16.26	189.20	15.98
17	CA-SCC	2016	TS_1	-0.10	108.09	260.12	-0.33	18.37	190.90	18.04
18	DE-Dgw	2015	NaN	NaN	NaN	NaN	NaN	NaN	NaN	NaN
19	DE-Dgw	2016	NaN	NaN	NaN	NaN	NaN	NaN	NaN	NaN
20	DE-Dgw	2017	NaN	NaN	NaN	NaN	NaN	NaN	NaN	NaN
21	DE-Hte	2011	NaN	NaN	NaN	NaN	NaN	NaN	NaN	NaN
22	DE-Hte	2012	TS_3	-0.20	76.96	344.01	4.98	12.26	215.50	17.23
23	DE-Hte	2013	TS_3	-0.20	60.92	377.99	3.96	11.99	207.90	15.95
24	DE-Hte	2014	TS_1	0.00	NaN	327.83	8.52	8.34	205.60	16.87
25	DE-Hte	2015	TS_1	0.00	62.92	360.55	5.17	11.67	187.40	16.84
26	DE-Hte	2016	TS_1	0.00	71.87	NaN	4.94	12.36	175.60	17.30
27	DE-Hte	2017	TS_1	0.00	61.55	343.32	4.50	11.76	186.00	16.26
28	DE-Hte	2018	NaN	NaN	NaN	NaN	NaN	NaN	NaN	NaN
29	DE-Sfn	2012	TS_1	-0.02	NaN	372.59	0.00	23.55	206.50	15.29
30	DE-Sfn	2013	TS_1	-0.02	55.84	381.50	0.92	13.62	216.40	14.54



31	DE-Sfn	2014	NaN	NaN	NaN	NaN	NaN	NaN	NaN	NaN	NaN	NaN	NaN	NaN	NaN	NaN	NaN	NaN	NaN	NaN	NaN	NaN	NaN	NaN
32	DE-Zrk	2013	NaN	NaN	NaN	NaN	NaN	NaN	NaN	NaN	NaN	NaN	NaN	NaN	NaN	NaN	NaN	NaN	NaN	NaN	NaN	NaN	NaN	NaN
33	DE-Zrk	2014	TS_1	-0.05	54.79	361.65	4.36	13.93	202.30	18.29	NaN	NaN	NaN	NaN	NaN	NaN	NaN	NaN	NaN	NaN	NaN	NaN	NaN	
34	DE-Zrk	2015	TS_1	-0.05	58.29	359.29	4.28	13.24	215.50	17.52	NaN	NaN	NaN	NaN	NaN	NaN	NaN	NaN	NaN	NaN	NaN	NaN	NaN	
35	DE-Zrk	2016	TS_1	-0.05	72.81	332.00	4.28	14.93	200.40	19.20	NaN	NaN	NaN	NaN	NaN	NaN	NaN	NaN	NaN	NaN	NaN	NaN	NaN	
36	DE-Zrk	2017	TS_1	-0.05	69.10	351.44	4.40	14.72	199.00	19.12	NaN	NaN	NaN	NaN	NaN	NaN	NaN	NaN	NaN	NaN	NaN	NaN	NaN	
37	DE-Zrk	2018	TS_1	-0.05	84.47	336.14	4.83	12.32	203.00	17.14	NaN	NaN	NaN	NaN	NaN	NaN	NaN	NaN	NaN	NaN	NaN	NaN	NaN	
38	FI-Lom	2006	TS_1	-0.07	114.15	290.83	-0.11	13.42	204.80	13.31	NaN	NaN	NaN	NaN	NaN	NaN	NaN	NaN	NaN	NaN	NaN	NaN	NaN	
39	FI-Lom	2007	TS_1	-0.07	126.84	302.05	0.11	13.05	200.00	13.16	NaN	NaN	NaN	NaN	NaN	NaN	NaN	NaN	NaN	NaN	NaN	NaN	NaN	
40	FI-Lom	2008	TS_1	-0.07	135.62	296.74	0.16	12.73	202.90	12.88	NaN	NaN	NaN	NaN	NaN	NaN	NaN	NaN	NaN	NaN	NaN	NaN	NaN	
41	FI-Lom	2009	TS_1	-0.07	117.16	291.86	0.14	11.73	214.00	11.87	NaN	NaN	NaN	NaN	NaN	NaN	NaN	NaN	NaN	NaN	NaN	NaN	NaN	
42	FI-Lom	2010	TS_1	-0.07	129.91	318.54	0.05	12.13	208.00	12.18	NaN	NaN	NaN	NaN	NaN	NaN	NaN	NaN	NaN	NaN	NaN	NaN	NaN	
43	FI-Si2	2012	TS_1	-0.05	NaN	323.46	0.00	19.85	204.60	16.02	NaN	NaN	NaN	NaN	NaN	NaN	NaN	NaN	NaN	NaN	NaN	NaN	NaN	
44	FI-Si2	2013	TS_1	-0.05	106.90	341.05	-0.05	16.04	199.40	15.98	NaN	NaN	NaN	NaN	NaN	NaN	NaN	NaN	NaN	NaN	NaN	NaN	NaN	
45	FI-Si2	2014	TS_1	-0.05	104.63	331.10	-0.04	17.07	208.50	17.03	NaN	NaN	NaN	NaN	NaN	NaN	NaN	NaN	NaN	NaN	NaN	NaN	NaN	
46	FI-Si2	2015	TS_1	-0.05	76.49	352.34	-0.87	16.31	211.00	15.44	NaN	NaN	NaN	NaN	NaN	NaN	NaN	NaN	NaN	NaN	NaN	NaN	NaN	
47	FI-Si2	2016	TS_1	-0.05	102.64	329.42	-0.88	16.48	206.00	15.60	NaN	NaN	NaN	NaN	NaN	NaN	NaN	NaN	NaN	NaN	NaN	NaN	NaN	
48	FI-Sii	2013	NaN	NaN	NaN	NaN	NaN	NaN	NaN	NaN	NaN	NaN	NaN	NaN	NaN	NaN	NaN	NaN	NaN	NaN	NaN	NaN	NaN	
49	FI-Sii	2014	NaN	NaN	NaN	NaN	NaN	NaN	NaN	NaN	NaN	NaN	NaN	NaN	NaN	NaN	NaN	NaN	NaN	NaN	NaN	NaN	NaN	
50	FI-Sii	2015	NaN	NaN	NaN	NaN	NaN	NaN	NaN	NaN	NaN	NaN	NaN	NaN	NaN	NaN	NaN	NaN	NaN	NaN	NaN	NaN	NaN	
51	FI-Sii	2016	NaN	NaN	NaN	NaN	NaN	NaN	NaN	NaN	NaN	NaN	NaN	NaN	NaN	NaN	NaN	NaN	NaN	NaN	NaN	NaN	NaN	
52	FI-Sii	2017	NaN	NaN	NaN	NaN	NaN	NaN	NaN	NaN	NaN	NaN	NaN	NaN	NaN	NaN	NaN	NaN	NaN	NaN	NaN	NaN	NaN	
53	FI-Sii	2018	NaN	NaN	NaN	NaN	NaN	NaN	NaN	NaN	NaN	NaN	NaN	NaN	NaN	NaN	NaN	NaN	NaN	NaN	NaN	NaN	NaN	
54	HK-MPM	2016	TS_2	NaN	NaN	566.87	0.00	7.79	219.80	28.92	NaN	NaN	NaN	NaN	NaN	NaN	NaN	NaN	NaN	NaN	NaN	NaN	NaN	
55	HK-MPM	2017	TS_2	NaN	NaN	NaN	0.00	8.73	218.50	29.13	NaN	NaN	NaN	NaN	NaN	NaN	NaN	NaN	NaN	NaN	NaN	NaN	NaN	
56	HK-MPM	2018	TS_2	NaN	NaN	NaN	0.00	7.23	204.90	28.66	NaN	NaN	NaN	NaN	NaN	NaN	NaN	NaN	NaN	NaN	NaN	NaN	NaN	
57	ID-Pag	2016	NaN	NaN	NaN	NaN	NaN	NaN	NaN	NaN	NaN	NaN	NaN	NaN	NaN	NaN	NaN	NaN	NaN	NaN	NaN	NaN	NaN	
58	JP-BBY	2015	TS_1	-0.18	87.83	340.83	0.94	21.59	218.10	22.53	NaN	NaN	NaN	NaN	NaN	NaN	NaN	NaN	NaN	NaN	NaN	NaN	NaN	
59	JP-BBY	2016	TS_1	-0.18	80.75	330.60	0.36	22.19	217.80	22.55	NaN	NaN	NaN	NaN	NaN	NaN	NaN	NaN	NaN	NaN	NaN	NaN	NaN	
60	JP-BBY	2017	TS_1	-0.18	80.38	347.77	0.20	21.75	213.80	21.95	NaN	NaN	NaN	NaN	NaN	NaN	NaN	NaN	NaN	NaN	NaN	NaN	NaN	
61	JP-BBY	2018	TS_1	-0.18	78.28	355.38	0.50	20.38	222.00	20.88	NaN	NaN	NaN	NaN	NaN	NaN	NaN	NaN	NaN	NaN	NaN	NaN	NaN	
62	JP-Mse	2012	TS_1	-0.01	60.38	348.86	2.15	23.76	211.80	25.91	NaN	NaN	NaN	NaN	NaN	NaN	NaN	NaN	NaN	NaN	NaN	NaN	NaN	
63	KR-CRK	2015	NaN	NaN	NaN	NaN	NaN	NaN	NaN	NaN	NaN	NaN	NaN	NaN	NaN	NaN	NaN	NaN	NaN	NaN	NaN	NaN	NaN	
64	KR-CRK	2016	NaN	NaN	NaN	NaN	NaN	NaN	NaN	NaN	NaN	NaN	NaN	NaN	NaN	NaN	NaN	NaN	NaN	NaN	NaN	NaN	NaN	



99	US-BZF	2014	TS_1	-0.08	96.05	322.79	-1.56	16.12	205.40	14.56
100	US-BZF	2015	TS_1	-0.08	108.39	331.07	-1.20	14.88	197.50	13.68
101	US-BZF	2016	TS_1	-0.08	95.50	315.89	-1.03	17.18	205.10	16.15
102	US-BZS	2015	TS_1	NaN	116.48	275.22	-0.07	4.87	202.90	4.79
103	US-BZS	2016	TS_1	NaN	119.07	278.90	-0.05	5.58	208.40	5.54
104	US-DPW	2013	NaN	NaN	NaN	NaN	NaN	NaN	NaN	NaN
105	US-DPW	2014	NaN	NaN	NaN	NaN	NaN	NaN	NaN	NaN
106	US-DPW	2015	NaN	NaN	NaN	NaN	NaN	NaN	NaN	NaN
107	US-DPW	2016	NaN	NaN	NaN	NaN	NaN	NaN	NaN	NaN
108	US-HRA	2017	NaN	NaN	NaN	NaN	NaN	NaN	NaN	NaN
109	US-HRC	2018	NaN	NaN	NaN	NaN	NaN	NaN	NaN	NaN
110	US-ICS	2014	TS_1	-0.08	147.27	263.08	-0.08	5.47	205.60	5.39
111	US-ICS	2015	TS_1	-0.08	141.61	255.70	-0.02	6.12	195.20	6.10
112	US-ICS	2016	TS_1	-0.08	146.75	265.86	-0.05	5.67	206.20	5.62
113	US-Ivo	2013	NaN	NaN	NaN	NaN	NaN	NaN	NaN	NaN
114	US-Ivo	2014	TS_1	-0.05	136.92	264.34	-0.20	10.84	195.70	10.64
115	US-Ivo	2015	TS_1	-0.05	139.42	257.06	-0.14	14.86	185.60	14.72
116	US-Ivo	2016	TS_1	-0.05	133.60	262.43	-0.10	8.90	197.30	8.80
117	US-LA1	2012	TS_1	-0.10	29.15	331.44	15.59	13.50	197.20	29.08
118	US-LA2	2012	TS_1	-0.10	36.65	336.05	15.04	14.35	193.20	29.39
119	US-LA2	2013	TS_1	-0.10	65.79	377.93	14.70	16.06	201.50	30.76
120	US-Los	2014	TS_1	0.00	136.18	417.40	1.95	8.26	244.30	10.22
121	US-Los	2015	TS_1	0.00	148.23	422.27	2.43	7.76	258.70	10.19
122	US-Los	2016	TS_1	0.00	135.20	415.75	2.47	8.08	255.10	10.56
123	US-Los	2017	TS_1	0.00	141.15	414.62	1.89	7.45	256.00	9.34
124	US-Los	2018	TS_1	0.00	169.83	421.79	1.46	7.42	260.00	8.88
125	US-MAC	2013	NaN	NaN	NaN	NaN	NaN	NaN	NaN	NaN
126	US-MAC	2014	NaN	NaN	NaN	NaN	NaN	NaN	NaN	NaN
127	US-MAC	2015	NaN	NaN	NaN	NaN	NaN	NaN	NaN	NaN
128	US-Myb	2010	NaN	NaN	NaN	NaN	NaN	NaN	NaN	NaN
129	US-Myb	2011	TS_3	-0.08	NaN	329.50	12.12	8.86	231.70	20.98
130	US-Myb	2012	TS_3	-0.08	35.60	372.21	9.39	10.96	216.10	20.36
131	US-Myb	2013	TS_3	-0.08	34.38	354.74	9.25	11.28	210.90	20.52
132	US-Myb	2014	TS_3	-0.08	26.04	365.88	9.64	12.28	210.00	21.93



133	US-Myb	2015	TS_3	-0.08	17.34	340.72	9.77	11.85	212.00	21.62
134	US-Myb	2016	TS_3	-0.08	5.05	357.82	9.61	11.19	201.00	20.80
135	US-Myb	2017	TS_3	-0.08	27.31	352.90	9.86	13.10	214.00	22.96
136	US-Myb	2018	TS_3	-0.08	36.27	326.10	10.20	10.72	207.00	20.92
137	US-NC4	2012	TS_1	-0.05	42.43	336.03	7.87	15.75	215.40	23.62
138	US-NC4	2013	TS_1	-0.05	59.96	368.85	6.92	16.83	210.50	23.74
139	US-NC4	2014	TS_1	-0.05	54.42	362.34	6.73	16.81	208.50	23.54
140	US-NC4	2015	TS_1	-0.05	68.13	387.31	8.27	16.06	205.00	24.33
141	US-NC4	2016	TS_1	-0.05	52.97	351.38	9.41	15.04	220.00	24.45
142	US-ORv	2011	NaN	NaN	NaN	NaN	NaN	NaN	NaN	NaN
143	US-ORv	2012	TS	NaN	57.42	352.55	4.36	20.61	203.90	24.97
144	US-ORv	2013	TS	NaN	63.67	356.74	2.93	19.98	210.80	22.90
145	US-ORv	2014	TS	NaN	68.11	364.96	2.11	20.17	205.30	22.28
146	US-ORv	2015	TS	NaN	68.77	387.78	1.77	21.26	206.00	23.04
147	US-OWC	2015	NaN	NaN	NaN	NaN	NaN	NaN	NaN	NaN
148	US-OWC	2016	TS_1	-0.05	0.00	0.00	0.00	0.00	211.20	23.91
149	US-Sne	2016	NaN	NaN	NaN	NaN	NaN	NaN	NaN	NaN
150	US-Sne	2017	TS_1	-0.01	46.07	337.92	10.33	13.14	212.70	23.47
151	US-Sne	2018	TS_1	-0.01	48.41	325.09	10.28	12.15	217.30	22.43
152	US-Srr	2014	NaN	NaN	NaN	NaN	NaN	NaN	NaN	NaN
153	US-Srr	2015	NaN	NaN	NaN	NaN	NaN	NaN	NaN	NaN
154	US-Srr	2016	TS_1	NaN	NaN	326.29	10.03	10.71	200.50	20.74
155	US-Srr	2017	TS_1	NaN	11.34	346.85	7.22	13.71	199.50	20.93
156	US-StJ	2016	TS_2	-0.05	68.37	347.38	4.05	16.22	213.70	20.27
157	US-Tw1	2011	NaN	NaN	NaN	NaN	NaN	NaN	NaN	NaN
158	US-Tw1	2012	TS_1	-0.02	50.54	359.96	5.99	11.52	225.20	17.51
159	US-Tw1	2013	TS_1	-0.02	35.80	337.57	4.39	14.59	206.60	18.97
160	US-Tw1	2014	TS_1	-0.02	41.23	395.41	6.67	10.89	208.30	17.56
161	US-Tw1	2015	TS_1	-0.02	50.66	342.55	9.02	7.83	235.00	16.85
162	US-Tw1	2016	TS_1	-0.02	34.57	361.06	8.78	7.94	218.00	16.72
163	US-Tw1	2017	TS_1	-0.02	41.17	343.75	7.55	10.22	228.00	17.77
164	US-Tw1	2018	TS_1	-0.02	60.47	327.43	6.70	10.42	222.00	17.12
165	US-Tw4	2014	NaN	NaN	NaN	NaN	NaN	NaN	NaN	NaN
166	US-Tw4	2015	TS_1	-0.02	15.93	327.22	10.04	11.56	199.40	21.60



167	US-Tw4	2016	TS_1	-0.02	9.56	358.75	8.16	11.29	201.70	19.45
168	US-Tw4	2017	TS_1	-0.02	38.35	347.31	8.07	11.52	211.90	19.59
169	US-Tw4	2018	TS_1	-0.02	58.11	344.87	8.00	10.93	218.00	18.93
170	US-Tw5	2018	TS_1	-0.02	NaN	414.83	0.00	8.89	222.20	18.37
171	US-Twt	2009	NaN	NaN	NaN	NaN	NaN	NaN	NaN	NaN
172	US-Twt	2010	NaN	NaN	NaN	NaN	NaN	NaN	NaN	NaN
173	US-Twt	2011	NaN	NaN	NaN	NaN	NaN	NaN	NaN	NaN
174	US-Twt	2012	NaN	NaN	NaN	NaN	NaN	NaN	NaN	NaN
175	US-Twt	2013	NaN	NaN	NaN	NaN	NaN	NaN	NaN	NaN
176	US-Twt	2014	NaN	NaN	NaN	NaN	NaN	NaN	NaN	NaN
177	US-Twt	2015	NaN	NaN	NaN	NaN	NaN	NaN	NaN	NaN
178	US-Twt	2016	NaN	NaN	NaN	NaN	NaN	NaN	NaN	NaN
179	US-Uaf	2011	TS_1	-0.09	86.20	372.46	-12.29	21.95	199.60	9.67
180	US-Uaf	2012	TS_1	-0.09	73.77	338.53	-11.83	20.86	202.40	9.03
181	US-Uaf	2013	TS_1	-0.09	109.63	395.51	-10.08	20.52	200.40	10.44
182	US-Uaf	2014	TS_1	-0.09	76.07	365.40	-10.94	19.94	206.00	9.00
183	US-Uaf	2015	TS_1	-0.09	80.99	423.19	-9.77	19.76	190.00	10.00
184	US-Uaf	2016	TS_1	-0.09	77.38	315.75	-7.74	19.13	198.00	11.39
185	US-Uaf	2017	TS_1	-0.09	84.88	380.17	-7.39	19.08	196.00	11.69
186	US-Uaf	2018	TS_1	-0.09	96.04	333.33	-5.60	17.72	199.00	12.11
187	US-WPT	2011	TS_1	-0.10	80.95	342.17	5.27	19.27	202.60	24.54
188	US-WPT	2012	TS_1	-0.10	40.29	345.57	3.70	21.60	197.40	25.30
189	US-WPT	2013	TS_1	-0.10	74.61	340.47	3.73	18.23	207.20	21.96

Column Descriptions

Site	Site name
Year	Data year
Probe_name	Temperature probe name as given in data files
Soil_temp_depth_m	Depth of soil temperature probe (m), with negative values being under the surface
Start_TS_(DOY)	Season start for elevated TS (DOY), point "f" in Figure 1
End_TS_(DOY)	Season end for elevated TS (DOY), point "h" in Figure 1
Base_value_(C)	Baseline TS during non-elevated season (C), average of points "a" and "b" in Figure 1



Ampl_TS_(C)	Amplitude of TS during elevated temperature season (C), difference between point "e" in Figure 1 and Base_value_TS
Peak_TS_(DOY)	Day of maximum elevated TS (DOY), point "g" in Figure 1
Peak_value_TS_(C)	Maximum value of TS (C) point "e" in Figure 1



Table B5: Timesat output for all soil temperature probes

Site	Year	Probe_name	Soil_temp_depth_m	Start_TS_(DOY)	End_TS_(DOY)	Base_value_TS_(C)	Ampl_T_S_(C)	Peak_TS_(DOY)	Peak_value_TS_(C)
1	AT-Neu	2010 TS_1	-0.05	61.32	339.44	0.15	17.54	200.9	17.7
2	AT-Neu	2011 TS_1	-0.05	51.04	328.84	0.40	16.37	201	16.77
3	AT-Neu	2012 TS_1	-0.05	61.12	341.88	0.73	17.57	202.9	18.3
4	BR-Npw	2016 TS_1	NaN	18.41	343.22	22.41	5.982	188	28.4
5	CA-SCB	2014 TS_1	0	105.94	292.18	-0.63	20.62	196.6	19.99
6	CA-SCB	2014 TS_2	-0.02	105.15	294.06	-0.74	20.42	197.5	19.68
7	CA-SCB	2014 TS_3	-0.04	112.00	294.38	0.05	19.07	199.6	19.11
8	CA-SCB	2014 TS_5	-0.16	123.21	317.72	-1.38	18.6	205.3	17.23
9	CA-SCB	2015 TS_1	0	106.92	287.14	-0.39	17.23	186.8	16.84
10	CA-SCB	2015 TS_2	-0.02	107.06	287.40	-0.42	17.08	187.4	16.66
11	CA-SCB	2015 TS_3	-0.04	107.45	289.83	-0.51	16.81	188.9	16.3
12	CA-SCB	2015 TS_5	-0.16	114.95	305.55	-0.39	15.84	195.7	15.45
13	CA-SCB	2016 TS_1	0	101.64	284.09	-0.31	19.07	193.2	18.77
14	CA-SCB	2016 TS_2	-0.02	101.81	284.11	-0.30	18.96	193.5	18.66
15	CA-SCB	2016 TS_3	-0.04	102.22	285.19	-0.30	18.6	194.3	18.3
16	CA-SCB	2016 TS_5	-0.16	101.16	298.99	-0.24	16.99	201.1	16.74
17	CA-SCB	2017 TS_1	0	107.44	289.72	-0.25	17.67	198	17.42
18	CA-SCB	2017 TS_2	-0.02	107.22	288.88	-0.25	17.59	198	17.33
19	CA-SCB	2017 TS_3	-0.04	108.58	289.29	-0.26	17.28	199	17.02
20	CA-SCB	2017 TS_5	-0.16	116.34	300.28	-0.24	14.95	214	14.71
21	CA-SCC	2014 TS_1	-0.1	123.36	287.06	-0.55	15.64	203	15.09
22	CA-SCC	2014 TS_2	-0.15	114.89	287.71	-0.83	14.49	200.8	13.66
23	CA-SCC	2014 TS_3	-0.2	111.36	288.63	-0.69	11.52	194.9	10.84
24	CA-SCC	2014 TS_4	-0.25	129.50	287.24	-0.22	8.612	207.4	8.391
25	CA-SCC	2014 TS_5	-0.3	142.36	287.99	-0.10	6.329	212.1	6.225
26	CA-SCC	2015 TS_1	-0.1	113.88	285.22	-0.28	16.26	189.2	15.98
27	CA-SCC	2015 TS_2	-0.15	113.05	284.18	-0.24	14.56	192.8	14.32
28	CA-SCC	2015 TS_3	-0.2	111.76	285.45	-0.22	12.71	199.1	12.48
29	CA-SCC	2015 TS_4	-0.25	120.81	287.09	-0.16	10.08	204.8	9.922
30	CA-SCC	2015 TS_5	-0.3	131.92	285.42	-0.09	7.705	209.2	7.616



31	CA-SCC	2016 TS_1	-0.1	108.09	260.12	-0.33	18.37	190.9	18.04
32	CA-SCC	2016 TS_2	-0.15	108.96	260.19	-0.30	17.31	192.1	17.01
33	CA-SCC	2016 TS_3	-0.2	110.49	260.44	-0.26	15.4	194.1	15.14
34	CA-SCC	2016 TS_4	-0.25	119.21	260.34	-0.20	13.38	200.2	13.18
35	CA-SCC	2016 TS_5	-0.3	130.75	261.73	-0.12	10.03	202.2	9.906
36	DE-Hte	2012 TS_3	-0.2	76.96	344.01	4.98	12.26	215.5	17.23
37	DE-Hte	2013 TS_3	-0.2	60.92	377.99	3.96	11.99	207.9	15.95
38	DE-Hte	2014 TS_1	0	NaN	327.83	8.52	8.342	205.6	16.87
39	DE-Hte	2015 TS_1	0	62.92	360.55	5.17	11.67	187.4	16.84
40	DE-Hte	2016 TS_1	0	71.87	NaN	4.94	12.36	175.6	17.3
41	DE-Hte	2017 TS_1	0	61.55	343.32	4.50	11.76	186	16.26
42	DE-SFN	2012 TS_1	-0.02	NaN	372.59	0.00	23.55	206.5	15.29
43	DE-SFN	2012 TS_3	-0.1	NaN	366.65	1.64	12.91	219.7	14.55
44	DE-SFN	2012 TS_4	-0.2	NaN	367.40	4.86	7.276	242.7	12.14
45	DE-SFN	2012 TS_5	-0.5	NaN	367.40	4.86	7.276	242.7	12.14
46	DE-SFN	2013 TS_1	-0.02	55.84	381.50	0.92	13.62	216.4	14.54
47	DE-SFN	2013 TS_3	-0.1	60.45	384.77	1.56	12.5	221.1	14.06
48	DE-SFN	2013 TS_4	-0.2	83.55	394.53	3.62	8.417	243.4	12.04
49	DE-SFN	2013 TS_5	-0.5	83.55	394.53	3.62	8.417	243.4	12.04
50	DE-Zrk	2014 TS_1	-0.05	54.79	361.65	4.36	13.93	202.3	18.29
51	DE-Zrk	2014 TS_2	-0.1	59.27	366.51	4.87	12.65	207.3	17.52
52	DE-Zrk	2014 TS_3	-0.2	62.95	371.30	5.53	11.5	211.7	17.03
53	DE-Zrk	2014 TS_4	-0.3	67.45	375.14	6.05	10.4	216.5	16.45
54	DE-Zrk	2014 TS_5	-0.5	72.50	378.95	6.57	9.359	221	15.93
55	DE-Zrk	2015 TS_1	-0.05	58.29	359.29	4.28	13.24	215.5	17.52
56	DE-Zrk	2015 TS_2	-0.1	62.61	364.99	4.79	12	219.8	16.8
57	DE-Zrk	2015 TS_3	-0.2	66.01	369.78	5.42	10.87	223.7	16.29
58	DE-Zrk	2015 TS_4	-0.3	70.47	374.40	5.93	9.771	228	15.7
59	DE-Zrk	2015 TS_5	-0.5	74.71	378.76	6.43	8.751	232.2	15.19
60	DE-Zrk	2016 TS_1	-0.05	72.81	332.00	4.28	14.93	200.4	19.2
61	DE-Zrk	2016 TS_2	-0.1	76.31	337.37	4.79	13.6	204.4	18.39
62	DE-Zrk	2016 TS_3	-0.2	79.73	343.16	5.43	12.33	208.1	17.77
63	DE-Zrk	2016 TS_4	-0.3	83.58	347.57	5.94	11.14	212	17.09
64	DE-Zrk	2016 TS_5	-0.5	87.15	354.22	6.40	10.07	216	16.47



65	DE-Zrk	2017 TS_1	-0.05	69.10	351.44	4.40	14.72	199	19.12
66	DE-Zrk	2017 TS_2	-0.1	73.29	356.52	4.91	13.33	204	18.23
67	DE-Zrk	2017 TS_3	-0.2	77.19	362.40	5.56	12.02	208	17.58
68	DE-Zrk	2017 TS_4	-0.3	82.20	367.20	6.04	10.8	212	16.84
69	DE-Zrk	2017 TS_5	-0.5	86.22	372.96	6.48	9.675	217	16.15
70	DE-Zrk	2018 TS_1	-0.05	84.47	336.14	4.83	12.32	203	17.14
71	DE-Zrk	2018 TS_2	-0.1	86.60	342.59	5.30	11.27	208	16.57
72	DE-Zrk	2018 TS_3	-0.2	87.68	348.07	5.89	10.25	212	16.14
73	DE-Zrk	2018 TS_4	-0.3	89.82	354.77	6.31	9.308	217	15.61
74	DE-Zrk	2018 TS_5	-0.5	92.01	360.46	6.69	8.412	222	15.11
75	FI-Lom	2006 TS_1	-0.07	114.15	290.83	-0.11	13.42	204.8	13.31
76	FI-Lom	2006 TS_2	-0.3	117.21	307.88	0.27	12.01	214.1	12.28
77	FI-Lom	2006 TS_3	-0.5	128.82	329.03	1.06	9.071	225.8	10.13
78	FI-Lom	2007 TS_1	-0.07	126.84	302.05	0.11	13.05	200	13.16
79	FI-Lom	2007 TS_2	-0.3	134.00	321.03	0.42	11.5	207.5	11.92
80	FI-Lom	2007 TS_3	-0.5	138.37	348.03	1.06	8.873	221.1	9.936
81	FI-Lom	2008 TS_1	-0.07	135.62	296.74	0.16	12.73	202.9	12.88
82	FI-Lom	2008 TS_2	-0.3	141.46	318.74	0.58	10.62	209.6	11.2
83	FI-Lom	2008 TS_3	-0.5	146.70	349.21	1.17	8.214	221.2	9.382
84	FI-Lom	2009 TS_1	-0.07	117.16	291.86	0.14	11.73	214	11.87
85	FI-Lom	2009 TS_2	-0.3	123.51	314.51	0.67	9.692	221	10.36
86	FI-Lom	2009 TS_3	-0.5	133.69	336.65	1.30	7.896	233	9.193
87	FI-Lom	2010 TS_1	-0.07	129.91	318.54	0.05	12.13	208	12.18
88	FI-Lom	2010 TS_2	-0.3	138.09	338.24	0.52	9.962	218	10.48
89	FI-Lom	2010 TS_3	-0.5	147.34	359.95	1.19	7.344	231	8.532
90	FI-Si2	2012 TS_1	-0.05	NaN	323.46	0.00	19.85	204.6	16.02
91	FI-Si2	2012 TS_2	-0.2	103.64	333.52	-0.04	15.75	217.5	15.71
92	FI-Si2	2012 TS_3	-0.35	105.57	NaN	0.00	19.38	230.6	15.09
93	FI-Si2	2012 TS_4	-0.5	110.87	NaN	0.00	17.26	237.5	14.66
94	FI-Si2	2013 TS_1	-0.05	106.90	341.05	-0.05	16.04	199.4	15.98
95	FI-Si2	2013 TS_2	-0.2	102.57	356.13	0.23	14.91	207.3	15.14
96	FI-Si2	2013 TS_3	-0.35	NaN	376.47	0.00	18.26	209.6	14.23
97	FI-Si2	2013 TS_4	-0.5	NaN	392.35	0.00	16.71	216.4	13.48
98	FI-Si2	2014 TS_1	-0.05	104.63	331.10	-0.04	17.07	208.5	17.03



99	FI-SI2	2014 TS_2	-0.2	107.82	359.78	0.59	15.33	215.3	15.92
100	FI-SI2	2014 TS_3	-0.35	112.02	385.94	0.99	13.61	222.2	14.61
101	FI-SI2	2014 TS_4	-0.5	118.24	400.15	1.59	12.01	229.1	13.59
102	FI-SI2	2015 TS_1	-0.05	76.49	352.34	-0.87	16.31	211	15.44
103	FI-SI2	2015 TS_2	-0.2	80.08	364.72	-0.41	14.83	218	14.42
104	FI-SI2	2015 TS_3	-0.35	82.01	374.79	0.12	13.27	225	13.39
105	FI-SI2	2015 TS_4	-0.5	88.25	382.37	0.84	11.7	233	12.53
106	FI-SI2	2016 TS_1	-0.05	102.64	329.42	-0.88	16.48	206	15.6
107	FI-SI2	2016 TS_2	-0.2	102.16	361.04	-0.77	16.02	212	15.25
108	FI-SI2	2016 TS_3	-0.35	103.15	383.82	-0.63	14.7	219	14.07
109	FI-SI2	2016 TS_4	-0.5	104.76	399.01	-0.20	13.36	227	13.16
110	HK-MPM	2016 TS_2	NaN	NaN	566.87	0.00	7.789	219.8	28.92
111	HK-MPM	2016 TS_3	NaN	NaN	373.06	20.56	7.386	227.3	27.95
112	HK-MPM	2017 TS_2	NaN	NaN	NaN	0.00	8.726	218.5	29.13
113	HK-MPM	2017 TS_3	NaN	69.55	364.53	19.53	8.572	233.6	28.1
114	HK-MPM	2018 TS_2	NaN	NaN	NaN	0.00	7.231	204.9	28.66
115	HK-MPM	2018 TS_3	NaN	64.82	383.39	19.17	8.406	221.4	27.58
116	JP-BBY	2015 TS_1	-0.183	87.83	340.83	0.94	21.59	218.1	22.53
117	JP-BBY	2015 TS_2	-0.233	90.59	340.99	1.34	20.9	219.9	22.25
118	JP-BBY	2015 TS_3	-0.283	90.34	341.60	1.58	20.42	221.4	22
119	JP-BBY	2015 TS_4	-0.383	96.01	341.35	2.39	19.09	225.1	21.48
120	JP-BBY	2015 TS_5	-0.483	95.83	341.49	2.91	18.09	228.9	21
121	JP-BBY	2016 TS_1	-0.183	80.75	330.60	0.36	22.19	217.8	22.55
122	JP-BBY	2016 TS_2	-0.233	82.30	335.40	0.67	21.64	220.8	22.3
123	JP-BBY	2016 TS_3	-0.283	84.28	332.64	0.99	21.1	222	22.09
124	JP-BBY	2016 TS_4	-0.383	89.00	332.43	1.76	19.92	225.6	21.68
125	JP-BBY	2016 TS_5	-0.483	94.29	331.91	2.44	18.83	228.9	21.27
126	JP-BBY	2017 TS_1	-0.183	80.38	347.77	0.20	21.75	213.8	21.95
127	JP-BBY	2017 TS_2	-0.233	84.54	347.79	0.82	21.02	214.6	21.83
128	JP-BBY	2017 TS_3	-0.283	86.19	347.10	1.06	20.56	216.3	21.62
129	JP-BBY	2017 TS_4	-0.383	92.20	346.01	1.97	19.34	218.5	21.31
130	JP-BBY	2017 TS_5	-0.483	98.15	345.18	2.70	18.34	221	21.03
131	JP-BBY	2018 TS_1	-0.183	78.28	355.38	0.50	20.38	222	20.88
132	JP-BBY	2018 TS_2	-0.233	83.55	357.60	1.48	19.23	224	20.7



133	JP-BBY	2018 TS_3	-0.283	85.93	355.90	1.69	18.78	225	20.47
134	JP-BBY	2018 TS_4	-0.383	95.89	351.34	2.81	17.25	229	20.07
135	JP-BBY	2018 TS_5	-0.483	103.83	349.39	3.63	16.1	232	19.73
136	JP-Mse	2012 TS_1	-0.01	60.38	348.86	2.15	23.76	211.8	25.91
137	MY-MLM	2014 TS	NaN	NaN	358.37	25.06	3.968	194.5	29.03
138	MY-MLM	2015 TS	NaN	27.32	NaN	25.57	1.973	172.7	27.55
139	NZ-Kop	2012 TS_1	-0.5	62.54	360.29	8.30	8.394	219.8	16.7
140	NZ-Kop	2012 TS_2	-0.1	65.53	362.35	8.45	8.093	222.1	16.54
141	NZ-Kop	2012 TS_3	-0.2	68.77	365.64	8.73	7.243	228.2	15.98
142	NZ-Kop	2013 TS_1	-0.5	45.63	367.00	8.41	7.635	210.5	16.04
143	NZ-Kop	2013 TS_2	-0.1	47.60	370.98	8.54	7.486	212.3	16.03
144	NZ-Kop	2013 TS_3	-0.2	52.74	377.20	8.82	6.87	217.8	15.69
145	NZ-Kop	2014 TS_1	-0.5	56.88	365.68	8.16	8.79	219	16.95
146	NZ-Kop	2014 TS_2	-0.1	59.45	367.47	8.29	8.512	221	16.8
147	NZ-Kop	2014 TS_3	-0.2	62.93	372.48	8.55	7.792	226	16.34
148	NZ-Kop	2015 TS_1	-0.5	56.49	371.82	7.73	9.355	214	17.09
149	NZ-Kop	2015 TS_2	-0.1	58.32	374.74	7.87	9.063	217	16.93
150	NZ-Kop	2015 TS_3	-0.2	62.67	378.44	8.19	8.217	222	16.4
151	RU-Ch2	2014 TS_1	-0.04	138.76	263.76	-0.13	14.42	206.6	14.29
152	RU-Ch2	2014 TS_2	-0.08	146.08	262.11	-0.14	13.03	206.5	12.9
153	RU-Ch2	2014 TS_3	-0.16	155.95	264.51	-0.05	4.581	210.5	4.535
154	RU-Ch2	2015 TS_1	-0.04	143.88	269.56	-0.14	13.97	193.3	13.83
155	RU-Ch2	2015 TS_2	-0.08	147.34	265.69	-0.10	12.3	195.7	12.2
156	RU-Ch2	2015 TS_3	-0.16	159.93	266.60	-0.04	3.995	205.2	3.96
157	RU-Ch2	2016 TS_1	-0.04	126.98	273.54	-0.16	11.64	200.2	11.48
158	RU-Ch2	2016 TS_2	-0.08	133.92	272.58	-0.10	10.06	203.2	9.964
159	RU-Ch2	2016 TS_3	-0.16	147.99	275.45	-0.04	4.042	217.7	4.001
160	RU-Che	2014 TS_1	-0.04	138.05	267.57	-0.12	15.04	208	14.92
161	RU-Che	2014 TS_2	-0.08	149.72	263.67	-0.09	8.959	206.6	8.873
162	RU-Che	2014 TS_3	-0.16	154.97	265.49	-0.07	7.006	210.3	6.938
163	RU-Che	2015 TS_1	-0.04	143.85	274.68	-0.17	14.81	193.7	14.64
164	RU-Che	2015 TS_2	-0.08	149.49	267.08	-0.06	8.336	197.9	8.273
165	RU-Che	2015 TS_3	-0.16	154.48	271.03	-0.04	5.942	202.4	5.9
166	RU-Che	2016 TS_1	-0.04	126.72	274.03	-0.19	12.95	200.4	12.76



167	RU-Che	2016 TS_2	-0.08	137.01	273.70	-0.07	7.076	205.4	7.01
168	RU-Che	2016 TS_3	-0.16	142.51	275.62	-0.05	5.498	211.8	5.451
169	SE-Deg	2014 TS_1	-0.02	111.85	303.55	-0.53	17.22	201.6	16.69
170	SE-Deg	2014 TS_2	-0.05	119.11	308.12	-0.31	13.23	207.4	12.93
171	SE-Deg	2014 TS_3	-0.1	125.46	315.55	-0.10	12.54	212	12.44
172	SE-Deg	2014 TS_4	-0.15	134.61	321.20	0.29	11.63	215.6	11.93
173	SE-Deg	2014 TS_5	-0.3	126.75	330.85	0.52	11.61	220	12.13
174	SE-Deg	2014 TS_6	-0.5	130.62	341.66	0.89	11.33	223.1	12.21
175	SE-Deg	2015 TS_1	-0.02	104.25	310.59	-0.28	15.2	207.2	14.91
176	SE-Deg	2015 TS_2	-0.05	110.64	312.57	0.09	13.86	209.5	13.95
177	SE-Deg	2015 TS_3	-0.1	112.94	321.41	0.41	12.94	212.9	13.36
178	SE-Deg	2015 TS_4	-0.15	115.72	329.21	0.60	11.94	216.6	12.54
179	SE-Deg	2015 TS_5	-0.3	118.31	339.17	0.90	11.08	220.5	11.98
180	SE-Deg	2015 TS_6	-0.5	121.80	347.97	1.30	10.19	224.6	11.48
181	SE-Deg	2016 TS_1	-0.02	108.14	306.39	-0.19	14.88	200.3	14.68
182	SE-Deg	2017 TS_1	-0.02	133.38	326.87	-0.20	12.35	215	12.15
183	SE-Deg	2018 TS_1	-0.02	111.67	310.21	-0.17	14.7	198	14.52
184	US-Atq	2014 TS_1	NaN	10.75	139.53	-0.20	8.068	61	7.864
185	US-Atq	2014 TS_2	NaN	18.00	137.32	-0.08	4.191	74.3	4.109
186	US-Atq	2014 TS_3	NaN	28.49	138.48	-0.03	2.366	83.5	2.334
187	US-Beo	2014 TS_1	NaN	155.09	270.13	-0.04	4.874	211.1	4.829
188	US-Beo	2014 TS_2	NaN	168.62	270.60	-0.02	2.94	219.6	2.922
189	US-Beo	2014 TS_3	NaN	170.53	269.49	-0.02	3.128	219.9	3.104
190	US-Bes	2013 TS_1	NaN	143.22	261.99	-0.05	5.649	201.3	5.602
191	US-Bes	2013 TS_2	NaN	150.57	267.49	-0.04	6.744	205.7	6.706
192	US-Bes	2013 TS_3	NaN	146.03	267.28	-0.06	8.248	202.3	8.187
193	US-Bes	2014 TS_1	NaN	151.79	282.29	-0.10	3.924	198.5	3.822
194	US-Bes	2015 TS_1	NaN	140.45	270.98	-0.11	4.763	195.3	4.65
195	US-Bes	2015 TS_2	NaN	148.76	269.64	-0.11	5.512	202.8	5.401
196	US-Bes	2015 TS_3	NaN	146.77	271.72	-0.16	7.182	197.8	7.027
197	US-BZB	2014 TS_1	-0.075	123.11	298.35	-0.44	15.35	215.8	14.91
198	US-BZB	2014 TS_2	-0.05	115.15	292.07	-0.59	15.49	209.9	14.9
199	US-BZB	2015 TS_1	-0.075	107.82	295.60	-0.38	14.04	210.2	13.67
200	US-BZB	2015 TS_2	-0.05	98.63	293.17	-0.67	14.56	203.5	13.9



201	US-BZB	2016 TS_1	-0.075	125.09	292.39	-0.33	16.39	214.3	16.06
202	US-BZB	2016 TS_2	-0.05	109.89	290.95	-0.74	16.89	211.7	16.15
203	US-BZF	2014 TS_1	-0.075	96.05	322.79	-1.56	16.12	205.4	14.56
204	US-BZF	2014 TS_2	-0.05	112.68	322.83	-1.22	15.9	208.3	14.68
205	US-BZF	2015 TS_1	-0.075	108.39	331.07	-1.20	14.88	197.5	13.68
206	US-BZF	2015 TS_2	-0.05	111.46	336.09	-1.12	14.83	200.2	13.72
207	US-BZF	2016 TS_1	-0.075	95.50	315.89	-1.03	17.18	205.1	16.15
208	US-BZF	2016 TS_2	-0.05	100.12	317.57	-0.90	17.72	206	16.81
209	US-BZS	2015 TS_1	NaN	116.48	275.22	-0.07	4.866	202.9	4.792
210	US-BZS	2015 TS_2	NaN	97.29	283.75	-0.27	8.135	187.7	7.862
211	US-BZS	2015 TS_3	NaN	105.93	272.47	-0.13	10.61	193.1	10.47
212	US-BZS	2016 TS_1	NaN	119.07	278.90	-0.05	5.584	208.4	5.535
213	US-BZS	2016 TS_2	NaN	87.59	278.96	-0.25	12.09	203.1	11.84
214	US-BZS	2016 TS_3	NaN	98.29	277.92	-0.16	11.67	198.8	11.51
215	US-ICS	2014 TS_1	-0.075	147.27	263.08	-0.08	5.467	205.6	5.39
216	US-ICS	2014 TS_2	-0.05	147.13	262.66	-0.01	6.41	205.1	6.402
217	US-ICS	2015 TS_1	-0.075	141.61	255.70	-0.02	6.12	195.2	6.098
218	US-ICS	2015 TS_2	-0.05	140.38	256.88	-0.02	7.07	193.1	7.047
219	US-ICS	2016 TS_1	-0.075	146.75	265.86	-0.05	5.67	206.2	5.623
220	US-ICS	2016 TS_2	-0.05	146.79	265.67	-0.05	6.654	206.1	6.599
221	US-Ivo	2014 TS_1	-0.05	136.92	264.34	-0.20	10.84	195.7	10.64
222	US-Ivo	2014 TS_1	-0.4	136.92	264.34	-0.20	10.84	195.7	10.64
223	US-Ivo	2014 TS_2	-0.1	142.52	266.53	-0.16	9.908	195.5	9.744
224	US-Ivo	2014 TS_3	-0.15	144.98	262.74	-0.19	6.761	204.8	6.574
225	US-Ivo	2014 TS_4	-0.3	166.58	262.05	-0.03	4.068	214.3	4.034
226	US-Ivo	2015 TS_1	-0.05	139.42	257.06	-0.14	14.86	185.6	14.72
227	US-Ivo	2015 TS_1	-0.4	139.42	257.06	-0.14	14.86	185.6	14.72
228	US-Ivo	2015 TS_2	-0.1	141.20	256.70	-0.09	11.99	189.1	11.9
229	US-Ivo	2015 TS_3	-0.15	145.76	260.99	-0.07	6.85	199.1	6.785
230	US-Ivo	2015 TS_4	-0.3	158.88	259.63	-0.03	4.032	208.2	3.997
231	US-Ivo	2016 TS_1	-0.05	133.60	262.43	-0.10	8.895	197.3	8.796
232	US-Ivo	2016 TS_1	-0.4	133.60	262.43	-0.10	8.895	197.3	8.796
233	US-Ivo	2016 TS_2	-0.1	139.70	264.19	-0.04	6.76	202.2	6.719
234	US-Ivo	2016 TS_3	-0.15	153.78	269.47	-0.05	4.305	211.5	4.253



235	US-Ivo	2016 TS_4	-0.3	171.24	271.03	-0.01	2.644	221.2	2.631
236	US-LA1	2012 TS_1	-0.1	29.15	331.44	15.59	13.5	197.2	29.08
237	US-LA2	2012 TS_1	-0.1	36.65	336.05	15.04	14.35	193.2	29.39
238	US-LA2	2013 TS_1	-0.1	65.79	377.93	14.70	16.06	201.5	30.76
239	US-Los	2014 TS_1	0	136.18	417.40	1.95	8.263	244.3	10.22
240	US-Los	2015 TS_1	0	148.23	422.27	2.43	7.761	258.7	10.19
241	US-Los	2016 TS_1	0	135.20	415.75	2.47	8.083	255.1	10.56
242	US-Los	2017 TS_1	0	141.15	414.62	1.89	7.451	256	9.343
243	US-Los	2018 TS_1	0	169.83	421.79	1.46	7.419	260	8.883
244	US-Myb	2011 TS_3	-0.08	NaN	329.50	12.12	8.859	231.7	20.98
245	US-Myb	2011 TS_4	-0.16	NaN	333.87	12.36	8.288	235.8	20.65
246	US-Myb	2011 TS_5	-0.32	NaN	338.98	12.72	7.56	241.4	20.28
247	US-Myb	2011 TS_1	-0.02	NaN	326.62	11.96	9.156	229.3	21.12
248	US-Myb	2012 TS_3	-0.08	35.60	372.21	9.39	10.96	216.1	20.36
249	US-Myb	2012 TS_4	-0.16	40.39	375.48	9.90	10.23	220.7	20.13
250	US-Myb	2012 TS_5	-0.32	47.39	379.29	10.56	9.212	227.2	19.78
251	US-Myb	2012 TS_1	-0.02	29.91	372.10	8.98	11.77	214.4	20.74
252	US-Myb	2013 TS_3	-0.08	34.38	354.74	9.25	11.28	210.9	20.52
253	US-Myb	2013 TS_4	-0.16	40.07	359.02	9.87	10.41	215	20.28
254	US-Myb	2013 TS_5	-0.32	45.10	363.81	10.53	9.441	221.9	19.97
255	US-Myb	2013 TS_1	-0.02	NaN	355.11	8.47	12.24	208.2	20.7
256	US-Myb	2014 TS_3	-0.08	26.04	365.88	9.64	12.28	210	21.93
257	US-Myb	2014 TS_4	-0.16	38.09	364.15	10.74	11.23	211	21.97
258	US-Myb	2014 TS_5	-0.32	44.34	366.12	11.25	10.25	218	21.5
259	US-Myb	2015 TS_3	-0.08	17.34	340.72	9.77	11.85	212	21.62
260	US-Myb	2015 TS_4	-0.16	12.76	339.04	10.79	10.84	221	21.63
261	US-Myb	2015 TS_5	-0.32	18.83	343.94	11.35	9.93	226	21.28
262	US-Myb	2016 TS_3	-0.08	5.05	357.82	9.61	11.19	201	20.8
263	US-Myb	2016 TS_4	-0.16	3.39	356.20	9.84	10.87	208	20.72
264	US-Myb	2016 TS_5	-0.32	12.02	360.46	10.73	9.627	214	20.36
265	US-Myb	2017 TS_3	-0.08	27.31	352.90	9.86	13.1	214	22.96
266	US-Myb	2017 TS_4	-0.16	28.29	357.41	9.92	12.74	215	22.66
267	US-Myb	2017 TS_5	-0.32	36.79	360.41	10.85	11.23	223	22.08
268	US-Myb	2017 TS_1	-0.02	62.79	325.72	12.70	10.71	216.8	23.41



269	US-Myb	2018 TS_3	-0.08	36.27	326.10	10.20	10.72	207	20.92
270	US-Myb	2018 TS_4	-0.16	41.30	332.83	10.47	10.35	209	20.82
271	US-Myb	2018 TS_5	-0.32	48.43	336.09	11.18	9.293	215	20.47
272	US-Myb	2018 TS_1	-0.02	38.38	344.86	10.05	11.93	200.3	21.98
273	US-NC4	2012 TS_1	-0.05	42.43	336.03	7.87	15.75	215.4	23.62
274	US-NC4	2013 TS_1	-0.05	59.96	368.85	6.92	16.83	210.5	23.74
275	US-NC4	2014 TS_1	-0.05	54.42	362.34	6.73	16.81	208.5	23.54
276	US-NC4	2015 TS_1	-0.05	68.13	387.31	8.27	16.06	205	24.33
277	US-NC4	2016 TS_1	-0.05	52.97	351.38	9.41	15.04	220	24.45
278	US-ORV	2012 TS	NaN	57.42	352.55	4.36	20.61	203.9	24.97
279	US-ORV	2013 TS	NaN	63.67	356.74	2.93	19.98	210.8	22.9
280	US-ORV	2014 TS	NaN	68.11	364.96	2.11	20.17	205.3	22.28
281	US-ORV	2015 TS	NaN	68.77	387.78	1.77	21.26	206	23.04
282	US-OWC	2016 TS_1	-0.05	0.00	0.00	0.00	0	211.2	23.91
283	US-Sne	2017 TS_1	-0.01	46.07	337.92	10.33	13.14	212.7	23.47
284	US-Sne	2017 TS_2	-0.02	41.06	341.82	10.76	12.66	205.7	23.41
285	US-Sne	2017 TS_3	-0.08	42.89	343.85	11.04	12.17	208.5	23.22
286	US-Sne	2017 TS_4	-0.16	46.36	346.18	11.39	11.79	211	23.18
287	US-Sne	2017 TS_5	-0.32	50.59	350.46	11.98	10.7	216	22.67
288	US-Sne	2018 TS_1	-0.01	48.41	325.09	10.28	12.15	217.3	22.43
289	US-Sne	2018 TS_2	-0.02	33.91	331.01	10.55	11.34	210.2	21.89
290	US-Sne	2018 TS_3	-0.08	36.76	331.50	10.87	10.63	212.1	21.5
291	US-Sne	2018 TS_4	-0.16	35.64	335.45	11.23	10.09	220.1	21.32
292	US-Sne	2018 TS_5	-0.32	49.09	335.94	11.88	9.045	218	20.92
293	US-Srr	2016 TS_1	NaN	NaN	326.29	10.03	10.71	200.5	20.74
294	US-Srr	2017 TS_1	NaN	11.34	346.85	7.22	13.71	199.5	20.93
295	US-StJ	2016 TS_2	-0.05	68.37	347.38	4.05	16.22	213.7	20.27
296	US-StJ	2016 TS_3	-0.1	68.38	347.38	5.84	14.1	213.7	19.94
297	US-Tw1	2012 TS_1	-0.02	50.54	359.96	5.99	11.52	225.2	17.51
298	US-Tw1	2012 TS_2	-0.04	48.02	358.76	6.14	11.32	227	17.46
299	US-Tw1	2012 TS_3	-0.08	50.07	367.92	5.18	12.31	222.1	17.49
300	US-Tw1	2012 TS_4	-0.16	49.05	367.52	5.31	12.19	224.5	17.5
301	US-Tw1	2012 TS_5	-0.32	-79.10	347.23	7.89	9.513	225.3	17.4
302	US-Tw1	2013 TS_1	-0.02	35.80	337.57	4.39	14.59	206.6	18.97



303	US-Tw1	2013 TS_2	-0.04	36.08	337.66	4.39	14.57	206.8	18.96
304	US-Tw1	2013 TS_3	-0.08	36.81	338.09	4.40	14.54	207.5	18.94
305	US-Tw1	2013 TS_4	-0.16	37.57	338.82	4.41	14.59	208.4	19.01
306	US-Tw1	2013 TS_5	-0.32	38.64	340.06	4.46	14.62	209.6	19.07
307	US-Tw1	2014 TS_1	-0.02	41.23	395.41	6.67	10.89	208.3	17.56
308	US-Tw1	2014 TS_2	-0.04	41.86	397.14	6.70	10.85	208.6	17.55
309	US-Tw1	2014 TS_3	-0.08	43.55	400.01	6.78	10.72	209.8	17.49
310	US-Tw1	2014 TS_4	-0.16	45.61	404.82	6.88	10.56	211.3	17.44
311	US-Tw1	2014 TS_5	-0.32	49.62	416.29	7.09	10.24	213.9	17.33
312	US-Tw1	2015 TS_1	-0.02	50.66	342.55	9.02	7.831	235	16.85
313	US-Tw1	2015 TS_2	-0.04	52.00	342.38	9.09	7.706	235	16.8
314	US-Tw1	2015 TS_3	-0.08	55.61	341.98	9.26	7.385	238	16.64
315	US-Tw1	2015 TS_4	-0.16	59.57	342.95	9.51	6.972	240	16.48
316	US-Tw1	2015 TS_5	-0.32	69.39	345.18	10.00	6.208	246	16.21
317	US-Tw1	2016 TS_1	-0.02	34.57	361.06	8.78	7.943	218	16.72
318	US-Tw1	2016 TS_2	-0.04	35.49	362.19	8.86	7.837	219	16.69
319	US-Tw1	2016 TS_3	-0.08	38.58	363.10	9.04	7.546	221	16.59
320	US-Tw1	2016 TS_4	-0.16	44.73	365.88	9.33	7.14	223	16.47
321	US-Tw1	2016 TS_5	-0.32	56.22	370.54	9.86	6.35	229	16.21
322	US-Tw1	2017 TS_1	-0.02	41.17	343.75	7.55	10.22	228	17.77
323	US-Tw1	2017 TS_2	-0.04	41.75	344.56	7.61	10.11	229	17.72
324	US-Tw1	2017 TS_3	-0.08	42.61	345.02	7.75	9.803	231	17.55
325	US-Tw1	2017 TS_4	-0.16	45.05	347.17	7.97	9.368	234	17.34
326	US-Tw1	2017 TS_5	-0.32	48.82	349.23	8.38	8.5	240	16.88
327	US-Tw1	2018 TS_1	-0.02	60.47	327.43	6.70	10.42	222	17.12
328	US-Tw1	2018 TS_2	-0.04	61.54	327.44	6.75	10.36	223	17.1
329	US-Tw1	2018 TS_3	-0.08	64.60	328.44	6.85	10.18	225	17.03
330	US-Tw1	2018 TS_4	-0.16	67.67	329.40	7.01	9.925	227	16.93
331	US-Tw1	2018 TS_5	-0.32	75.09	331.40	7.31	9.459	230	16.77
332	US-Tw4	2015 TS_1	-0.02	15.93	327.22	10.04	11.56	199.4	21.6
333	US-Tw4	2015 TS_3	-0.08	20.21	329.78	10.48	10.96	202.3	21.44
334	US-Tw4	2015 TS_4	-0.16	23.88	332.52	10.86	10.42	205.7	21.28
335	US-Tw4	2015 TS_5	-0.32	29.16	338.59	11.49	9.449	212.4	20.94
336	US-Tw4	2016 TS_1	-0.02	9.56	358.75	8.16	11.29	201.7	19.45



337	US-Tw4	2016 TS_3	-0.08	13.17	360.06	8.67	10.58	205.7	19.25
338	US-Tw4	2016 TS_4	-0.16	15.94	362.56	9.11	9.991	209.2	19.11
339	US-Tw4	2016 TS_5	-0.32	21.05	367.55	9.91	8.876	216.2	18.78
340	US-Tw4	2017 TS_1	-0.02	38.35	347.31	8.07	11.52	211.9	19.59
341	US-Tw4	2017 TS_3	-0.08	42.12	351.81	8.45	10.91	215.3	19.36
342	US-Tw4	2017 TS_4	-0.16	46.03	354.70	8.83	10.35	218.6	19.18
343	US-Tw4	2017 TS_5	-0.32	53.54	361.37	9.52	9.275	224.9	18.79
344	US-Tw4	2018 TS_1	-0.02	58.11	344.87	8.00	10.93	218	18.93
345	US-Tw4	2018 TS_3	-0.08	63.91	349.15	8.38	10.41	222	18.79
346	US-Tw4	2018 TS_4	-0.16	67.95	352.10	8.71	9.862	225	18.57
347	US-Tw4	2018 TS_5	-0.32	75.31	357.88	9.33	8.8	231	18.13
348	US-Tw5	2018 TS_1	-0.02	NaN	414.83	0.00	8.894	222.2	18.37
349	US-Tw5	2018 TS_2	-0.1	NaN	401.00	0.00	12.32	204.4	22.24
350	US-Tw5	2018 TS_3	-0.02	NaN	414.83	0.00	8.894	222.2	18.37
351	US-Tw5	2018 TS_4	-0.08	NaN	423.43	0.00	7.898	227.3	18.14
352	US-Tw5	2018 TS_5	-0.16	NaN	430.15	0.00	7.531	230	17.94
353	US-Uaf	2011 TS_1	-0.09	86.20	372.46	-12.29	21.95	199.6	9.667
354	US-Uaf	2012 TS_1	-0.09	73.77	338.53	-11.83	20.86	202.4	9.028
355	US-Uaf	2013 TS_1	-0.09	109.63	395.51	-10.08	20.52	200.4	10.44
356	US-Uaf	2014 TS_1	-0.09	76.07	365.40	-10.94	19.94	206	8.999
357	US-Uaf	2015 TS_1	-0.09	80.99	423.19	-9.77	19.76	190	9.998
358	US-Uaf	2016 TS_1	-0.09	77.38	315.75	-7.74	19.13	198	11.39
359	US-Uaf	2017 TS_1	-0.09	84.88	380.17	-7.39	19.08	196	11.69
360	US-Uaf	2018 TS_1	-0.09	96.04	333.33	-5.60	17.72	199	12.11
361	US-WPT	2011 TS_1	-0.1	80.95	342.17	5.27	19.27	202.6	24.54
362	US-WPT	2011 TS_2	-0.3	NaN	347.04	6.38	16.62	209.7	23.01
363	US-WPT	2012 TS_1	-0.1	40.29	345.57	3.70	21.6	197.4	25.3
364	US-WPT	2012 TS_2	-0.3	44.91	354.96	4.52	19.21	203.8	23.72
365	US-WPT	2013 TS_1	-0.1	74.61	340.47	3.73	18.23	207.2	21.96
366	US-WPT	2013 TS_2	-0.3	77.62	352.35	4.32	16.69	211.7	21.01

Column Descriptions
 Site Site name



Year	Data year
Probe_name	Temperature probe name as given in data files
Soil_temp_depth_m	Depth of soil temperature probe (m), with negative values
Start_TS_(DOY)	Season start for elevated TS (DOY), point "f" in Figure 1
End_TS_(DOY)	Season end for elevated TS (DOY), point "h" in Figure 1
Base_value_TS_(C)	Baseline TS during non-elevated season (C), average of points
Ampl_TS_(C)	Amplitude of TS during elevated temperature season (C), difference between point "e" in Figure 1 and Base_value_TS
Peak_TS_(DOY)	Day of maximum elevated TS (DOY), point "g" in Figure 1
Peak_value_TS_(C)	Maximum value of TS (C) point "e" in Figure 1



Table B6 - Soil temperature probe depths (m)

	Site	Year	Probe name	Soil_temp_d epth_m	Additional_n otes
1	AT-NEU		TS_1	-0.05	
2	AT-NEU		TS_2	-0.1	
3	AT-NEU		TS_3	-0.2	
4	BR-NPW		TS_1		
5	BR-NPW		TS_2		
6	BW-GUM		no data		
7	BW-NXR		no data		
8	CA-SCB		TS_1	0	
9	CA-SCB		TS_2	-0.02	
10	CA-SCB		TS_3	-0.04	
11	CA-SCB		TS_4	-0.08	
12	CA-SCB		TS_5	-0.16	
13	CA-SCB		TS_6	-0.32	
14	CA-SCB		TS_7	-0.64	
15	CA-SCB		TS_8	-1.28	
16	CA-SCC		TS_1	-0.1	
17	CA-SCC		TS_2	-0.15	
18	CA-SCC		TS_3	-0.2	
19	CA-SCC		TS_4	-0.25	
20	CA-SCC		TS_5	-0.3	
21	CA-SCC		TS_6	-0.5	
22	CA-SCC		TS_7	-0.6	
23	CA-SCC		TS_8	-0.7	
24	CH-CHA		TS_1	-0.01	
25	CH-CHA		TS_2	-0.02	
26	CH-CHA		TS_3	-0.04	
27	CH-CHA		TS_4	-0.07	
28	CH-CHA		TS_5	-0.1	
29	CH-CHA		TS_6	-0.15	
30	CH-CHA		TS_7	-0.25	
31	CH-CHA		TS_8	-0.4	
32	CH-CHA		TS_9	-0.95	
33	CH-DAV		TS_1	-0.05	
34	CH-DAV		TS_2	-0.15	
35	CH-DAV		TS_3	-0.5	
36	CH-DAV		TS_4	-	
37	CH-DAV		TS_5	-	
38	CH-DAV		TS_6	-	
39	CH-OE2		TS_1	-0.05	
40	CH-OE2		TS_2	-0.1	
41	CH-OE2		TS_3	-0.15	
42	CH-OE2		TS_4	-	



43	CH-OE2		TS_5	-0.3
44	CH-OE2		TS_6	-0.5
45	CH-OE2		TS_7	-
46	CN-HGU		TS	
47	DE-DGW		no data	
48	DE-HTE		TS_1	0
49	DE-HTE		TS_2	-0.1
50	DE-HTE		TS_3	-0.2
51	DE-SFN		TS_1	-0.02
52	DE-SFN		TS_3	-0.1
53	DE-SFN		TS_4	-0.2
54	DE-SFN		TS_5	-0.5
55	DE-ZRK		TS_1	-0.05
56	DE-ZRK		TS_2	-0.1
57	DE-ZRK		TS_3	-0.2
58	DE-ZRK		TS_4	-0.3
59	DE-ZRK		TS_5	-0.5
60	FI-HYY		TS_1	-0.02
61	FI-HYY		TS_2	-0.04
62	FI-HYY		TS_3	-0.12
63	FI-HYY		TS_4	-0.25
64	FI-HYY		TS_5	-0.5
65	FI-LOM		TS_1	-0.07
66	FI-LOM		TS_2	-0.3
67	FI-LOM		TS_3	-0.5
68	FI-SI2		TS_1	-0.05
69	FI-SI2		TS_2	-0.2
70	FI-SI2		TS_3	-0.35
71	FI-SI2		TS_4	-0.5
72	FI-SII	pre 2016	TS_1	-0.05
73	FI-SII	pre 2016	TS_2	-0.2
74	FI-SII	pre 2016	TS_3	-0.35
75	FI-SII	pre 2016	TS_4	-0.5
76	FI-SII	after 2017	TS_1	0
77	FI-SII	after 2017	TS_2	-0.5
78	FI-SII	after 2017	TS_3	-0.1
79	FI-SII	after 2017	TS_4	-0.15
80	FI-SII	after 2017	TS_5	-0.25
81	FI-SII	after 2017	TS_6	-0.45
82	FI-SII	after 2017	TS_7	-0.95
83	FR-LGT		TS_1	-0.02
84	FR-LGT		TS_2	-0.05
85	FR-LGT		TS_3	-0.1
86	FR-LGT		TS_4	-0.2



87	FR-LGT	TS_5	-0.4
88	HK-MPM	TS_1	
89	HK-MPM	TS_2	
90	HK-MPM	TS_3	
91	ID-PAG	TS_1	-0.05
92	IT-BCI	TS_1	-0.05
93	IT-BCI	TS_2	-0.1
94	IT-BCI	TS_3	-0.3
95	IT-BCI	TS_4	-0.5
96	IT-BCI	TS_5	-1
97	IT-CAS	TS_1	-0.035
98	IT-CAS	TS_2	-0.075
99	IT-CAS	TS_3	-0.15
100	JP-BBY	TS_1	-0.183
101	JP-BBY	TS_2	-0.233
102	JP-BBY	TS_3	-0.283
103	JP-BBY	TS_4	-0.383
104	JP-BBY	TS_5	-0.483
105	JP-MSE	TS_1	-0.01
106	JP-MSE	TS_2	-0.025
107	JP-MSE	TS_3	-0.05
108	JP-MSE	TS_4	-0.1
109	JP-MSE	TS_5	-0.2
110	JP-MSE	TS_6	-0.4
111	JP-SWL	no data	
112	KR-CRK	TS_1	-0.05
113	KR-CRK	TS_2	-0.15
114	MAERC	TS	
115	MY-MLM	TS_1	-0.05
116	NL-HOR	TS_1	-0.01
117	NL-HOR	TS_2	-0.02
118	NL-HOR	TS_3	-0.04
119	NL-HOR	TS_4	-0.05
120	NL-HOR	TS_5	-0.1
121	NL-HOR	TS_6	-0.15
122	NL-HOR	TS_7	-0.25
123	NL-HOR	TS_8	-0.4
124	NL-HOR	TS_9	-0.6
125	NZ-KOP	TS_1	-0.5
126	NZ-KOP	TS_2	-0.1
127	NZ-KOP	TS_3	-0.2
128	PH-RIF	TS_1	
129	RU-CH2	TS_1	-0.04
130	RU-CH2	TS_2	-0.08



131	RU-CH2	TS_3	-0.16
132	RU-CHE	TS_1	-0.04
133	RU-CHE	TS_2	-0.08
134	RU-CHE	TS_3	-0.16
135	RU-COK	no data	
136	RU-FY2	TS_1	
137	RU-FY2	TS_2	
138	RU-FY2	TS_3	
139	RU-FY2	TS_4	
140	RU-FY2	TS_5	
141	SE-DEG	TS_1	-0.02
142	SE-DEG	TS_2	-0.05
143	SE-DEG	TS_3	-0.1
144	SE-DEG	TS_4	-0.15
145	SE-DEG	TS_5	-0.3
146	SE-DEG	TS_6	-0.5
147	UK-LBT	no data	
148	US-A03	TS_1	-0.025
149	US-A03	TS_2	-0.1
150	US-A03	TS_3	-0.3
151	US-A10	TS_1	-0.025
152	US-A10	TS_2	-0.1
153	US-A10	TS_3	-0.3
154	US-ATQ	TS_1	
155	US-ATQ	TS_2	
156	US-ATQ	TS_3	
157	US-BEO	TS_1	
158	US-BEO	TS_2	
159	US-BEO	TS_3	
160	US-BES	TS_1	
161	US-BES	TS_2	
162	US-BES	TS_3	
163	US-BI1	TS_1	-0.02
164	US-BI1	TS_2	-0.04
165	US-BI1	TS_3	-0.08
166	US-BI1	TS_4	-0.16
167	US-BI1	TS_5	-0.32
168	US-BI2	TS_1	-0.02
169	US-BI2	TS_2	-0.04
170	US-BI2	TS_3	-0.08
171	US-BI2	TS_4	-0.16
172	US-BI2	TS_5	-0.32
173	US-BRW		
174	US-BZB	TS_1	-0.075



175	US-BZB	TS_2	-0.05
176	US-BZF	TS_1	-0.075
177	US-BZF	TS_2	-0.05
178	US-BZS	TS_1	
179	US-BZS	TS_2	
180	US-BZS	TS_3	
181	US-CRT	TS_1	
182	US-DPW	no data	
183	US-EDN	TS_1	-0.25
184	US-EDN	TS_2	-0.15
185	US-EDN	TS_3	-0.05
186	US-EDN	TS_4	0
187	US-EDN	TS_5	0.05
188	US-EDN	TS_6	0.1
189	US-EDN	TS_7	0.2
190	US-EDN	TS_8	0.3
191	US-EML	TS_1	-0.05
192	US-EML	TS_2	-0.1
193	US-EML	TS_3	-0.2
194	US-EML	TS_4	-0.4
195	US-HO1	TS_1	-0.05
196	US-HO1	TS_2	-0.1
197	US-HRA	no data	-0.02
198	US-HRC	no data	-0.02
199	US-ICS	TS_1	-0.075
200	US-ICS	TS_2	-0.05
201	US-IVO	TS_1	-0.05
202	US-IVO	TS_2	-0.1
203	US-IVO	TS_3	-0.15
204	US-IVO	TS_4	-0.3
205	US-IVO	TS_5	-0.4
206	US-LA1	TS	-0.1
207	US-LA2	TS	-0.1
208	US-LOS	TS_1	0
209	US-LOS	TS_2	-0.05
210	US-LOS	TS_3	-0.1
211	US-LOS	TS_4	-0.2
212	US-LOS	TS_5	-0.5
213	US-MRM	TS_1	
214	US-MRM	TS_2	
215	US-MYB	TS_1	-0.02
216	US-MYB	TS_2	-0.04
217	US-MYB	TS_3	-0.08
218	US-MYB	TS_4	-0.16



219	US-MYB	TS_5	-0.32
220	US-NC4	TS_1	-0.05
221	US-NC4	TS_2	-0.2
222	US-NGB	no data	
223	US-NGC	no data	
224	US-ORV	TS_1	-0.08
225	US-OWC	TS_1	-0.05
226	US-OWC	TS_2	-0.3
227	US-PFA		
228	US-SND	TS_1	-0.08
229	US-SND	TS_2	-0.16
230	US-SND	TS_3	
231	US-SND	TS_4	
232	US-SND	TS_5	
233	US-SND	TS_6	
234	US-SNE	TS_1	-0.01
235	US-SNE	TS_2	-0.02
236	US-SNE	TS_3	-0.08
237	US-SNE	TS_4	-0.16
238	US-SNE	TS_5	-0.32
239	US-SRR	TS_1	
240	US-SRR	TS_2	
241	US-SRR	TS_3	
242	US-SRR	TS_4	
243	US-SRR	TS_5	
244	US-STJ	TS_2	-0.05
245	US-STJ	TS_3	-0.1
246	US-TW1	TS_1	-0.02
247	US-TW1	TS_2	-0.04
248	US-TW1	TS_3	-0.08
249	US-TW1	TS_4	-0.16
250	US-TW1	TS_5	-0.32
251	US-TW3	TS_1	-0.02
252	US-TW3	TS_2	-0.04
253	US-TW3	TS_3	-0.08
254	US-TW3	TS_4	-0.16
255	US-TW3	TS_5	-0.32
256	US-TW4	TS_1	-0.02
257	US-TW4	TS_2	-0.04
258	US-TW4	TS_3	-0.08
259	US-TW4	TS_4	-0.16
260	US-TW4	TS_5	-0.32
261	US-TW5	TS_1	-0.02
262	US-TW5	TS_2	-0.1



263	US-TW5	TS_3	-0.02
264	US-TW5	TS_4	-0.08
265	US-TW5	TS_5	-0.16
266	US-TWT	TS_1	-0.02
267	US-TWT	TS_2	-0.04
268	US-TWT	TS_3	-0.08
269	US-TWT	TS_4	-0.16
270	US-TWT	TS_5	-0.32
271	US-UAF	TS_1	-0.09 average of 3 depths: -0.15, -0.02, -0.1
272	US-UAF	TS_2	-0.1833333 average of 3 depths: -0.3, -0.05, -0.2
273	US-UAF	TS_3	-0.2833333 average of 3 depths: -0.45, -0.1, -0.3
274	US-UAF	TS_4	-0.3666667 average of 3 depths: -0.5, -0.2, -0.4
275	US-UAF	TS_5	-0.5 average of 2 depths: -0.7, -0.3
276	US-UAF	TS_6	-0.6 average of 2 depths: -0.8, -0.4
277	US-UAF	TS_7	-0.75 average of 2 depths: -1, -0.5
278	US-UAF	TS_8	-0.925 average of 2 depths: -1.25, 0.6,
279	US-UAF	TS_9	-1
280	US-WPT	TS_1	-0.1
281	US-WPT	TS_2	-0.3

Column Descriptions

Site	Site name
Year	When relevant, information about time-span of probe location. If blank, assume probe depth was constant
Probe_name	Temperature probe name as given in data files
Soil_temp_depth_m	Depth of soil temperature probe (m), with negative values being under the surface
Additional_notes	When relevant, additional information about site



Table B7 Site year annual sums and uncertainties

	Site	Year	Ann_Flux_g_C_m-2	Ann_Flux_Uncertainty_g_C_m-2	Mean_Soil_Temp_C	Mean_Water_Table_Depth_m
1	ATNEU	2010	0.38	0.03	8.65	NaN
2	ATNEU	2011	0.25	0.02	8.61	NaN
3	ATNEU	2012	NaN	NaN	9.39	NaN
4	BRNPW	2013	NaN	NaN	NaN	NaN
5	BRNPW	2014	NaN	NaN	25.95	NaN
6	BRNPW	2015	20.95	1.18	26.2	-0.47
7	BRNPW	2016	17.48	1.14	25.31	-0.41
8	BWGUM	2018	51.73	10.59	NaN	NaN
9	BWNXR	2018	47.32	3.70	NaN	NaN
10	CASCB	2014	10.42	0.66	9.6	-0.15
11	CASCB	2015	NaN	NaN	5.58	-0.1
12	CASCB	2016	12.12	0.31	5.38	-0.15
13	CASCB	2017	9.48	0.27	6.32	-0.21
14	CASCC	2013	NaN	NaN	7.2	NaN
15	CASCC	2014	4.94	0.12	4.38	NaN
16	CASCC	2015	6.76	0.15	3.15	NaN
17	CASCC	2016	6.76	0.12	NaN	NaN
18	CHCHA	2012	2.13	0.38	11.88	NaN
19	CHCHA	2013	2.30	0.36	10.89	NaN
20	CHCHA	2014	3.46	0.40	12.2	NaN
21	CHCHA	2015	3.93	0.68	11.93	NaN
22	CHCHA	2016	NaN	NaN	12.28	NaN
23	CHDAV	2016	1.21	0.40	4.33	NaN
24	CHDAV	2017	NaN	NaN	4.41	NaN
25	CHOE2	2018	0.29	0.13	12.32	NaN
26	CNHGU	2015	NaN	NaN	NaN	NaN
27	CNHGU	2016	0.81	0.16	7.26	NaN
28	CNHGU	2017	0.82	0.45	7.66	NaN
29	DEDGW	2015	NaN	NaN	NaN	NaN
30	DEDGW	2016	7.51	0.22	NaN	NaN
31	DEDGW	2017	10.42	0.16	NaN	NaN
32	DEDGW	2018	NaN	NaN	NaN	NaN
33	DEHTE	2011	59.85	6.39	NaN	-0.41
34	DEHTE	2012	36.83	3.46	NaN	-0.21
35	DEHTE	2013	49.72	2.34	NaN	-0.25
36	DEHTE	2014	NaN	NaN	13.26	-0.19
37	DEHTE	2015	51.37	1.75	10.78	-0.26
38	DEHTE	2016	50.77	2.09	9.8	-0.25
39	DEHTE	2017	46.61	1.40	10.39	-0.4
40	DEHTE	2018	41.62	2.52	6.12	-0.22
41	DESFN	2012	NaN	NaN	NaN	-0.08



42	DESFN	2013	3.62	0.93	10.32	-0.05
43	DESFN	2014	NaN	NaN	8.16	NaN
44	DEZRK	2013	NaN	NaN	13.03	NaN
45	DEZRK	2014	NaN	NaN	11.67	NaN
46	DEZRK	2015	30.76	1.00	10.85	NaN
47	DEZRK	2016	31.14	1.23	11.28	0.12
48	DEZRK	2017	29.10	0.87	10.84	0.31
49	DEZRK	2018	31.10	1.20	10.54	0.25
50	FIHYY	2016	NaN	NaN	5.41	NaN
51	FILOM	2006	13.77	0.76	4.47	0
52	FILOM	2007	17.22	0.25	4.33	0.04
53	FILOM	2008	15.52	0.22	3.79	0.06
54	FILOM	2009	17.63	0.27	3.98	0.02
55	FILOM	2010	13.78	0.29	3.71	0.03
56	FISI2	2012	9.27	1.17	9.4	0.06
57	FISI2	2013	10.22	1.17	10.47	0.13
58	FISI2	2014	NaN	NaN	7.7	0.1
59	FISI2	2015	NaN	NaN	8.18	0.09
60	FISI2	2016	NaN	NaN	7.67	0.09
61	FISII	2013	14.58	0.32	6.45	0.04
62	FISII	2014	12.93	0.78	6.42	0.03
63	FISII	2015	NaN	NaN	6.92	-0.02
64	FISII	2016	16.56	0.68	5.87	-0.01
65	FISII	2017	8.63	0.23	8.4	0.06
66	FISII	2018	9.46	1.10	6.68	0.11
67	FRLGT	2017	NaN	NaN	10.45	-0.24
68	FRLGT	2018	2.45	0.60	10.87	-0.22
69	HKMPM	2016	11.62	0.61	25.06	-0.61
70	HKMPM	2017	10.60	0.30	23.14	-0.64
71	HKMPM	2018	11.04	0.59	NaN	-0.8
72	IDPAG	2016	0.09	0.07	NaN	NaN
73	IDPAG	2017	0.09	0.09	NaN	NaN
74	ITBCI	2017	NaN	NaN	17.16	NaN
75	ITBCI	2018	NaN	NaN	17.36	NaN
76	ITCAS	2009	25.44	1.46	9.62	NaN
77	ITCAS	2010	17.80	1.26	12.37	NaN
78	JPBBY	2015	9.53	0.29	10.12	0
79	JPBBY	2016	16.42	0.45	10.02	0
80	JPBBY	2017	19.61	0.65	9.33	-0.03
81	JPBBY	2018	NaN	NaN	9.79	-0.04
82	JPMSE	2012	9.50	1.97	14.52	0.03
83	JPSWL	2016	66.68	4.29	NaN	1.91
84	KRCRK	2015	NaN	NaN	14.41	0.02
85	KRCRK	2016	29.12	0.91	12.48	0.03



86	KRCRK	2017	25.84	0.86	13.94	0.02
87	KRCRK	2018	28.82	1.15	11.32	0.02
88	MYMLM	2014	9.55	0.59	26.8	-0.09
89	MYMLM	2015	NaN	NaN	26.9	-0.01
90	NLHOR	2007	NaN	NaN	12.4	NaN
91	NLHOR	2008	NaN	NaN	10.37	NaN
92	NLHOR	2009	NaN	NaN	11.61	NaN
93	NZKOP	2012	23.98	1.38	12.17	-0.08
94	NZKOP	2013	15.33	0.43	12.68	-0.13
95	NZKOP	2014	15.67	0.39	12.38	-0.11
96	NZKOP	2015	14.37	2.66	12.46	-0.1
97	PHRIF	2012	NaN	NaN	27.78	NaN
98	PHRIF	2013	12.41	0.99	28.17	NaN
99	PHRIF	2014	NaN	NaN	27.47	NaN
100	RUCH2	2014	6.99	0.14	-4.21	NaN
101	RUCH2	2015	5.86	0.14	-4.87	NaN
102	RUCH2	2016	NaN	NaN	-2.88	NaN
103	RUCHE	2014	3.84	0.14	-3.31	NaN
104	RUCHE	2015	4.19	0.22	-3.28	NaN
105	RUCHE	2016	4.24	0.19	-1.65	NaN
106	RUCOK	2008	NaN	NaN	NaN	NaN
107	RUCOK	2009	NaN	NaN	NaN	NaN
108	RUCOK	2010	NaN	NaN	NaN	NaN
109	RUCOK	2011	NaN	NaN	NaN	NaN
110	RUCOK	2012	NaN	NaN	-0.46	NaN
111	RUCOK	2013	NaN	NaN	-5.73	NaN
112	RUCOK	2014	NaN	NaN	-4.82	NaN
113	RUCOK	2015	4.45	0.15	-4.4	NaN
114	RUCOK	2016	NaN	NaN	-11.1	NaN
115	RUFY2	2015	NaN	NaN	9.83	NaN
116	RUFY2	2016	2.69	0.59	6.88	0.68
117	RUFY2	2017	2.17	0.52	6.1	0.19
118	RUFY2	2018	5.66	1.37	6.48	0.79
119	SEDEG	2014	11.24	1.98	5.02	-0.02
120	SEDEG	2015	11.11	0.08	5.04	0.02
121	SEDEG	2016	11.19	0.15	5.19	-0.01
122	SEDEG	2017	NaN	NaN	4.19	0
123	SEDEG	2018	9.42	0.09	5.49	-0.03
124	UKLBT	2011	NaN	NaN	NaN	NaN
125	UKLBT	2012	NaN	NaN	NaN	NaN
126	UKLBT	2013	50.50	0.97	NaN	NaN
127	UKLBT	2014	42.57	2.25	NaN	NaN
128	USA03	2015	NaN	NaN	-6.65	NaN
129	USA03	2016	NaN	NaN	-6.14	NaN



130	USA03	2017	7.26	2.58	-4.48	NaN
131	USA03	2018	4.35	0.62	-4.93	NaN
132	USA10	2012	NaN	NaN	NaN	NaN
133	USA10	2013	NaN	NaN	NaN	NaN
134	USA10	2014	NaN	NaN	NaN	NaN
135	USA10	2015	NaN	NaN	NaN	NaN
136	USA10	2016	NaN	NaN	NaN	NaN
137	USA10	2017	NaN	NaN	NaN	NaN
138	USA10	2018	NaN	NaN	NaN	NaN
139	USATQ	2013	NaN	NaN	-5.65	NaN
140	USATQ	2014	1.80	0.19	-4.48	NaN
141	USATQ	2015	1.75	0.11	-0.43	NaN
142	USATQ	2016	1.75	0.00	NaN	NaN
143	USBEO	2013	NaN	NaN	-2.67	NaN
144	USBEO	2014	2.74	0.05	-4.95	NaN
145	USBES	2013	NaN	NaN	-6.01	NaN
146	USBES	2014	3.32	0.04	-5.69	NaN
147	USBES	2015	3.06	0.54	-6.24	NaN
148	USB11	2016	NaN	NaN	15.62	NaN
149	USB11	2017	NaN	NaN	17.17	NaN
150	USB11	2018	0.69	0.29	16.82	NaN
151	USB12	2017	0.86	0.20	20.42	NaN
152	USB12	2018	1.69	0.29	17.12	NaN
153	USBZB	2014	8.02	4.61	4.03	NaN
154	USBZB	2015	7.52	0.82	3.9	NaN
155	USBZB	2016	11.61	2.25	4.89	NaN
156	USBZF	2014	6.61	0.63	4.32	NaN
157	USBZF	2015	10.82	0.90	3.99	NaN
158	USBZF	2016	NaN	NaN	5.93	NaN
159	USBZS	2015	0.68	0.68	0.48	NaN
160	USBZS	2016	0.89	0.27	0.67	NaN
161	USCRT	2011	2.21	0.15	11.49	-0.92
162	USCRT	2012	2.21	0.11	12.38	-1.45
163	USDPW	2013	NaN	NaN	NaN	NaN
164	USDPW	2014	58.91	0.69	NaN	NaN
165	USDPW	2015	NaN	NaN	NaN	NaN
166	USDPW	2016	43.60	1.29	NaN	NaN
167	USDPW	2017	43.60	0.06	NaN	NaN
168	USEDN	2018	-0.04	0.06	NaN	NaN
169	USEML	2015	NaN	NaN	5.71	NaN
170	USEML	2016	1.04	0.08	3.07	NaN
171	USEML	2017	0.36	0.27	3.8	NaN
172	USEML	2018	0.36	0.07	NaN	NaN
173	USHO1	2012	NaN	NaN	NaN	-0.43



174	USHO1	2013	-0.05	0.02	NaN	-0.33
175	USHO1	2014	-0.04	0.02	NaN	-0.38
176	USHO1	2015	-0.16	0.01	NaN	-0.48
177	USHO1	2016	-0.22	0.01	NaN	-0.57
178	USHO1	2017	-0.24	0.01	NaN	-0.56
179	USHO1	2018	-0.24	0.01	NaN	NaN
180	USHRA	2017	-0.24	0.56	NaN	NaN
181	USHRC	2017	-0.24	0.81	NaN	NaN
182	USICS	2014	NaN	NaN	-1.55	NaN
183	USICS	2015	NaN	NaN	-0.62	NaN
184	USICS	2016	NaN	NaN	-1.48	NaN
185	USIVO	2013	NaN	NaN	3.19	NaN
186	USIVO	2014	5.05	0.22	0.02	NaN
187	USIVO	2015	3.89	0.27	0.47	NaN
188	USIVO	2016	5.77	0.55	-1.01	NaN
189	USLA1	2011	NaN	NaN	18.92	NaN
190	USLA1	2012	12.68	0.63	24.23	NaN
191	USLA2	2011	12.68	0.19	NaN	NaN
192	USLA2	2012	48.42	1.57	23.09	NaN
193	USLA2	2013	43.34	1.32	23.19	NaN
194	USLOS	2014	6.66	1.48	8.3	-0.06
195	USLOS	2015	5.51	0.40	5.65	-0.1
196	USLOS	2016	8.67	0.35	6.3	-0.07
197	USLOS	2017	6.00	0.33	5.5	-0.09
198	USLOS	2018	5.71	0.37	4.29	-0.19
199	USMAC	2013	5.71	2.68	NaN	NaN
200	USMAC	2014	26.37	1.69	23.18	-0.71
201	USMAC	2015	15.40	0.85	23.29	-0.55
202	USMRM	2012	0.30	0.19	11.16	NaN
203	USMRM	2013	0.37	0.14	8.99	NaN
204	USMYB	2010	NaN	NaN	NaN	0.95
205	USMYB	2011	33.83	0.72	17.18	1.23
206	USMYB	2012	64.20	0.58	16.25	1.12
207	USMYB	2013	59.81	0.92	15.7	1.19
208	USMYB	2014	58.97	0.68	11.27	1.24
209	USMYB	2015	60.85	0.55	NaN	1.3
210	USMYB	2016	45.72	0.48	NaN	1.22
211	USMYB	2017	30.32	0.84	18.5	1.35
212	USMYB	2018	29.33	0.55	17.05	1.19
213	USNC4	2012	38.28	1.70	17.12	NaN
214	USNC4	2013	18.60	3.88	NaN	NaN
215	USNC4	2014	26.98	0.60	18.02	NaN
216	USNC4	2015	23.37	2.30	16.27	NaN
217	USNC4	2016	62.20	2.78	16.35	NaN



218	USNGB	2012	NaN	NaN	NaN	NaN
219	USNGB	2013	NaN	NaN	NaN	NaN
220	USNGB	2014	NaN	NaN	NaN	NaN
221	USNGB	2015	NaN	NaN	NaN	NaN
222	USNGB	2016	NaN	NaN	NaN	NaN
223	USNGB	2017	2.31	0.11	NaN	NaN
224	USNGB	2018	2.52	0.22	NaN	NaN
225	USNGC	2017	2.52	0.06	NaN	NaN
226	USNGC	2018	2.52	0.05	NaN	NaN
227	USORV	2011	3.53	0.54	16.64	NaN
228	USORV	2012	9.11	0.45	14.23	NaN
229	USORV	2013	7.70	0.41	13.19	NaN
230	USORV	2014	8.46	0.26	12	NaN
231	USORV	2015	NaN	NaN	13.36	NaN
232	USOWC	2015	NaN	NaN	22.11	0.9
233	USOWC	2016	113.99	3.25	21.19	0.54
234	USPFA	2010	NaN	NaN	NaN	NaN
235	USPFA	2011	0.34	0.05	NaN	NaN
236	USPFA	2012	0.30	0.04	NaN	NaN
237	USPFA	2013	0.31	0.05	NaN	NaN
238	USPFA	2014	NaN	NaN	NaN	NaN
239	USPFA	2015	0.63	0.03	NaN	NaN
240	USPFA	2016	0.85	0.02	NaN	NaN
241	USPFA	2017	0.80	0.06	NaN	NaN
242	USPFA	2018	NaN	NaN	NaN	NaN
243	USSND	2010	NaN	NaN	16.85	NaN
244	USSND	2011	NaN	NaN	14.96	NaN
245	USSND	2012	6.34	0.25	16.06	NaN
246	USSND	2013	6.04	0.48	16.59	-0.65
247	USSND	2014	3.23	0.36	17.52	-0.78
248	USSND	2015	3.23	0.21	NaN	NaN
249	USSNE	2016	NaN	NaN	17.85	-0.2
250	USSNE	2017	45.96	0.40	17.05	0.16
251	USSNE	2018	39.63	0.66	16.83	0.09
252	USSRR	2014	0.71	0.10	NaN	NaN
253	USSRR	2015	0.88	0.11	NaN	NaN
254	USSRR	2016	0.86	0.10	16.3	-0.18
255	USSRR	2017	0.86	0.11	NaN	NaN
256	USSTJ	2016	9.55	1.04	11.66	-0.26
257	USTW1	2011	26.09	2.70	14.01	NaN
258	USTW1	2012	NaN	NaN	11.58	0.24
259	USTW1	2013	33.93	1.78	11.92	0.25
260	USTW1	2014	49.60	1.67	13.14	0.25
261	USTW1	2015	54.80	2.58	12.79	0.33



262	USTW1	2016	45.93	1.90	12.91	0.41
263	USTW1	2017	38.66	2.09	12.53	0.38
264	USTW1	2018	27.60	1.64	12.1	0.24
265	USTW3	2013	NaN	NaN	19.63	NaN
266	USTW3	2014	NaN	NaN	17.91	NaN
267	USTW4	2013	NaN	NaN	NaN	NaN
268	USTW4	2014	16.26	0.39	NaN	0.48
269	USTW4	2015	27.61	0.43	17.2	0.36
270	USTW4	2016	33.49	0.37	14.8	0.18
271	USTW4	2017	47.95	0.58	13.78	0.07
272	USTW4	2018	37.41	0.48	13.02	0.08
273	USTW5	2018	59.72	1.15	16.67	0.69
274	USTWT	2009	NaN	NaN	17.66	-0.01
275	USTWT	2010	9.87	1.15	15.67	-0.18
276	USTWT	2011	12.32	4.92	14.95	-0.11
277	USTWT	2012	8.12	0.51	16.05	-0.04
278	USTWT	2013	12.64	0.48	15.98	-0.11
279	USTWT	2014	17.02	0.97	17.44	-0.09
280	USTWT	2015	14.43	0.38	17.04	-0.14
281	USTWT	2016	11.07	0.59	16.44	-0.29
282	USTWT	2017	11.07	0.31	NaN	NaN
283	USUAF	2011	0.32	0.04	-2.14	-0.17
284	USUAF	2012	NaN	NaN	-2.43	-0.18
285	USUAF	2013	NaN	NaN	-1.15	-0.18
286	USUAF	2014	NaN	NaN	-1.18	-0.13
287	USUAF	2015	NaN	NaN	-0.49	-0.12
288	USUAF	2016	0.68	0.05	-0.05	-0.1
289	USUAF	2017	0.58	0.06	1.09	-0.13
290	USUAF	2018	NaN	NaN	0.87	-0.13
291	USWPT	2011	41.05	1.57	17.22	0.43
292	USWPT	2012	54.96	1.71	14.27	0.28
293	USWPT	2013	52.76	1.29	12.89	0.44

Column Descriptions

Site	Site name
Year	Data year
Ann_Flux_g_C_m-2	Total annual methane flux (gC/m ²)
Ann_Flux_Uncertainty_g_C_m-2	Gap-filling and random uncertainty associated with annual flux (gC/m ²)
Mean_Soil_Temp_C	Annual mean soil temperature (degree C). For sites with multiple probes, we use the probe closest to the surface
Mean_Water_Table_Depth_m	Annual mean water table depth (m)